The Role of Down Syndrome Cell Adhesion Molecule in Development and Diseases

by

Hao Liu

A dissertation submitted in partial fulfillment
of the requirements for the degree of
Doctor of Philosophy
(Cell and Developmental Biology)
in the University of Michigan
2020

Doctoral Committee:

Assistant Professor Kenneth Kwan, Chair
Assistant Professor Dawen Cai
Associate Professor Ken Inoki
Professor Yukiko Yamashita
Associate Professor Bing Ye

Hao Liu
falleave@umich.edu
ORCID iD: 0000-0001-9155-409X

DEDICATION

To my beloved family.

ACKNOWLEDGEMENTS

I would like to first thank my dissertation advisor, Dr. Bing Ye, who offers me the opportunity to work in his laboratory and pursue the wonderful world of neuroscience. I have benefitted tremendously from his dedication to science, breadth of knowledge and the capacity of persistence. My critical thinking, scientific insight, writing and presentation skills elevated exponentially via the daily communication with him. In addition, I'd like to thank Dr. Ye for the baby items, which helped me a lot during the first several months after my daughter was born.

I would also like to thank my thesis committee members, Drs. Kenneth Kwan, Dawen Cai, Ken Inoki, and Yukiko Yamashita. Their insightful advice and generous help are invaluable to my Ph.D. training. Talking with them in the thesis committee meeting is one of the most enjoyable things in my Ph.D. study. Especially, I'd like to thank Dr. Kenneth Kwan for the critical suggestions on how to package the story, Dr. Dawen Cai for the critical reagents, Dr. Ken Inoki for the amazingly simple and effective genotyping protocol and Dr. Yukiko Yamashita for sharing the powerful SP8 confocal. Without their supports, this dissertation wouldn't have been possible.

I would like to thank all the people who contributed to my thesis research. I'd like to thank Jung Hwan Kim, Sarah Pizzano, Ruonan Li, Limin Yang, Wenquan Zhao, Macy W. Veling, Laura Smithson, Yujia Hu, René N. Caballero-Florán, Tao Yang, Jacob M. Hull, Geng Pan, Miao He,

Yongjie Hou, Pedro Lowenstein and Lori L. Isom for their critical suggestions and participation in my research projects. Especially, I'd like to thank Dr. Paul M. Jenkins and René N. Caballero-Florán for the productive collaboration. Furthermore, this thesis benefits a lot from the reagents shared by Drs. Z. Josh Huang, Peter G. Fuerst, Roman Giger, Jun Wu, Andrew Nelson, Jonathan Flak, Martin Myers, Lawrence Zipursky, Yi Chen, Jack Dixon, Catherine Collins, Ryan Insolera, David Lorberbaum and Scott Barolo.

I would like to thank CDB, a cozy department which makes me feel at home. In particular, I'd like to thank Dr. Roman Giger and Kristen Hug for their long support. I'd like to thank PIBS for accepting me and the University of Michigan for providing such a great environment for Ph.D. study.

Last but not least, I would like to thank my family. My parents are my first mentor, who taught me to make a living by one's own hand, to be thankful to those who helped me and to be optimistic about the future. These principles have been deeply craved in my mind and will last all my life. My elder brother is my first friend. He taught me how to share and stand in others shoes. I feel myself so lucky to have a brother with me in my childhood and my life. Of course, I'd like to thank whole-heartedly my wife, Qidi Feng. I still remember the first time I met her at the yard of Shanghai Institutes for Biological Sciences nine years ago. This is one of the most memorable day in my life. Qidi accompanies me through ups and downs over the past nine years. With my wife, the joy of life is doubled while misery divided. Especially, Qidi gave birth our first child, Kaiyang, this January. My daughter has brought me so much happiness these several months. I feel I'm blessed and I hope I may make their life more blissful in the future.

TABLE OF CONTENTS

LIST OF FIGURES

ABSTRACT

How neurons elaborate dendrites and axons and how they form synapses with targeted cells are fundamental questions in neurodevelopment. Although a number of genes have been identified to play a role in these processes, the following two aspects are largely unknown and interesting to study. First, while most genes go through alternative splicing to generate different protein isoforms, how each protein isoform contributes to the function of this gene in neurodevelopment remains a challenging question, especially at the cell-type specific and endogenous levels. Second, in neurodevelopmental diseases, such as those in Down syndrome, the expression levels of hundreds or thousands of genes are altered. The dysregulation of which gene cause the neurite and synaptic defects in these brain disorders remains largely unknown. My dissertation aims to answer these two questions with the focus of one gene, *Down syndrome cell adhesion molecule* (*Dscam*).

Dscam is an evolutionarily conserved single-pass transmembrane protein that plays critical roles in multiple aspects of neuronal wiring, including dendritic/axonal growth and synapse formation. In *Drosophila*, alternative splicing of *Dscam* produces two mutually exclusive isoforms, Dscam[TM1] and [TM2], which differ in their transmembrane and juxtamembrane region. By developing a novel genetic method, termed *isoTarget*, which enables the investigation of isoform-specific function and endogenous localization in specific cells, I report differential function and localization of Dscam isoforms in axons versus dendrites. In addition, I uncovered

an isoform-specific signaling pathway that involves DLK/Wallenda, Dock, and Dscam[TM2], but not Dscam[TM1], at the axon terminals of *Drosophila* sensory neurons. I provide evidence showing that Dscam[TM2]-specific function and signaling in axon terminals are caused by its isoform-specific localization, rather than by biochemical differences between Dscam[TM1] and [TM2]. These findings not only demonstrate the specific function, localization and signaling of Dscam isoforms but also demonstrate the critical role of subcellular localization in expanding isoform diversity.

In human, the *Dscam* gene is localized in the Down syndrome critical region on chromosome 21. By taking advantage of sparse neuron labeling for morphological analysis and whole-cell patch-clamp for functional assay, I found that *Dscam* regulates inhibitory neuron development in the neocortex in a dose-dependent fashion. Loss of *Dscam* impairs the presynaptic growth in chandelier and basket cells, two major types of inhibitory neurons in the neocortex. In the Ts65Dn mouse model for Down syndrome, where Dscam is overexpressed, GABAergic inhibition of pyramidal neurons (PyNs), the main excitatory neurons in the cortex, is increased. Genetic normalization of Dscam expression rescues the excessive GABAergic synapse formation and inhibition of PyNs. These findings reveal abnormal GABAergic innervation in the neocortex of Down syndrome mouse model and identify Dscam overexpression as the cause. They also implicate dysregulated Dscam levels as a potential pathogenic driver in related neurological disorders.

In summary, by using the novel genetic method *isoTarget*, this dissertation uncovers Dscam isoform-specific subcellular signaling cascade in neurodevelopment; using genetic normalization in Down syndrome mouse model, it establishes a causal effect between dysregulated Dscam

expression levels and cortical defects in Down syndrome pathology. These findings are expected to advance our understanding of the role of Dscam in neurodevelopment and neurological disorders.

Chapter 1

Introduction

1.1 Molecular mechanisms underlying neuronal development.

Since Ramon y Cajal proposed more than one hundred years ago that neurons are the basic building blocks of the nervous system (Ramón y Cajal 1893), these specialized cells have fascinated scientists and the public with their highly polarized morphologies. A typical neuron contains three major compartments: the dendrite, cell body and axon. The dendrite is the input compartment that receives electrochemical signals while the axon is the output compartment for passing the information on to downstream cells. The axon and dendrite differ in membrane composition, organelle enrichment and cytoskeletal orientation, which serve as the structural basis for the functional distinctions of these two compartments (Yogev and Shen 2017). For example, synaptic vesicles are specifically localized at axon terminals. These 35- to 45-nm spherical vesicles contain neurotransmitters that are released upon action potentials' arrival at the axon terminals (Sudhof 2012). By contrast, the small membranous protrusions, called spines, is only present in a neuron's dendrite. Dendritic spines receive input from single axons and convey electrochemical signals to the neuron's cell body (Sorra and Harris 2000) .

To achieve such a "two-part" design, several steps are needed for neuronal development (Caceres, Ye, and Dotti 2012; Yogev and Shen 2017): 1) the establishment of neuronal polarity. A symmetry-breaking signal causes a spatial orientation in the neuron and determine the site

where axon/dendrite initiates. 2) Neurite extension. The dendrite and axon elongate towards their target areas. 3) Pre/post-synaptic development. Upon reaching the destination, the neurite arborizes locally and forms synapses within these arbors for synaptic transmission. Each step requires an exquisite orchestration of cell-intrinsic signaling cascades and the extra-cellular environmental cues. This dissertation mainly focuses on the cell-intrinsic molecular regulators of presynaptic development.

1.1.1 Molecular regulators of presynaptic arborization.

A variety of experimental systems have been used to study the molecular mechanism of presynaptic arborization. These include cultured hippocampal neurons, *Drosophila* dendritic arborization (da) neurons, cortical inhibitory neurons, neuromuscular junction (NMJ) and retinal ganglion cells (Takano et al. 2015; Wang, Sterne, and Ye 2014; Sanes and Lichtman 1999; Sanes and Masland 2015). Due to the scope and interest of this dissertation, I will focus on the presynaptic regulators identified in the first three experimental systems.

Presynaptic regulators identified *in vitro*

Cultured neurons from mouse or rat hippocampi are a widely used *in vitro* model for investigating the signaling pathways that regulate presynaptic growth. After plating, a hippocampal neuron in culture shows a symmetric appearance and lamella extension around the soma (defined as stage 1). After around 6 hours, the cell displays several minor neurites (defined as stage 2), one of which acquires axonal properties and extends rapidly to reach neighboring neurons (defined as stage 3). After reaching the destination, the axonal growth cone branches and forms synapses within these arbors (defined as stage 4 and 5) (Banker 2018; van Spronsen et al.

2013). Stage 2 and 3 have been extensively used to explore mechanisms underlying neuronal polarity, while stage 4 and 5 serves as a good *in vitro* model for studying presynaptic arborization (Banker 2018; van Spronsen et al. 2013).

A series of presynaptic regulators have been identified, many of which belongs to tumor necrosis factor superfamily (TNFSF). For example, a proliferation-inducing ligand (*APRIL*), member 13 in TNFSF, promotes axonal branching and growth in cultured hippocampal pyramidal cells (Osorio et al. 2014). The effect of APRIL is through binding its receptor B-cell maturation antigen (BCMA) and activating PI3K/Akt/GSK-3β signaling in the developing neurons. Mutating either the receptor or the signaling component abolishes the axonal growth-promoting effect of APRIL. Interestingly, no dendrite phenotype was observed, suggesting an axon-dedicated regulation of APRIL (Osorio et al. 2014). In addition, Fas ligand or CD95L, member 6 in TNFSF, exhibits similar function of stimulating axonal branching as APRIL (Zuliani et al. 2006). CD95L was best known as a trigger of apoptosis through binding to its receptor CD95 and activation of downstream effector caspases. Interestingly, Zuliani et al. found that CD95 is expressed in developing neurons without inducing apoptosis. The branching effect of CD95L is caspase-independent but via the adaptor -- Fas-associated protein with death domain (*FADD*) (Zuliani et al. 2006).

By contrast, some TNFSF members play a negative role in regulating presynaptic arborization. For example, astrocytic glial cells secret tumor necrosis factor-α (TNFα), member 2 in TNFSF, to inhibit axonal branching (Neumann et al. 2002). In addition, TNFSF member 11, receptor activator of nuclear factor kappa-B ligand (RANKL), was reported to inhibit both axonal and dendritic branching in cultured neurons (Gutierrez et al. 2013). Altogether, these

studies demonstrate TNFSF, especially their corresponding receptors expressed in developing neuron, play a critical role in presynaptic arborization.

Other transmembrane proteins, such as Down syndrome cell adhesion molecule (Dscam), have been reported to be involved in presynaptic growth in cultured neurons (Zhang et al. 2015). Intriguingly, different molecular regulators may interact with each other to sculpt a final readout. For example, Dscam, which promotes axonal growth and branching, is negatively regulated by RANKL (Bando et al. 2018). Thus, it will be interesting to examine whether Dscam and RANKL antagonize each other to exert their function in regulating presynaptic arborization. A comprehensive view of the interaction network would be a necessary step for an in-depth understanding of presynaptic regulation at molecular levels.

Presynaptic regulators identified in *Drosophila*

Despite the valuable insights obtained from cultured cells, whether the functions of these regulators are conserved *in vivo* are largely unknown. Quantitative analyses of presynaptic arborization *in vivo* require sparse labeling and stereotyped morphology of the neurons of interest. In this regard, the *Drosophila* da neurons and mammalian cortical inhibitory neurons stand out.

Drosophila Class IV dendritic arborization (C4da) neurons are nociceptors with their cell body and dendrites located in the larval body wall, while axons projecting to the ventral nerve cord (VNC), the *Drosophila*'s equivalent of vertebrate spinal cord (Figure 1.1A) (Grueber, Jan, and Jan 2002). The dendrites of C4da neurons tile the body wall and sense the noxious stimuli. The axons project to VNC and branch into stereotyped anterior, posterior, and contralateral projections at the axon terminals (Figure 1.1B). C4da axon terminals collectively form a ladder-

like structure (Figure 1.1B) and convey the nociceptive signals to VNC to mediate escape behaviors (Hwang et al. 2007; Kim et al. 2012; Xiang et al. 2010). Like other *Drosophila* neurons, C4da neurons are amenable to advanced genetic manipulation, such as mosaic analysis with a repressible cell marker (MARCM) (Lee and Luo 1999). Single-cell labeling techniques, such as MARCM, allows precise measurement of presynaptic arbors of signal neurons *in vivo*. The specific driver *pickpocket* (*ppk*)-Gal4 further facilitates genetic screens and reverse genetic tests (Grueber et al. 2003).

A number of molecular regulators that control presynaptic arborization in C4da neurons have been identified. An important signaling axis is the PHR-DLK-Dscam-Abl signaling pathway. PHR refers to the Pam/Highwire/RPM-1 (PHR) family of E3 ubiquitin ligases. They ubiquitinate and trigger the degradation of the dual leucine zipper kinase (DLK). The PHR-DLK signaling cascade was first discovered in *C. elegans* motor neurons and then *Drosophila* NMJ (Collins et al. 2006; Nakata et al. 2005) . In *Drosophila* larvae, loss of function of the *Drosophila* homolog of PHR, *hiw*, causes the overexpression of Wnd, the *Drosophila* homolog of DLK, and presynaptic overgrowth in NMJ. Consistently, loss of *Wnd* rescues the NMJ phenotype caused by *hiw* mutation (Collins et al. 2006), demonstrating that Wnd functions downstream of Hiw.

Our lab found that the function of Hiw-Wnd signaling pathway is conserved in *Drosophila* C4da neurons (Kim et al. 2013). In addition, we identified the critical role of Dscam in presynaptic arborization (Kim et al. 2013). Dscam is a single-pass membrane protein that is enriched in developing, but not mature, neurons (Schmucker et al. 2000; Li et al. 2020). Consistent with the expression profile, Dscam plays a role in regulating axonal growth in different neuronal types (Kim et al. 2013; Zhang et al. 2015; Bruce et al. 2017; Santos et al. 2018; Chen et al. 2006). Dscam is positively regulated by Wnd and mediates Wnd's growth-

promoting effects on presynaptic arbors (Kim et al. 2013). In addition, the Ye lab identified the cytoplasmic tyrosine kinase Abl as a key downstream effector of Dscam. Abl physically interacts with Dscam to mediate its axon-promoting effects (Sterne, Kim, and Ye 2015a). The function of Abl in presynaptic extension is also conserved in other types of neurons (Wills, Bateman, et al. 1999; Wills, Marr, et al. 1999; Wills et al. 2002; Hsouna, Kim, and VanBerkum 2003; Lee et al. 2004; Forsthoefel et al. 2005). Altogether, these studies suggest a conserved role of the PHR-DLK-Dscam-Abl signaling axis in instructing presynaptic arborization. Importantly, multiple Abl inhibitors have been approved by the US Food and Drug Administration (FDA) for treating chronic myeloid leukemia. Our lab found that treatment of these inhibitors is sufficiently to reverse the axonal overgrowth caused by Dscam overexpression in *Drosophila* larvae (Sterne, Kim, and Ye 2015a). This raises a novel possibility of treating neurological diseases with altered PHR-DLK-Dscam-Abl signaling axis.

Presynaptic regulators identified in mammals

Another *in vivo* experimental system for assaying presynaptic growth is the mammalian GABAergic neurons. G-aminobutyric acid (GABA) is the major inhibitory neurotransmitter in mammalian brains. It is produced and released by GABAergic neurons to modulate-- usually inhibit-- the target cell activity (Lim et al. 2018; Tremblay, Lee, and Rudy 2016; Huang and Paul 2019). Thus, GABAergic interneurons serve as the “brake” to maintain normal levels of brain excitation. Dysfunction of GABAergic neurons has been shown to cause a variety of neurological disorders (Ramamoorthi and Lin 2011; Ko, Choii, and Um 2015; Krueger-Burg, Papadopoulos, and Brose 2017).

GABAergic neurons are highly diverse in anatomical, electrophysiological and functional properties. Among the different types of GABAergic neurons, chandelier cells (ChCs), the unique axo-axonic cells, have long captured the interest of neuroscientists because of its stereotyped morphology and innervation manner (DeFelipe 1999). Each ChC has hundreds of vertically oriented axon terminals that resemble a candelabrum, where its name is derived from (Figure 1.2A-B) (Blazquez-Llorca et al. 2015). Each axon terminal selectively innervates one or two pyramidal neurons (PyNs) at the axon initial segment (AIS), thus termed axo-axonic neuron (Figure 1.2C) (Jones 1975; Szentagothai 1975a). Unlike other types of GABAergic neurons that are highly variable in morphology, the stereotyped projection and innervation of ChC axon terminals make these neurons an advantageous model for investigating presynaptic arborization (Fazzari et al. 2010; Tai et al. 2014). Especially, with the advance of techniques, such as in utero electroporation (IUE) and ChC-specific mouse Cre-ER lines, mosaic labeling and manipulating of single ChCs become increasingly feasible (Tai et al. 2014; Fazzari et al. 2010; Taniguchi, Lu, and Huang 2013). It is exciting to see that a growing number of molecular regulators are being uncovered in controlling GABAergic neuron presynaptic arborization in mammalian brains.

The NRG1-ERBB4 signaling cascade regulates ChC presynaptic growth (Fazzari et al. 2010). Neuregulin1 (Nrg1) is a cell adhesion molecule with ERBB4, a receptor tyrosine kinase, as its receptor. NRG1 and ErbB4 are known to be schizophrenia-susceptibility genes and have been considered to regulate neuronal wiring in excitatory cells. Fazzari and the colleagues found that ERBB4 is mainly localized in GABAergic neurons and localized at the presynaptic site. Via combining IUE and embryonic virus injection, the authors carried out both gain- and loss-of-function experiments demonstrating that NRG1-ErbB4 signaling cell-autonomously promotes ChC axon terminal growth and synapse formation (Fazzari et al. 2010). This study identified the

first molecular regulators of ChC presynaptic growth and corroborated the previous finding of impaired ChC axon terminal growth in schizophrenia patients (Lewis 2011; Konopaske et al. 2006). Deleting ERBB4 in ChCs causes schizophrenia-like phenotypes in mice, demonstrating the importance of NRG1-ERBB4-controlled ChC development in neurological disorders (Del Pino et al. 2013; Yang et al. 2019). In addition to the NRG1-ErbB4 signaling, Nkx2.1, DOCK7, Fgf13 and L1CAM have also been found to regulate the ChC presynaptic formation (Fazzari et al. 2010; Tai et al. 2014; Favuzzi et al. 2019; Tai et al. 2019). Importantly, besides arbor extension, ChCs have also been used to identify factors that regulates presynaptic orientation and synaptic formation, suggesting the broad applications of this experimental model (Fazzari et al. 2010; Tai et al. 2014; Favuzzi et al. 2019; Tai et al. 2019).

1.1.2 Molecular regulators of synapse formation.

The human brain contains around 86 billion neurons. Each makes more than one thousand synaptic connections with other neurons on average (Herculano-Houzel 2009). Altogether, these trillions of synapses sculpt how we respond to internal and external stimuli. Elucidating how a synapse is organized has long been an interest in the neuroscience field. Based on the effect of released neurotransmitter on postsynaptic neuronal firing, synapses are divided into excitatory or inhibitory. In mammalian brains, glutamatergic synapses are the major excitatory synapses, while GABAergic the major inhibitory synapses. Because of the dissertation interest and space limitation, I will mainly focus on molecular organizers of GABAergic synapses at the presynaptic site.

Neurexins are presynaptic cell surface molecules crucial for synapse formation (Missler, Sudhof, and Biederer 2012). They are localized in presynaptic terminals of inhibitory synapses

and interact with particular postsynaptic transmembrane proteins. For example, neurexins bind to neuroligin-2, the first discovered inhibitory synapse-specific transsynaptic organizer, via the extracellular acetylcholinesterase domain (Poulopoulos et al. 2009; Krueger et al. 2012). This physical interaction mediates the specific postsynaptic localization of Neuroligin-2, and is required for its function in clustering postsynaptic GABA receptors and scaffolding proteins (Krueger-Burg, Papadopoulos, and Brose 2017). In addition, neurexins have been shown to interact with other postsynaptic proteins, such as dystroglycan and neurexophilin 1(Waite, Brown, and Blake 2012; Reissner et al. 2014). Interestingly, these pre/post-synaptic interactions are modulated to form a complex regulatory network for synapse development. For example, calsyntenin-3 is a member of the cadherin superfamily of cell adhesion molecules. Proteolytic cleavage of calsyntenin-3 releases the ectodomain that prevents neurexin- neuroligin -2 interaction, thus causing the inhibitory effects on synaptogenesis (Pettem et al. 2013; Um et al. 2014).

IgSF9 and IgSF9b are two members of the immunoglobulin superfamily member 9 (IgSF9) transmembrane protein family. These two homophilic cell adhesion proteins are thought to be localized at both pre and post-synaptic sites (Ko, Choii, and Um 2015; Krueger-Burg, Papadopoulos, and Brose 2017). IgSF9 was originally reported to promote excitatory synapse development based on RNA interference (Shi et al. 2004). However, recent studies using IgSF9-deficient mice refuted this hypothesis in that hippocampal dendrite growth or branching remains intact in this mutant mice (Mishra et al. 2008). By contrast, IgSF9-deficient mice show reduced inhibitory synapse density and synaptic transmission, suggesting a critical role in inhibitory synaptogenesis. Interestingly, IgSF9 exerts such effects independent of its cytoplasmic domain as the knock-in mice expressing IgSF9 without intracellular domain causes no inhibitory defects

(Mishra et al. 2014). By contrast, IgSF9b is thought to specifically regulate inhibitory synapse formation between GABAergic interneurons via its binding to neuroligin-2 at the intracellular domain (Woo et al. 2013). Additionally, several other transmembrane proteins have been shown to function presynaptically. Protein tyrosine phosphatase receptor, PTPd, binds postsynaptic slit- and trk-like (Slitrk) family member 3 (Slitrk3) to promote inhibitory synapse development and function in hippocampal CA1 neurons (Takahashi et al. 2012). Deletion of ERBB4, the receptor of neuregulin 1, cell autonomously impairs the presynaptic bouton growth in ChCs and synaptic transmission in inhibitory neurons (Fazzari et al. 2010).

Besides the transmembrane proteins, a variety of cytoplasmic synapse regulators have been identified, mainly in the GABAergic Dorsal D-type motor neurons (hereafter termed DD neurons) of *C. elegans*. During the maturation of *C. elegans* larvae, DD neurons forms new synapses with dorsal body wall muscles that are critical for worm locomotion. Interestingly, the synapse formation is not involved with overt changes in presynaptic arborization, thus providing an ideal model to study the molecular mechanisms underlying GABAergic synapse development (Kurup and Jin 2016).

Transcript levels of DLK, a regulator of presynaptic arborization as described in previous sections, is boosted to facilitate synapse formation during the maturation of DD neurons (Kurup et al. 2015; Grun et al. 2014). The effect of DLK is mediated by increasing the dynamic microtubule amount at the presynaptic sites by acting on microtubule catastrophe factors, such as Kinesin-13 and Spastin (Kurup et al. 2015; Nakata et al. 2005; Roll-Mecak and McNally 2010). The increased dynamic microtubule facilitates synaptic vesicle transport, which is mediated by UNC-116, the *C. elegans* homolog of vertebrate motor protein kinesin-1. Gain of function of UNC-116 is sufficient to rescue the impaired synapse formation in DD neurons caused by the

mutations including DLK (Kurup et al. 2015). In addition, cyclin-dependent kinase-5 (CDK-5) has been shown to promote new synapse formation in DD neurons of mature *C. elegans* by elevating the activity of UNC-104/Kinesin3 (Park et al. 2011). After synapse formation, TTBK-3, a member of the Casein-kinase (CK1) superfamily in *C. elegans*, inhibits the stabilization of these nascent synapses on the dorsal neurite (Kurup et al. 2017).

However, compared with the long list of postsynaptic organizers, the presynaptic organizers are relatively less understood. One technical challenge is that presynaptic active zones are more insoluble by detergents than postsynaptic density, and are thus difficult to purify (Sudhof 2012). Recently, spatially restricted proximity labeling has enabled mass spectrometry-based quantitative proteomics in various sub-neuronal structures, such as synaptic cleft, post-synaptic density, axon initial segment and neuronal surface (Loh et al. 2016; Uezu et al. 2016; Hamdan et al. 2019; Li et al. 2020). Such technique, when applied in presynaptic active zones, is expected to significantly advance the field.

1.2 Isoform diversity contributes to the signaling complexity of presynaptic development

Human has ~20,000 protein coding genes, but ~200,000 protein products. This is caused by alternative splicing. Alternative splicing is ubiquitous and evolutionarily conserved regulatory mechanism that enables eukaryotic cells to generate vast protein diversity from limited gene number. Through alternative splicing, a single pre-mature RNA can generate different mRNAs with distinct coding regions by mutually exclusive exons, exon skipping, alternative splicing site or intron retention. This distinct combination of coding sequences generates different protein isoforms with diverse biochemical and physiological properties. This proteome complexity

exponentially expands the signaling complexity in cells, especially when we consider it at the subcellular levels.

Alternative splicing may change the subcellular localization of targeted isoforms by introducing specific coding sequences that contain signals for subcellular localization, post-translational modification or protein interaction (Kelemen et al. 2013). Protein isoforms may exert distinct functions in different subcellular compartments. For example, determined by inclusion or exclusion of an alternative exon, the LPIN1 gene generates a nuclear isoform that acts as a transcription factor and a cytoplasmic variant with phosphatidate phosphatase activity (Han and Carman 2010; Zhang et al. 2012). Similar scenario is observed in other genes, such as that of Rbfox1, with a nuclear variant (excluding exon 19) that regulates RNA splicing and a cytoplasmic variant (including exon 19) that stabilizes mRNAs (Lee et al. 2016). However, a caution needs to be taken in that most of these studies are carried out *in vitro* with cDNA constructs that lack endogenous cis and trans-regulation. Whether these findings apply *in vivo* awaits further studies (Kelemen et al. 2013).

In *Drosophila*, alternative splicing of Dscam, a molecular regulator of presynaptic growth and neurite self-avoidance, produces two isoforms with mutually exclusive exons that encode distinct transmembrane and juxtamembrane region, called Dscam[TM1] and Dscam[TM2], respectively (Schmucker et al. 2000). Previous studies suggest that Dscam[TM1] and Dscam[TM2] may differentially regulate presynaptic growth in *Drosophila*. For example, overexpression of Dscam[TM2] in *Drosophila* mushroom body, a CNS neural ensemble involved in *Drosophila* learning and memory, cause its ubiquitous presence in both axons and dendrites. By contrast, Dscam[TM1] is largely restrained in somatodendrites (Zhan et al. 2004; Wang et al. 2004b). These data suggest that Dscam[TM2] and [TM1] may have distinct

subcellular localization. Consistently, Dscam[TM2] better rescues the branching defects in *Drosophila* mushroom body caused by Dscam mutant than Dscam[TM1] (Zhan et al. 2004). However, in *Drosophila* C4da neurons, which are nociceptors, overexpression of Dscam[TM1] results in a expression profile reminiscent that of [TM2] (Soba et al. 2007). And both Dscam[TM1] and [TM2] have been reported to cause the same defects in axonal segregation when overexpressed in mushroom body (Zhan et al. 2004). Are these discrepancies caused by neuronal specificity or artificial effects of overexpression? Answering this question requires the interrogation the endogenous localization and function of Dscam isoforms at the endogenous and subcellular levels *in vivo*, which is not feasible with current techniques.

In the first part of my dissertation, I developed a novel genetic method, termed *isoTarget*, which enables the investigation of isoform-specific function, endogenous localization and signaling at cell type-specific levels *in vivo*. By applying *isoTarget* in Dscam[TM1] and [TM2], I found that presynaptic growth is specifically regulated by Dscam[TM2] by its unique presence there. In addition, I uncovered a Wnd-Dscam[TM2]-Dock signaling cascade that specifically occurs at the presynaptic site. Interestingly, I found that this compartmentalized signaling is not caused by the unique biochemical properties of Dscam[TM2] but by the presynaptic enrichment of Wnd and Dock. Thus, *isoTarget* is expected to be a useful tool to dissect the signaling complexity caused by isoform diversity at the subcellular levels, including that of presynaptic arbors.

1.3 Dysregulated expression levels of presynaptic regulators in neurodevelopmental disorders.

GABAergic neurons are the major inhibitory neurons in the mammalian brain (Lim et al. 2018; Tremblay, Lee, and Rudy 2016). Dysregulated GABAergic system causes a variety of neurodevelopmental disorders (Ramamoorthi and Lin 2011). For example, impaired forebrain GABAergic neurons cause autism-like symptoms, such as repetitive behavior (Chao et al. 2010). While GABAergic hyper-functioning causes Down syndrome symptoms, such as impaired spatial leaning (Fernandez et al. 2007; Braudeau, Delatour, et al. 2011; Colas et al. 2013a; Martinez-Cue et al. 2013). To date, a growing number of molecular regulators have been identified to control presynaptic development in GABAergic neurons. Intriguingly, copy number variations of these genes are commonly found in a variety of neurological diseases (Ko, Choii, and Um 2015), suggesting that dysregulated expression of these genes may cause the disease pathology. However, whether or not this is true remains largely unknown.

Down syndrome is caused by an extra copy of chromosome 21 or a segment of it, which results in the triplication of up to about 200 genes in human patients. It is the most common aneuploid disorder that causes intellectual disability (Gardiner et al. 2010). The most widely used mouse model of Down syndrome is Ts65Dn, which contains a trisomic chromosomal region that is homologous to about half of human chromosome 21 (Reeves et al. 1995). Ts65Dn mice exhibit a variety of behavioral deficits reminiscent that of human patients (Reeves et al. 1995). A milestone in DS pathogenesis is the discovery that Ts65Dn behavioral deficits can be blocked by GABA receptor antagonist (Fernandez et al. 2007; Braudeau, Delatour, et al. 2011; Colas et al. 2013a; Martinez-Cue et al. 2013), suggesting that activated GABAergic signaling is the pathological driver. Uncovering the molecular mechanisms of GABAergic hyperfunctioning is the key for pharmaceutical treatment of Down syndrome.

One gene that is triplicated in DS and involved in neurodevelopment is *Dyrk1A*, the human orthologue of the *Drosophila minibrain* gene. *Dyrk1A* encodes a serine-threonine kinase that is highly expressed in neuroblast during embryonic neurogenesis (Okui et al. 1999) (Hammerle, Elizalde, and Tejedor 2008; Hammerle et al. 2002). Loss of *Dyrk1A* has been shown to cause microcephaly in humans and reduced brain size in mice (Moller et al. 2008; Fotaki et al. 2002). Transgenic overexpression of *Dyrk1A* causes impaired motor behavior, spatial learning and cognitive function, reminiscent of the symptoms in DS patients (Altafaj et al. 2001; Martinez de Lagran et al. 2004). Indeed, Normalizing *Dyrk1A* dosage in Ts65Dn DS mouse model has been shown to rescue the GABAergic synapse overgrowth and cognitive defects (Garcia-Cerro et al. 2014) , suggesting a direct contribution of *Dyrk1A* triplication to DS pathogenesis. Interestingly, green tea flavonol epigallocatechin-gallate (EGCG), an inhibitor of Dyrk1A, rescues the cognitive deficits in both Ts65Dn mice and DS patients (De la Torre et al. 2014), raising Dyrk1A as a promising therapeutic target for cognitive treatment in DS. Besides *Dyrk1A*, the extra copy of amyloid precursor protein gene, *App*, causes the degeneration of basal forebrain cholinergic neurons in Ts65Dn and Ts1Cje mouse models of DS (Salehi et al. 2006). Triplication of *Kcnj6*, a gene that encodes the $GABA_B$ receptor-coupled G protein-coupled inward rectifying potassium channel subunit 2 (GIRK2), has been shown to promote the infantile spasms induced by $GABA_B$ receptor agonists in Ts65Dn mice(Joshi et al. 2016).

Chakrabarti and the colleagues found that triplication of *Olig1* and *Olig2* cause the overproliferation of parvalbumin- and somatostatin-expressing inhibitory neurons in Ts65Dn neocortex and hippocampus (Chakrabarti et al. 2010). These findings provide the first celluar basis for GABAergic overinhibition in the DS mouse model (Chakrabarti et al. 2010; Contestabile, Magara, and Cancedda 2017; Haydar and Reeves 2012). Meanwhile, several lines

of evidence suggest that heterogeneous etiology may exist. For example, the sizes of synaptic boutons and inhibitory synapses are enlarged in the neocortex of Ts65Dn mice, suggesting a post-mitotic GABAergic synaptic dysfunctions in the neocortex (Belichenko et al. 2009; Kurt et al. 2000; Belichenko et al. 2004). However, which subtype of GABAergic neurons are affected and the triplication of which gene causes the pathogenic defects remains unknown.

Down syndrome cell adhesion molecule (Dscam) is an evolutionarily conserved type I transmembrane protein (Yamakawa et al. 1998). In human, *Dscam* gene is localized in the Down syndrome critical region on chromosome 21 (hCh21) (Yamakawa et al. 1998). Altered Dscam expression levels have been reported in multiple brain disorders, including Down syndrome, autism spectrum disorders, intractable epilepsy and bipolar disorder (Saito et al. 2000; O'Roak et al. 2014; Krumm et al. 2015; Turner et al. 2016; Shen et al. 2011; Amano et al. 2008), suggesting a potential pathogenic role. Indeed, we show that Dscam promote neuronal growth in a dosage-dependent manner (Kim et al. 2013; Cvetkovska et al. 2013; Lowe, Hodge, and Usowicz 2018). In addition, Dscam is enriched in developing neurons, when dendrite/axon are differentiating (Li et al. 2020; Mayer et al. 2018; Mi et al. 2018). These findings suggest that dysregulated Dscam levels might contribute to the post-mitotic GABAergic defects in Down syndrome.

The second part of my dissertation focus on the role of *Dscam* gene triplication in GABAergic dysfunctions in Down syndrome. By using Ts65Dn as the mouse model of Down syndrome, we found that the presynaptic arborization and synaptogenesis are boosted in ChCs and basket cells, two major types of GABAergic neurons. Genetic normalization of Dscam expression rescues the excessive GABAergic innervation and synaptic transmission. Conversely, Loss of *Dscam* impairs the presynaptic development and functioning in inhibitory neurons. These findings identify the genetic basis of post-mitotic GABAergic defects in Down syndrome

and implicate dysregulated Dscam levels as a common pathogenic driver in related neurological disorders.

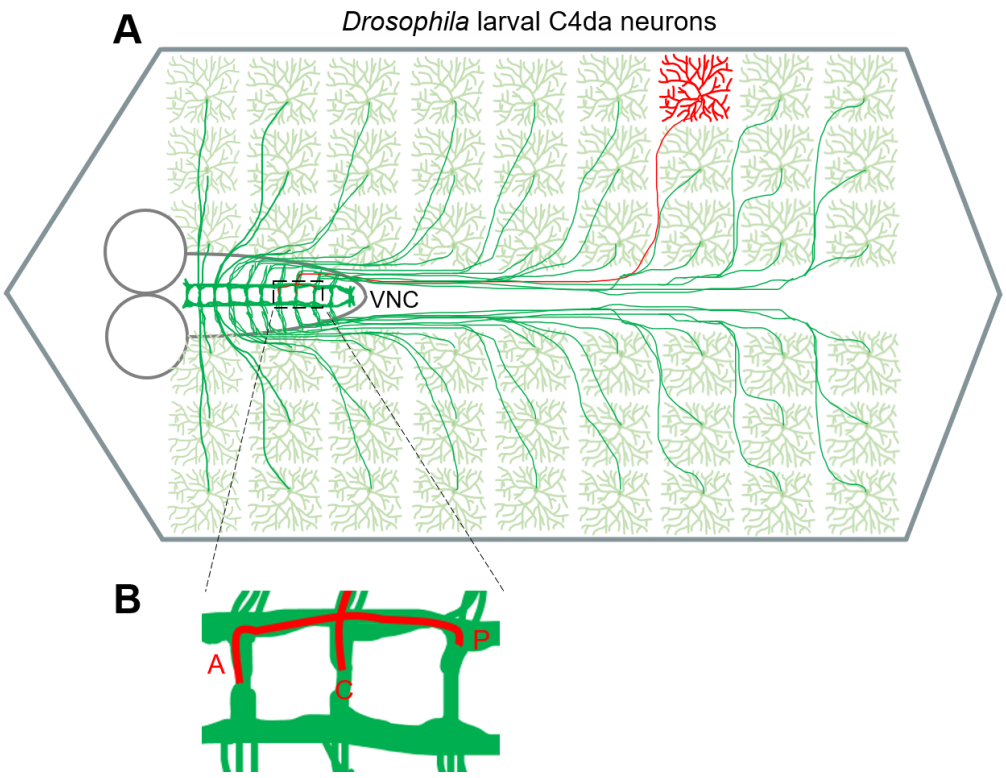

Figure 1.1. Scheme of *Drosophila* larval C4da neurons.
(**A**) Schematic image of *Drosophila* larval C4da neurons. Each hemisegment is tiled by the dendrites of three C4 da neurons (light green). For each C4da neuron (red), the dendrites and cell body are on the body wall while the axons are sent to the VNC of larval brain.
(**B**) Magnified image of C4da neuron axons. The presynaptic arbor of a single C4da neuron shows anterior (A), posterior (P) and contralateral (C) projects (Red). The axons of C4da neuron together form a ladder- like structure (Green).

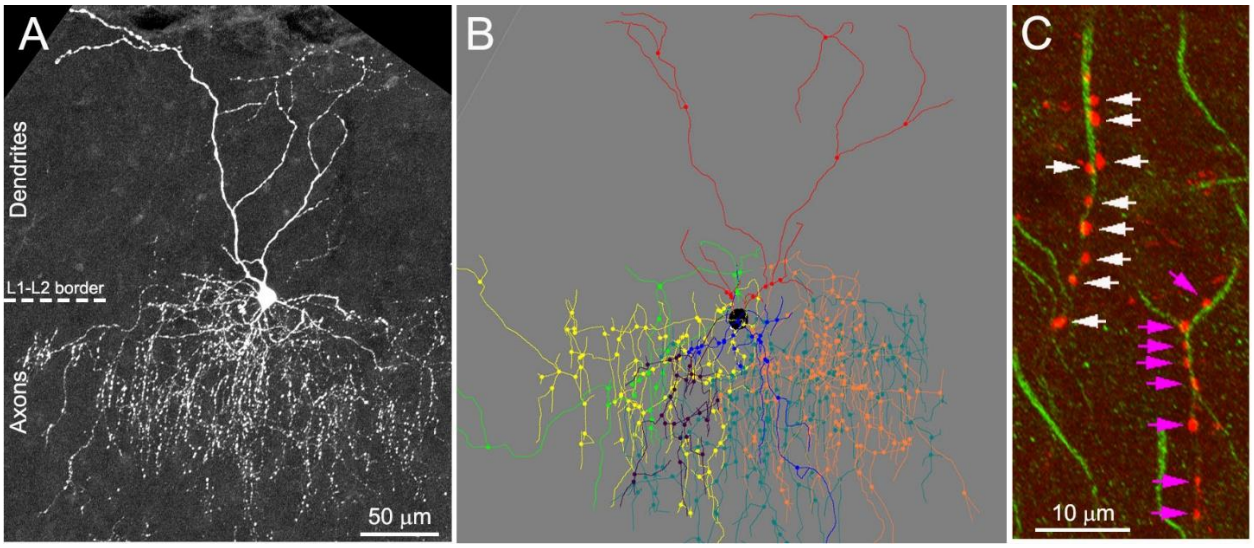

Figure 1.2. Representative images of single ChCs and ChC-PyN synases.
(**A**) A single ChC labeled by tdTomato through Nkx2.1CreERT2. The soma of this ChC is located at the border of layers I and II in neocortex.
(**B**) 3-D tracing of a single ChC. The soma of this ChC is located at the L1-L2 border in somatosensory cortex. The dendrites are marked in red, and the axons—including terminals—are labeled in various colors, each representing a separate arbor.
(**C**) The cartridges of ChC axon terminals. Red: boutons on ChC axon terminals labeled by tdTomato; Green: pyramidal cell AIS labeled by anti-phospho-IκBα. White and pink arrows point to the boutons on two different cartridges.

Chapter 2

isoTarget: a Genetic Method for Analyzing the Functional Diversity of Splicing Isoforms *in vivo*

This chapter is modified after a research article that is under revision for publication with authors listed as Hao Liu, Sarah Pizzano, Ruonan Li, Wenquan Zhao, Macy W. Veling, Yujia Hu, Limin Yang, and Bing Ye.

2.1 Abstract

Protein isoforms generated by alternative splicing contribute to proteome diversity. Due to the lack of effective techniques, isoform-specific functions, expression, localization, and signaling mechanisms of endogenous proteins *in vivo* are unknown for most genes. Here we report a genetic method, termed *isoTarget*, for blocking the expression of a targeted isoform without affecting the other isoforms and for conditional tagging the targeted isoform for multi-level analyses in select cells. Applying *isoTarget* to two mutually exclusive isoforms of *Drosophila* Dscam, Dscam[TM1] and [TM2], we found that endogenous Dscam[TM1] is localized in dendrites while Dscam[TM2] is in both dendrites and axons. We demonstrate that the difference in subcellular localization between Dscam[TM1] and [TM2], rather than any difference in biochemical properties, leads to the two isoforms' differential contributions to dendrite and axon development. Moreover, with *isoTarget*, we discovered that the subcellular

enrichment of functional partners results in a DLK/Wallenda-Dscam[TM2]-Dock signaling cascade specifically in axons. *isoTarget* is an effective technique for studying how alternative splicing enhances proteome complexity.

2.2 Introduction

Alternative splicing is a fundamental biological process that expands proteome diversity in eukaryotes. Genome-wide transcriptome analyses have shown that 90%-95% of human genes encode two or more isoforms (Baralle and Giudice 2017). The percentage of multi-exonic genes that undergo alternative splicing is estimated to be 63% in mouse, 45% in *Drosophila*, and 25% in *C. elegans* (Lee and Rio 2015). Alternative splicing is regulated by the coordination of RNA-binding proteins, RNA polymerase II, and epigenetic modifications of DNA (Baralle and Giudice 2017). Perturbations of RNA splicing cause neurodevelopmental, cardiovascular, and other diseases (Baralle and Giudice 2017; Scotti and Swanson 2016). Despite these important findings, how distinct protein isoforms resulted from alternative splicing differ in their functions and regulations are poorly understood. In fact, the cellular functions, endogenous expression and localization, and signaling cascades of individual splicing isoforms are only known for a very small number of genes (Baralle and Giudice 2017).

Protein isoforms encoded by alternative exons often differ in their structures and biochemical properties, which lead to distinct functions of the isoforms (Kelemen et al. 2013). In addition, different types of cells may express different splicing variants (Baralle and Giudice 2017), which further diversifies the biological functions of different isoforms. Intriguingly, different protein isoforms of some genes are localized to distinct subcellular compartments within the same cell (Kelemen et al. 2013; Baralle and Giudice 2017; Lee et al. 2016; Yap and Makeyev 2016; Lerch et al. 2012). Compared to our understanding of how biochemical and expressional differences contribute to distinct functions of splicing isoforms, much less is known about whether and how isoform-specific subcellular localization contributes to distinct cellular

functions. This is a challenging problem because solving it requires manipulating a specific isoform at its endogenous locus—without affecting other isoforms—in a cell-specific fashion.

Transgene-mediated overexpression of splicing variants of interest is widely used for studying isoform-specific functions and subcellular localization in specific cells. However, it is well documented that overexpressed proteins often do not mimic the endogenous proteins in their spatiotemporal expression, localization, and functions (Kelemen et al. 2013; Baralle and Giudice 2017; Prelich 2012; Moriya 2015).

Here, we report a genetic method, termed *isoTarget*, for studying isoform-specific function, localization, and signaling of endogenous splicing isoforms of interest. This method allows to knock out a select isoform for functional studies and to tag conditionally the endogenous proteins for multi-disciplinary analyses in specific cells without affecting other isoforms. To achieve these, we created a translational stop sequence, used it to generate a cleavable cassette that contains an epitope tag for conditional tagging, and inserted the cassette into the exon encoding the isoform of interest. As a proof-of-concept, we applied *isoTarget* to study two mutually exclusive isoforms of *Drosophila* Down syndrome cell adhesion molecule (Dscam), Dscam[TM1] and [TM2] (Schmucker et al. 2000; Wang et al. 2004a; Zhan et al. 2004). We report isoform-specific functions for Dscam[TM1] and [TM2] resulting from the distinct endogenous subcellular localization patterns of these two isoforms. We further describe a compartment-specific signaling pathway in the axon terminals, which involves Dscam[TM2], but not [TM1], as a result of the differential localization of the two isoforms and their functional partners. These findings illustrate the versatility of *isoTarget* in isoform studies and its effectiveness in uncovering mechanisms governing the expansion of proteome diversity by alternative splicing *in vivo*. In addition, they establish the causality between the subcellular

localization and cellular function of Dscam splicing isoforms, demonstrating the critical role of subcellular localization in expanding the functional diversity of splicing isoforms.

2.3 Results

The design of *isoTarget*

The transcriptional stop cassettes commonly used for conditional knockouts or knockins (Lakso et al. 1992) do not specifically disrupt the expression a select splicing isoform and are hence not applicable for isoform-specific studies. This is because RNA splicing occurs after transcription and, as a consequence, transcriptional stop cassettes disrupts the expression of all isoforms downstream of the targeted isoform (Figure 2.1A). To meet this challenge, we created a *translational stop* (*tlstop*) sequence by introducing multiple stop codons (TAA, TAG or TGA) into the DNA sequence encoding a non-catalytic region of β-Galactosidase (β-Gal) (Figures 2.1A, 2.2A). If the *tlstop* is present in an isoform-specific exon, it would lead to isoform-specific truncation during mRNA translation (Figure 2.1A).

To achieve cell-type-specific labeling of targeted isoforms, the *tlstop* sequence is flanked by two R recombinase recognition sites (RSRT) followed by an epitope tag (Chen et al. 2014; Nern et al. 2011). When R recombinase is expressed to remove *tlstop*, the epitope tag is inserted in-frame into the targeted isoform, allowing the detection and biochemical analyses of endogenous proteins in cells of interest (Figure 2.1B). We refer to the RSRT-*tlstop*-RSRT as "iso-KO cassette" (for "*isoTarget* knockout cassette"), as its insertion into an isoform-specific exon is expected to create a loss-of-function mutant of this particular isoform. In *Drosophila*, the *iso-KO* alleles can be used in combination with the mosaic analysis with a repressible cell marker (MARCM) (Lee and Luo 1999) to study isoform-specific function in targeted single neurons (Figure 2.1B). We refer to the RSRT-epitope resulted from the excision of the *tlstop* sequence as "iso-Tagging cassette". As we show below, the iso-Tagging approach allows the

investigation of upstream and downstream signaling mechanisms that involve targeted isoform at the organismal, cell-type-specific, or subcellular levels (Figure 2.1B).

The validation of *isoTarget* and mitigation of off-target effects of translational-stop cassettes

To fulfill the designed applications, the *isoTarget* technique should meet the following requirements. First, the iso-KO cassette must abolish the function of the targeted isoform. Second, the iso-KO or iso-Tagging cassette in one isoform should not impair the expression of other isoforms. Third, iso-Tagging—resulted from the excision of the iso-KO cassette—should restore the isoform functions that are disrupted by the iso-KO cassette. We determined whether *isoTarget* met these prerequisites by testing on the *Drosophila Dscam* gene.

In *Drosophila*, exon 17.1 and 17.2 of *Dscam* gene encode two different transmembrane/juxtamembrane domains (Schmucker et al. 2000). Alternative splicing of these two mutually exclusive exons produces two isoforms called Dscam[TM1] and Dscam[TM2] (Figure 2.2B). We inserted the iso-KO cassette into the juxtamembrane domain in exon 17.1 (TM1) and 17.2 (TM2) (Figures 2.2B-C). In homozygous *Dscam[TM2]* iso-KO (*Dscam[TM2]*$^{iso\text{-}KO}$) larvae, the axon terminal growth was dramatically impaired in the class IV dendritic arborization (C4da) neurons (Figures 2.3A-B, and H), a widely used model for studying dendrite and axon development (Grueber and Jan 2004; Grueber et al. 2007; Jan and Jan 2010; Ye et al. 2007). This is consistent with previous reports that *Dscam* is required for axon terminal growth in C4da neurons (Kim et al. 2013), and suggests that iso-KO cassette abolishes *Dscam[TM2]* functions. The impaired growth of axon terminals was completely rescued in homozygous global Dscam[TM2] iso-Tagging (*Dscam[TM2]*$^{iso\text{-}Tagging}$) larvae resulted from the excision of the iso-

KO cassette (Figures 2.2C, 2.4A-B), suggesting that tagging endogenous Dscam[TM2] with the epitope tag (V5) does not disrupt the function of the isoform.

Next, we determined whether *isoTarget* of one isoform affected the expression of another isoform by using quantitative real-time PCR and immunohistochemistry on *isoTarget* samples. *Dscam[TM1]* mRNA levels were not affected in the brains of homozygous *Dscam[TM2]*$^{iso\text{-}KO}$ or *Dscam[TM2]*$^{iso\text{-}Tagging}$ 3rd-instar larvae (Figure 2.4C). Unexpectedly, the [TM1] iso-KO cassette abolished *Dscam[TM2]* mRNA and protein expression, creating a *Dscam[TM1/2]*$^{iso\text{-}KO}$ mutant (Figures 2.5A-C). By contrast, the expression of *Dscam[TM2]* mRNA was not affected by *Dscam[TM1]* iso-Tagging cassette (Figure 2.5A). These results suggest that inserting a long piece of DNA in TM1-encoding exon disrupts the splicing of TM2-encoding exon of *Dscam* pre-mRNA (Figure 2.5F), possibly by overly extending the distance between exon 16 and the TM2-encoding exon (Anastassiou, Liu, and Varadan 2006). To test this possibility, we reduced the size of the iso-KO cassette from 561 bp to 285 bp by cutting a 276 bp-fragment from the *tlstop* sequence. Strikingly, insertion of the short iso-KO cassette in [TM1] did not impair Dscam[TM2] expression, including both mRNA and protein expression (Figures 2.5A and 2.5D-E). Through these studies, we discovered that the impact of an *isoTarget* cassette on off-target isoforms can be mitigated by reducing the cassette length and found a new translational stop sequence for achieving this.

Taken together, these results validate the use of *isoTarget* for studying endogenous Dscam[TM1] and [TM2] isoforms.

Uncovering the functions of Dscam isoforms in axon terminals with *isoTarget*

We previously demonstrated that in larval PNS neurons Dscam instructs the presynaptic terminal growth, which is a function that is distinct from Dscam's role in neurite self-avoidance (Kim et al. 2013). However, whether both Dscam[TM1] and [TM2] contribute to this process is unknown. With *iso-KO* larvae, we found that knocking out the [TM2] isoform impaired axon terminal growth in larval C4da neurons (Figures 2.3A-B and H). By contrast, the axonal development remained intact in *Dscam[TM1]*$^{iso\text{-}KO}$ larvae (Figures 2.3C and H). Next, we combined *isoTarget* with the MARCM technique to determine whether the Dscam isoforms functioned cell-autonomously to regulate C4da axon terminal growth. Single C4da neurons that were homozygous for *Dscam[TM1]*$^{iso\text{-}KO}$ had normal axon terminal growth (Figures 2.3D-E and I). By contrast, loss of *Dscam[TM2]* in C4da neurons significantly impaired axon terminal growth to the same levels as loss of *Dscam* (Figures 2.3F-G and I).

Similar to C4da neurons, while C3da neurons in homozygous *Dscam[TM1]*$^{iso\text{-}KO}$ larvae showed normal growth of axon terminals, those in homozygous *Dscam[TM2]*$^{iso\text{-}KO}$ displayed dramatically reduced axon terminals growth, as evident in the gaps in longitudinal axon tracts (Figures 2.3J-L). The disruption in longitudinal axon tracts was also observed in *Dscam[TM1/2]*^{KO} larvae (Figure 2.3M).

These results suggest that *Dscam[TM2]*, but not *Dscam[TM1]*, regulates the growth of axon terminals.

Uncovering the functions of Dscam isoforms in dendrites with *isoTarget*

Dscam has been shown to mediate dendritic self-avoidance without affecting dendritic growth in the PNS neurons of *Drosophila* larvae (Matthews et al. 2007; Soba et al. 2007; Hughes et al. 2007). Again, it is unknown whether both Dscam[TM1] and [TM2] isoforms are

responsible for this process. We applied *isoTarget* to answer this question. As expected from previous studies, homozygous *Dscam[TM1/2]*$^{iso\text{-}KO}$ mutant larvae, which lack both [TM1] and [TM2] functions, exhibited increased dendritic crossing in both C3da mechanosensors (Figures 2.6A-B and E) and C4da nociceptors (Figures 2.7A-B and E), indicating defective avoidance among dendrites of the same neuron. Different from what we observed in axons, neither *Dscam[TM1]*$^{iso\text{-}KO}$ nor *Dscam[TM2]*$^{iso\text{-}KO}$ caused any defect in dendritic self-avoidance in these neurons (Figures 2.6C-D and E, 2.7C-D and E).

We further combined MARCM with *isoTarget* to study cell-autonomous functions of targeted isoforms in single cells. As previously shown (Matthews et al. 2007; Soba et al. 2007; Hughes et al. 2007), single C4da neurons that were homozygous of *Dscam*^{18}, which abolishes both [TM1] and [TM2] isoforms, showed significant self-avoidance defect (Figures 2.6G and J). By contrast, loss of either *Dscam[TM1]* or *[TM2]* in single C4da neurons did not cause any defect in dendritic self-avoidance (Figures 2.6H-I and J).

These results suggest that *Dscam[TM1]* and *[TM2]* function redundantly in dendritic self-avoidance. Thus, these two isoforms function differently in dendrite and axon development.

Using *isoTarget* to identify the subcellular localizations of endogenous protein isoforms

Previous studies have shown that in CNS neurons transgenic Dscam[TM1] is restrained in somatodendritic compartments while [TM2] is in both dendrites and axons (Wang et al. 2004a; Yang, Bai, and Lee 2008; Zhan et al. 2004). However, transgenic Dscam[TM1] and [TM2] were both found to be ubiquitously present in PNS neurons (Soba et al. 2007) (Figures 6B and D and data not shown). Does this discrepancy indicate that the subcellular localization of Dscam isoforms varies in different neuronal types? To answer this question, we applied iso-

Tagging to examine the subcellular localizations of *endogenous* Dscam isoforms in both PNS and CNS neurons. We found that in PNS neurons both endogenous Dscam[TM1] and [TM2] were localized in the dendrites (Figures 2.8A-C). Interestingly, different from what we observed with *Dscam* transgenes, only endogenous Dscam[TM2] was localized in the presynaptic terminals of PNS neurons (Figures 2.8D and E). Similar isoform-specific localization patterns were observed in CNS neurons. By iso-Tagging in mushroom body (MB) neurons in the 3rd-instar larva, we observed both endogenous Dscam[TM1] and [TM2] in MB calyx (Figures 2.8F-H), which is a cluster of dendritic branches, but only [TM2] in the core fibers of axonal peduncles (Figures 2.8I-K). The finding that only [TM2] is localized in axons was further supported by the observation of Dscam proteins in axonal shafts that connect the PNS and CNS. In iso-Tagging larvae, despite a substantial amount of Dscam[TM1] signals in the neuropil region of the ventral nerve cord (VNC), no [TM1] signal was observed in axonal shafts (Figures 2.9A-B). By contrast, Dscam[TM2] puncta were abundant in axonal shafts in global *Dscam[TM2]$^{iso\text{-}Tagging}$* larvae (Figure 2.9C). Taken together, we found that in PNS and CNS, both endogenous Dscam[TM1] and [TM2] isoforms are present in dendrites, while only [TM2] is in axons.

Notably, endogenous Dscam expression seemed to be enriched in developing neurons, but not in mature ones. While both endogenous Dscam[TM1] and [TM2] were observed in PNS neurons at the early 2nd-instar stage, no signal was detectable in the 3rd instar stage (data not shown). In larval MB, endogenous Dscam[TM2] was detected only in the core fiber, which is the axonal projections of nascent developing neurons. These observations are consistent with previous immunostaining results with an anti-Dscam antibody (Zhan et al. 2004). The

discrepancies of spatiotemporal expression pattern between transgenes and endogenous Dscam isoforms underscore the importance of studying protein isoforms at the physiological level.

Dendrite-specific localization restrains endogenous Dscam[TM1] from functioning in axons

The studies above show that endogenous Dscam[TM1] is required for dendritic, but not axonal, development. Although this could be a result of the compartmentalized localization of Dscam[TM1] in dendrites, trans-compartmental communication has been shown for many membrane proteins . It is thus essential to determine whether or not the dendrite-specific localization of Dscam[TM1], instead of its biochemical properties, restrains it from functioning in axons. This important issue has not been addressed, despite previous insightful studies on the differences between Dscam[TM1] and [TM2].

We determined whether forced localization of Dscam[TM1] in axon terminals was sufficient to rescue the axon phenotype caused by *Dscam[TM2]*$^{iso\text{-}KO}$. Overexpression of a *Dscam[TM1]* transgene in C4da neurons led to a modest level of Dscam[TM1] in axon terminals and significantly mitigated axonal growth defects caused by *Dscam[TM2]*$^{iso\text{-}KO}$ (Figures 2.10A-B, and F). As expected, two different [TM2] transgenes (#1 and #2) both caused higher levels of [TM2] in axon terminals and stronger rescue than the [TM1] transgene (Figures 2.10C, E-G). Strikingly, when we used 2 copies of the C4da-specific driver *ppk*-Gal4 to increase the axonal level of Dscam[TM1] to that expressed by *Dscam[TM2]* transgenes, the rescue effects were comparable (Figures 2.10C, D, F, and G). By quantitatively assessing transgenic Dscam::GFP levels in C4da axon terminals (Figure 2.10G), we found a linear correlation (R^2=0.969) between presynaptic Dscam isoform levels and their rescue effects (Figure 2.10H). These results suggest that when localized in the same subcellular compartment, Dscam[TM1] function equally as

Dscam[TM2] in promoting axonal growth. Thus, the dendritic function of endogenous Dscam[TM1] is a result of its compartmentalized localization.

Axonally enriched Dscam[TM2]-Dock signaling is essential for the axonal function of Dscam[TM2]

While the study above demonstrates that the dendrite-specific localization of Dscam[TM1] prevents it from functioning in axon development, it remains unknown whether Dscam[TM1] and [TM2] exhibit any biochemical difference that might also explain the difference in their cellular functions. To test this possibility, we took advantage of *isoTarget* to compare Dscam[TM1] and [TM2] for their interactions with functional partners. Among the molecules known to bind to the intracellular domain of Dscam and mediate its signaling (Schmucker et al. 2000; Liu et al. 2009; Purohit et al. 2012; Kamiyama et al. 2015; Sterne, Kim, and Ye 2015b), we found that Dock, an SH2/SH3 adapter protein that is preferentially localized in axons (Hing et al. 1999; Desai et al. 1999; Fan et al. 2003), preferentially associated with Dscam[TM2] in *Drosophila* larval brains (Figure 2.11A). We further confirmed this finding with transgenic flies that overexpress Dscam[TM1]::GFP or [TM2]::GFP through their endogenous promoters (Wang et al. 2004a). Immunoprecipitation was performed using an anti-GFP antibody. Endogenous Dock preferentially co-precipitated with [TM2]::GFP from brain lysates of 3rd instar larvae (Figure 2.11B). Consistent with this notion, we found that Dock is required for Dscam[TM2] to promote axon terminal growth. While overexpressing [TM2] significantly promoted axon terminal growth in C4da neurons, its effect was completely eliminated by loss of *dock* (Figures 2.11C-G). Interestingly, we found that the [TM2]-Dock signaling is compartment-dependent. Dock bound to both isoforms with equal affinity in cultured Schneider 2 (S2) cells,

which do not have dendrite-axon compartmentalization (Figure 2.11H). This result is consistent with the previous finding that the Dock-binding sites, including PXXP sites and polyproline motifs, are located in the cytoplasmic region shared by [TM1] and [TM2] (Schmucker et al. 2000). Consistent with the biochemical results, the axon terminal overgrowth resulted from [TM1] overexpression was also eliminated by loss of *dock* (Figures 2.11I-L). Thus, given the same subcellular compartment, Dscam[TM1] and [TM2] are biochemically comparable and share the same signaling mechanism. Moreover, the ectopic localization, function and signaling of transgenic [TM1] in axons underscore the importance of studying splicing isoforms at physiological levels of expression.

Axonal enrichment of Wnd compartmentalizes the Wnd-Dscam[TM2] signaling

We showed previously that the signaling pathway involving the E3 ubiquitin ligase Highwire (Hiw) and the dual leucine zipper kinase Wallenda (Wnd) promotes Dscam expression (Kim et al. 2013). However, whether the Hiw-Wnd pathway regulates the expression of both [TM1] and [TM2] isoforms is unknown. To address this, we determined whether loss of *hiw* or overexpression of Wnd changed the levels of [TM1]::HA and [TM2]::V5. To test the effects of loss of *hiw*, Western blotting was performed on CNS lysates from trans-heterozygous [TM1]::HA / [TM2]::V5 larvae that were generated through global iso-Tagging. We found that loss of *hiw* led to increased expression of both Dscam[TM1] and [TM2] in the CNS (Figure 2.12A). Next, we compared Wnd's effect on the expression of Dscam[TM1] and [TM2]. As global overexpression of Wnd caused larval lethality, we co-expressed Wnd and R recombinase (for iso-Tagging of endogenous Dscam[TM1] and [TM2]) in a subset of CNS neurons with $GAL4^{4\text{-}77}$ (Kim et al. 2013). Interestingly, Wnd overexpression only increased the level of

Dscam[TM2] (Figure 2.12B), but not that of [TM1], suggesting that unlike Hiw, Wnd preferentially regulates the expression of Dscam[TM2]. This finding from biochemical studies was confirmed in C4da neurons by immunostaining of the endogenous Dscam[TM2] tagged through iso-Tagging. Immunostaining of Dscam[TM2]::$V5^{iso\text{-}Tagging}$ showed that endogenous Dscam[TM2] was undetectable in C4da axon terminals in 3rd-instar larvae, but detectable at this developmental stage when Wnd was overexpressed in these neurons (Figure 2.12C).

Next, we investigated the mechanism underlying the differential effect of Wnd on Dscam[TM1] and [TM2]. Firstly, we determine whether Wnd is capable of increasing Dscam[TM1] expression in a cell type without the dendrite-axon compartmentalization. We overexpressed Dscam isoforms with endogenous 5' and 3' UTR in S2 cells, and found that Wnd similarly promoted [TM1] and [TM2] expression (Figure 2.12D-E). This result suggest that Dscam[TM1] and [TM2] are molecularly indistinguishable for the Wnd regulation. Secondly, we identified the distribution of Wnd in neurons, and found that Wnd was enriched in axons but not dendrites. A GFP-tagged kinase-dead version of Wnd (GFP-Wnd^{KD})(Xiong et al. 2010) was expressed in C4da neurons; substantial signals were detected in axon terminals but not in dendrites (Figure 2.12F). These data suggest that axonal localization of Wnd compartmentalizes the Wnd-Dscam[TM2] signaling.

2.4 Discussion

In this study, we developed *isoTarget* to generate splicing isoform-specific loss-of-function mutants and conditional tagging in specific neurons. As a proof of concept, we applied *isoTarget* to investigate two mutually exclusive isoforms of Dscam, which differ in their transmembrane and juxtamembrane domains, for their subcellular localization, regulation of expression, function in dendrite/axon development, and subcellular signaling. These findings highlight the versatility of *isoTarget* and the importance of studying splicing isoform at endogenous levels *in vivo*. In addition, they establish the causality between the subcellular localization and cellular function of splicing isoforms, demonstrating the critical role of subcellular localization in expanding the functional diversity of splicing isoforms.

Our study demonstrates that Dscam isoforms use two different modes to achieve distinct compartment-specific functions *in vivo* (Figure 2.12G). While the dendrite-specific localization restrains Dscam[TM1] from functioning in axons, axonal enrichment of functional partners forms a subcellular signaling pathway involving the ubiquitously distributed Dscam[TM2].

Subcellular localizations define the distinct cellular functions of alternative splicing isoforms that have the same biochemical functions

Alternative isoforms often differ in their protein structures and thus the biochemical properties (Kelemen et al. 2013). Recent studies suggest the importance of subcellular localization in defining the cellular functions of alternative splicing isoforms. For example, in cultured neurons, the RBFOX1 gene generates a nuclear variant (by excluding exon 19) that regulates RNA splicing and a cytoplasmic variant (by including exon 19) that stabilizes mRNAs (Lee et al. 2016). However, whether subcellular localization causes the nuclear and cytoplasmic

variants differ in their cellular functions remains to be determined, as it is possible that the two isoforms have distinct biochemical functions. More broadly, a challenging question in the field is whether the difference in subcellular localization determines the compartmentalized functions for the isoform (i.e., the issue of causality), especially at the endogenous levels *in vivo*. By applying *isoTarget* in *Drosophila* sensory system, we establish the causality between the subcellular localization and cellular functions of the Dscam isoforms. Our findings highlight the critical role of subcellular localization in expanding the functional diversity of isoforms.

Even if they are localized in different subcellular compartments, splicing isoforms with the same biochemical function might exhibit the same cellular functions because their downstream partners might spread throughout the cell (e.g., via trans-compartmental communication (Terenzio, Schiavo, and Fainzilber 2017)). In order to achieve cellular functions specific to a compartment, one solution is to localize the functional partners shared by the isoforms to specific subcellular compartments. Indeed, we found that compartmental enrichment of interactors leads to isoform-specific signaling. The Dscam[TM1] and [TM2] do not differ in their biochemical interactions with Wnd and Dock (Figures 2.11H, 2.12C-D). Yet, the axonal enrichment of Wnd and Dock forms a compartmentalized Wnd-Dscam[TM2]-Dock signaling cascade *in vivo*, despite that Dscam[TM2] is present in both dendrites and axons (Figures 2.8C, E, H, K). These findings suggest that, for splicing isoforms with the same biochemical functions, specific cellular functions can be achieved by the compartment-specific colocalization of the isoforms and their functional partners (Figures 2.12G).

Advantages of *isoTarget*

The studies reported in this paper demonstrate several advantages of *isoTarget* over traditional techniques.

First, it can be used to generate classic genetic mutants for analyzing the functions of specific splicing isoforms. RNA interference has been adopted to investigate Dscam isoform functions in CNS neurons (Shi et al. 2007). However, we found that this method is not applicable for studying Dscam in larval PNS neurons (data not shown). This is likely because endogenous Dscam primarily functions at early developmental stages and a late efficacy of RNAi precluded the discovery of Dscam functions in these neurons. By contrast, *isoTarget* can be used to create a loss-of-function mutant a specific isoform without affecting other isoforms, allowing us to investigate the functions of Dscam isoforms in larval PNS neurons.

Second, *isoTaget* enables the identification of isoform-specific localization at the subcellular level in neurons of interest *in vivo*, which is otherwise challenging due to the difficulty in discerning immunofluorescent signals in subcellular compartments among a number of neurons expressing the same protein in the vicinity. In addition, this method expresses tagged proteins at more physiological levels than transgenes. Prior studies on Dscam have relied on transgenes to investigate the functions and subcellular localizations of Dscam[TM1] and [TM2] (Zhan et al. 2004; Wang et al. 2004a; Soba et al. 2007; Yang, Bai, and Lee 2008; Goyal et al. 2019; Kim et al. 2013), but transgenic proteins are often ectopically localized. For example, whereas the endogenous Dscam[TM1] is absent in axons (Figures 2.8D and 2.9B), overexpressing [TM1] leads to its axonal localization (Figures 2.10A-G). In fact, tagging endogenous Dscam[TM1] and [TM2] with *isoTarget* led to the observation of consistent patterns of subcellular localization in different types of neurons (Figure 2.8), which reconciles the cell-type discrepancies observed previously with transgenes.

Third, *isoTarget* allows studying isoform-specific compartmentalized signaling. Using *isoTarget*, we identified a Wnd-Dscam[TM2]-Dock signaling pathway enriched at the presynaptic terminals of C4da neurons. Complementing the *in vivo* studies with *isoTarget*, we performed biochemical studies in S2 cells and found that Dscam[TM1] and [TM2] did not differ in their biochemical interactions with Wnd and Dock (Figures 2.11H, 2.12C-D). Consistent with this, forced localization of ectopic Dscam[TM1] in axons also increased axonal growth *in vivo* (Figures 2.10A-G) through the same downstream effector Dock used by Dscam[TM2] (Figures 2.11I-L). In this series of studies, *isoTarget* was essential for establishing the cellular functions and biochemical interactions *in vivo*.

Limitations

There are three limitations to the *isoTarget* technique. First, for the successful application of *isoTarget*, the isoform inserted with iso-KO cassette is expected to lose its function. This is not necessarily always the case, especially when the targeted exon encodes a fragment located at the C-terminus of the protein. This problem is common in isoform studies by genetic modifications, including Cre-LoxP and isoEXPRESS (Gu et al. 2019). Developing isoform-specific nanobody might be a way to solve this problem (Roth, Fulcher, and Sapkota 2019). Second, we discovered that the original translational stop cassette may cause off-target effects (Figures 2.5A-C and F), and that such effects depend on the length of the cassette. Thus, the expression of isoforms other than the targeted one should always be examined by techniques such as RT-qPCR. Finally, successful uses of *isoTarget* require that the epitope tagging preserves the function of the splicing isoform. Structural information would be helpful in

choosing the proper inserting site. For example, inserting the isoTarget cassette into the loop region of a polypeptide is likely to increase the chance of success.

In summary, we have developed *isoTarget* as a versatile genetic tool that is compatible with a variety of techniques for analyzing isoform-specific properties and uncovering the mechanisms underlying isoform diversity at multiple levels *in vivo*. We anticipate this methodology be useful for isoform studies in various cell types and organisms.

2.5 Future directions

Application of *isoTarget* in isoforms of other genes

Here we successfully applied *isoTarget* to two Dscam isoforms. As few isoforms have been studies at endogenous and subcellular levels *in vivo*, there would be a rich list of candidate genes to target. Notably, we found that the full-length tlstop cassette may alter the expression levels of other isoform in a length-dependent manner. Thus, we recommend the usage of short tlstop cassette in future studies.

One interesting candidate is *FoxP*. The Foxp proteins are evolutionarily conserved transcription factors that are linked to a variety of human diseases, such as autism, speech disorders, tumor and autoimmune disease (Takahashi, Takahashi, and Liu 2009). Though four members, FoxP1-P4, exist in humans, *Drosophila* exhibits a single ortholog, called FoxP. *Drosophila* FoxP is extensively expressed in the nervous system, including cholinergic, glutamatergic and GABAergic neurons (Castells-Nobau et al. 2019). It has been shown to play critical roles in pre and post-synaptic development, motor coordination, operant self-learning, perceptual decision and producing courtship songs (Castells-Nobau et al. 2019; Lawton, Wassmer, and Deitcher 2014; Mendoza et al. 2014; DasGupta, Ferreira, and Miesenbock 2014). Though it's well known that 3 different isoforms exist in *Foxp* gene, whether these isoforms differ in their expression, localization and function remains a mystery. Application of *isoTarget* to FoxP isoforms is expected to advance the understanding to unprecedented levels.

Application of *isoTarget* in conditional protein tagging

Here we used the *isoTarget* cassettes to conditionally knockout and tag isoforms. In principle, these cassettes can be inserted to last exon before stop codon to conditionally tag

proteins. Compared with the commonly used transcriptional stop cassette, the translational stop cassette would not introduce exogenous 3'-UTR, which is critical for the expression, localization and post-translation modification of targeted genes. *isoTarget* cassettes can be widely used to examine the endogenous localization and signaling of targeted proteins at the endogenous and cell-specific levels *in vivo*.

One potential direction is using *isoTarget* to conditionally tagging the endogenous receptors of neurotransmitters, such as GABA, acetylcholine, dopamine, serotonin and glutamate. Such a tool will be invaluable for assaying the subcellular localization of neurotransmitter receptor, the relative expression levels of receptor subunits, how neural circuitry and plasticity are regulated at certain cellular compartments. These results will significantly contribute to a more comprehensive and in-depth understanding of brain wiring in *Drosophila*.

Dscam isoform levels may underlie the morphological diversity of neurons

Drosophila neurons exhibit extensive diversity in the relative sizes of dendrite and axons. For example, lobula plate tangential cells (LPTCs), a family of giant neurons involved in visual feedback for self-motion, have remarkably large dendritic arbors and simple axons with short axon terminals (Wei et al. 2020). By contrast, *Drosophila* mushroom bodies, a neuronal ensemble critical for olfactory learning and memory, show long axonal arbors but relatively short dendrites (Heisenberg 2003). Despite these observations, the molecular mechanism underlying the morphological diversity is poorly understood.

Here we discover that endogenous Dscam[TM1] function restrictedly in dendrites while [TM2] is responsible for axonal growth. These spatial differences raise the hypothesis that

neurons control morphogenesis by differentially manipulating the expression of Dscam[TM1] and [TM2]. Neurons with high Dscam[TM1]-to-[TM2] ratio exhibit extensive dendrites but short axons, while low Dscam[TM1]-to-[TM2] ratio corresponding to diminished dendrites but extensive presynaptic arborization. For example, in LPTC neurons, Dscam[TM1] may be highly expressed to ensure proper dendritic elaboration while [TM2] expression is restricted to guarantee small axon size. To test this hypothesis, it would be interesting to assay the association of Dscam[TM1]-to-[TM2] mRNA ratio with the relative dendritic/axonal arbor size in different neuronal types. With *isoTarget* fly lines at hand, LPTC neurons could be a good starting point. It would be exciting if endogenous Dscam[TM1] is highly expressed and transgenic overexpression of Dscam[TM2] confers aberrant long axons in LPTC neurons.

Interestingly, mammalian *Dscam* are not alternatively spliced in the trans/juxta-membrane region as *Drosophila Dscam* gene. How does a single form of Dscam protein potentially regulate the differential dendritic/axonal growth in distinct neuronal types in mammals? One possibility is that Dscam expression levels can be differentially controlled in dendrites versus axons. This could be achieved by molecular trafficking or local translation in targeted subcellular compartment. The other possibility is that despite of its even distribution, the subcellular localization of the Dscam downstream effectors or functional antagonizers confer differential function of Dscam signaling in different cellular compartments. Similar scenarios are observed in *Drosophila* sensory neurons by the finding of the axonal Wnd-Dscam[TM2]-Dock signaling. Applying *isoTarget* to conditionally tagging endogenous Dscam in targeted neuronal population in mouse model would be a key method to distinguish these two possibilities.

Mechanisms underlying compartmentalized Wnd-Dscam[TM2] signaling

Our lab previously found that Wnd, the fly homolog of DLK, promotes Dscam expression levels via 3'UTR in the *Drosophila* brain. Here with *isoTarget*, we found wnd specifically promotes Dscam[TM2] expression at axon terminals of a neuron. As Wnd is enriched in axon terminals, one interesting question is whether this isoform-specific regulation depends on the axonal localization of Dscam[TM2] mRNA. As the mRNA difference between Dscam[TM1] and [TM2] is too short for fluorescent in situ hybridization (FISH), the traditional method is not feasible to answer this question. Here, *isoTarget* offers us one way to address this issue. For example, we may specifically iso-Tag [TM2] in C4da neurons. As only axon terminals of C4 da neurons reach VNC, it's expected to detect [TM2]::V5 mRNA by PCR if Dscam[TM2] is localized in axons.

Another interesting question would be how Wnd, a MAP3K, promotes Dscam expression. We propose that the RNA binding protein (RBP) may be a go-between. As we found that this regulation is conserved in S2 cells, one experiment would be using Dscam[TM2]::GFP-3'UTR as a reporter gene and carry out a systematic RNAi of RBPs with the presence of Wnd. One will be the candidate if knocking down the expression causes impaired Dscam[TM2]::GFP expression. Especially, it would be interesting to apply *isoTarget* to examine whether this RBP is specifically localized in axon terminals so that the compartmentalized Wnd-RBP-Dscam[TM2] signaling is caused by the presence of all three components. This observation will highlight the importance of subcellular localization in expanding signaling complexity in cells.

2.6 Author contribution

H.L. and B.Y. conceived the project and designed the experiments. H.L. designed, generated and validated *isoTarget* flies, examined the functions, endogenous expression and signaling cascade of Dscam isoforms. S.P., R.L. and M.W.Z. performed MARCM on C4da neurons and assisted in quantification of global iso-KO. W.Z. examined isoform functions in C3da neurons. Y. H. assisted in generating *isoTarget* flies. L.Y. assisted in experiments of endogenous isoform expression. B.Y. supervised the project. H.L. and B.Y. wrote the paper.

2.7 Materials and methods

Drosophila strains

The following published fly strains were used: *ppk*-Gal4 (chromosome III) (Kuo, Jan, and Jan 2005); GMR83B04-GAL4 (Pfeiffer et al. 2011); UAS-Dscam[TM2]::GFP (3.36.25, chromosome III and X), UAS-Dscam[TM1]::GFP (3.36.25, chromosome X), *DscamP*-Dscam[TM1]::GFP (3.36.25) (Wang et al. 2004a), *DscamP*-Dscam[TM2]::GFP (3.36.25) (Wang et al. 2004a); OK107-Gal4 (Connolly et al. 1996); $Dscam^{18}$ (Wang, Zugates, et al. 2002); $hiw^{\Delta N}$ (Wu et al. 2005); wnd^{1}, wnd^{3}, and UAS-Wnd (Collins et al. 2006); $dock^{4732}$ and $dock^{C506}$ (Garrity et al. 1996); *nos*-Gal4 (Van Doren, Williamson, and Lehmann 1998); 20xUAS-R recombinase (Nern et al. 2011).

Generation of DNA constructs

The design of *isoTarget* system is described in Figure S1A. The translational stop cassette was amplified by PCR from non-catalytic region of lacZ with frame shift to introduce multiple premature termination codons. The loxP-dsRed-loxP sequence is described in Gratz et al., (2014) (Gratz et al. 2014). The pBluescript donor plasmid, which contains *isoTarget* KI cassettes (GS linker-RSRT-*tlstop*-loxP-dsRed-loxP-RSRT-epitope-G3 linker) and Dscam isoform homologous sequences with mutated PAM, was generated with the In-Fusion HD Cloning Kit (Clontech Laboratories, Inc.). The pCFD3-dU63gRNA plasmid, which produces gRNA in fly embryos, is described in Ran et al., (2013) (Ran et al. 2013). The pUAST-*Dscam5'UTR-Dscam[TM1]::GFP-Dscam3'UTR* (4.3-6.36-9.25) plasmid was made by modifying pUAST-*Dscam5'UTR- Dscam[TM2]::GFP-Dscam3'UTR* (4.3-6.36-9.25)(Kim et al. 2013). Specifically, the fragment containing *Dscam5*'UTR and exons 1-16 and that containing exons 18-24 plus

Dscam3'UTR were amplified from pUAST-*Dscam5'UTR- Dscam[TM2]::GFP-Dscam3'UTR* by PCR. The fragments, together with PCR products of *Dscam* exon 17.1, were fused with the pUASTattB vector (linearized by EcoRV) by In-Fusion HD Cloning (Clontech Laboratories, Inc.).

Sequences of *isoTarget* cassettes

tlstop (in-frame stop codons that we introduced are underlined):

TAACGTAAGCTAGCTAGACCGGTCCCAACTTAATCGCCTTGCAGCACATCCCCCTTT
CGCCAGCTGGCGTAATAGCGAAGAGGCCCGCACCGATCGCCCTTCCCAACAGTTGC
GCAGCCTGAATGGCGAATGGCGCTTTGCCTGGTTTCCGGCACCAGAAGCGGTGCCG
GAAAGCTGGCTGGAGTGCGATCTTCCTGAGGCCGATACTGTCGTCGTCCCCTCAAAC
TGGCAGATGCACGGTTACGATGCGCCCATCTACACCAACGTAACCTATCCCATTACG
GTCAATCCGCCGTTTGTTCCCACGGAGAATCCGACGGGTTGTTACTCGCTCACATTT
AATGTTGATGAAAGCTGGCTACAGGAAGGCCACGCGTA

Short *tlstop* (in-frame stop codons that we introduced are underlined):

TAACGTAAGCTAGCTAGACCGGTTTCCCACGGAGAATCCGACGGGTTGTTACTCGCT
CACATTTAATGTTGATGAAAGCTGGCTACAGGAAGGCCACGCGTA

GS-linker: GGTGGCGGCGGAAGCGGAGGTGGAGGCTCC

RSRT: CTTGATGAAAGAATAACGTATTCTTTCATCAAG

loxP: ATAACTTCGTATAATGTATGCTATACGAAGTTAT

dsRed box (consisting of 3XP3 enhancer/HSP70 promoter (Gratz et al. 2014), the cDNA encoding the dsRed fluorescent protein and *SV40 3' UTR*)

CGTACGGGATCTAATTCAATTAGAGACTAATTCAATTAGAGCTAATTCAATTAGGAT
CCAAGCTTATCGATTTCGAACCCTCGACCGCCGGAGTATAAATAGAGGCGCTTCGTC
TACGGAGCGACAATTCAATTCAAACAAGCAAAGTGAACACGTCGCTAAGCGAAAGC
TAAGCAAATAAACAAGCGCAGCTGAACAAGCTAAACAATCGGCTCGAAGCCGGTCG
CCACCATGGCCTCCTCCGAGGACGTCATCAAGGAGTTCATGCGCTTCAAGGTGCGCA
TGGAGGGCTCCGTGAACGGCCACGAGTTCGAGATCGAGGGCGAGGGCGAGGGCCG
CCCCTACGAGGGCACCCAGACCGCCAAGCTGAAGGTGACCAAGGGCGGCCCCCTGC
CCTTCGCCTGGGACATCCTGTCCCCCCAGTTCCAGTACGGCTCCAAGGTGTACGTGA
AGCACCCCGCCGACATCCCCGACTACAAGAAGCTGTCCTTCCCCGAGGGCTTCAAGT
GGGAGCGCGTGATGAACTTCGAGGACGGCGGCGTGGTGACCGTGACCCAGGACTCC
TCCCTcCAGGACGGCTCCTTCATCTACAAGGTGAAGTTCATCGGCGTGAACTTCCCCT
CCGACGGCCCCGTAATGCAGAAGAAGACTATGGGCTGGGAGGCgTCCACCGAGCGC
CTGTACCCCCGCGACGGCGTGCTGAAGGGCGAGATCCACAAGGCCCTGAAGCTGAA
GGACGGCGGCCACTACCTGGTGGAGTTCAAGTCCATCTACATGGCCAAGAAGCCCG
TGCAGCTGCCCGGCTACTACTACGTGGACTCCAAGCTGGACATCACCTCCCACAACG
AGGACTACACCATCGTGGAGCAGTACGAGCGCGCCGAGGGCCGCCACCACCTGTTC
CTGTAG*GGGCCGCGACTCTAGATCATAATCAGCCATACCACATTTGTAGAGGTTTTACTTG*
CTTTAAAAAACCTCCCACACCTCCCCCTGAACCTGAAACATAAAATGAATGCAATTGTTGTT
GTTAACTTGTTTATTGCAGCTTATAATGGTTACAAATAAAGCAATAGCATCACAAATTTCACA
AATAAAGCATTTTTTTCACTGCATTCTAGTTGTGGTTTGTCCAAACTCATCAATGTATCTTAA
CCGGT

V5: GGCAAGCCCATCCCAAACCCACTGCTCGGCCTGGATAGCACC

HA: TACCCATACGATGTTCCAGATTACGCT

G3 linker (Gratz et al. 2014): GGTGGCGGC

Generation of *isoTarget* flies

The donor plasmid (750 ng/µl) and gRNA plasmid (250 ng/µl) were co-injected into fly embryos to generate mosaic G0 flies, which were crossed to *white*$^{-/-}$ flies to get G1 heterozygous knock-in flies that express the selection marker dsRed in their eyes. G1 flies with red fluorescence in their eyes were crossed to Cre-expressing flies (BL1092) to generate iso-KO flies. To generate global iso-Tagging flies, iso-KO flies were mated with the germline driver *nos*-Gal4 (BL4442) and 20x UAS-R recombinase (BL55795). According to our experiences, around 20% of fertile mosaic G0 flies were able to generate G1 knock-in flies with fluorescent red eyes. The G1 knock-in flies constitute 1-30% of total G1 flies, depending on individual lines. To generate cell-type-specific iso-Tagging, iso-KO flies were mated with cell-type-specific Gal4 drivers, such as *ppk*-Gal4, and 20x UAS-R recombinase.

S2 cell culture and transfection

S2 cells were maintained in *Drosophila* Schneider's medium supplemented with 10% fetal bovine serum at 25°C in a humidified chamber. Plasmids were transfected into cultured S2 cells with polyethylenimine (PEI) (Ehrhardt et al. 2006). Cells were harvested for Western blotting 2 days after transfection.

Co-immunoprecipitation and Western blotting

To perform co-immunoprecipitation with neural tissues, the CNS of 3rd-instar larvae (~120 per experimental condition) were dissected out and placed in ice-cold PBS containing 2 mM sodium vanadate. After a pulse of centrifugation, larval CNS were isolated and then lysed on ice with the lysis buffer (50 mM Tris-HCl/pH 7.4, 150 mM NaCl, 2 mM sodium vanadate, 10 mM sodium fluoride, 1% Triton X-100, 10% glycerol, 10 mM imidazole and 0.5 mM phenylmethylsulfonyl fluoride). Lysates were centrifuged at 15,000 g for 20 min at 4°C. The resulting supernatants were either saved as inputs or incubated with magnetic beads conjugated with appropriate antibodies for 4 hours at 4°C. After washing once with the lysis buffer, twice with lysis buffer containing 0.1% deoxycholate, and 3 times with lysis buffer lacking Triton X-100, the immunoprecipitates and total lysates were resolved on 7.5% SDS-PAGE gels followed by Western blotting as previously described (Kim et al., 2013). Protein samples were transferred to nitrocellulose membranes and detected by chemiluminescence (Catalog# 32106, Pierce ECL Western Blotting Substrate) with either a BIO-RAD ChemiDoc Touch Imaging system or a Kodak X-OMAT 2000 film processor.

The procedure of co-immunoprecipitation with lysates from S2 cells was similar except that cultured S2 cells were re-suspended in ice-cold PBS before lysis.

Imaging and image analysis

Larvae immunostaining was described previously (Ye et al. 2011). Confocal imaging was done with a Leica SP5 confocal system with 20x or 63x glycerol immersion lenses. To minimize the variation, we only imaged neuronal dendrites and presynaptic terminals of C3da or C4da neurons in abdominal segments 4, 5, and 6. Images were collected with z stacks of 1-μm-step size for

dendrites and 0.3-μm-step size for axons. The resulting three-dimensional images were projected into two-dimensional images by maximum projection. The same imaging setting was applied throughout the imaging process.

The Neurolucida software was used to quantify dendritic morphology and axon terminal growth. For dendrites, the overlap of sister branches is counted as a cross. For quantifying axon terminals of single C4 da neuron, branches shorter than 5 μm were excluded from the analysis. For quantifying the number of longitudinal axonal branches visible between abdominal segment 4-6 (i.e., the connectives) of C4 da neurons, only complete connectives spanning neighboring segments were quantified. Fasciculated connectives are counted as two.

To eliminate experimenter's bias, these experiments were carried out in double-blind fashion. The images acquired by the primary experimenter were coded and randomized by another lab member. After the primary experimenter quantified the data, the data were decoded for statistical analysis.

Reverse-transcription real-Time PCR

The procedure was as described before (Kim et al., 2013). Briefly, mRNA was extracted from around 20 3rd-instar larval CNS with a standard Trizol method (Invitrogen). cDNA was synthesized with Invitrogen SuperScript III First-Strand Synthesis SuperMix (Invitrogen). 10 ng cDNA was used as the template for each real-time PCR reaction by SYBR Green mix (Thermo Scientific) with the Applied Biosystems 7300. To normalize *Dscam* transcripts to those of reference genes, we calculated ΔCt (*Dscam*) = Ct (*Dscam*) – Ct (reference gene). Statistical analysis was performed to compare ΔCt (*Dscam*)(wild-type) and ΔCt (*Dscam*)(mutant) to determine whether there is the expression of test gene is different between wild-type and mutants

(Yuan et al. 2006). Relative mRNA levels is calculated as: $2^{-\Delta\Delta Ct}$, where ΔΔCt (*Dscam*) = ΔCt (*Dscam*)(mutant) -ΔCt (*Dscam*)(wild-type). We used *elav* as the reference gene and *Chmp1* as the internal control. Following primers were used: *Chmp1*: 5'-AAAGGCCAAGAAGGCGATTC-3' and 5'-GGGCACTCATCCTGAGGTAGTT-3'; *elav*: 5'-CTGCCAAAGACGATGACC-3' and 5'-TAAAGCCTACTCCTTTCGTC-3'; *Dscam[TM1]*: 5'-CGTTACCGGAGGCACTATCG-3' and 5'- ATCGTCTTTGTGGTGA TTGCC-3'; *Dscam[TM2]*: 5'- CGTTACCGGAGGCACCATT-3' and 5'- ACTACATCG TAGTACACATCCTTT-3'.

Statistical Analysis

Data are presented as mean ± SEM. Comparisons of mean differences between groups were performed by One-way ANOVA followed by Student's *t*-test. $P < 0.05$ was considered to be statistically significant. For all quantification, *: $p < 0.05$; **: $p < 0.01$; ***: $p < 0.001$; ns: not significant ($p > 0.05$).

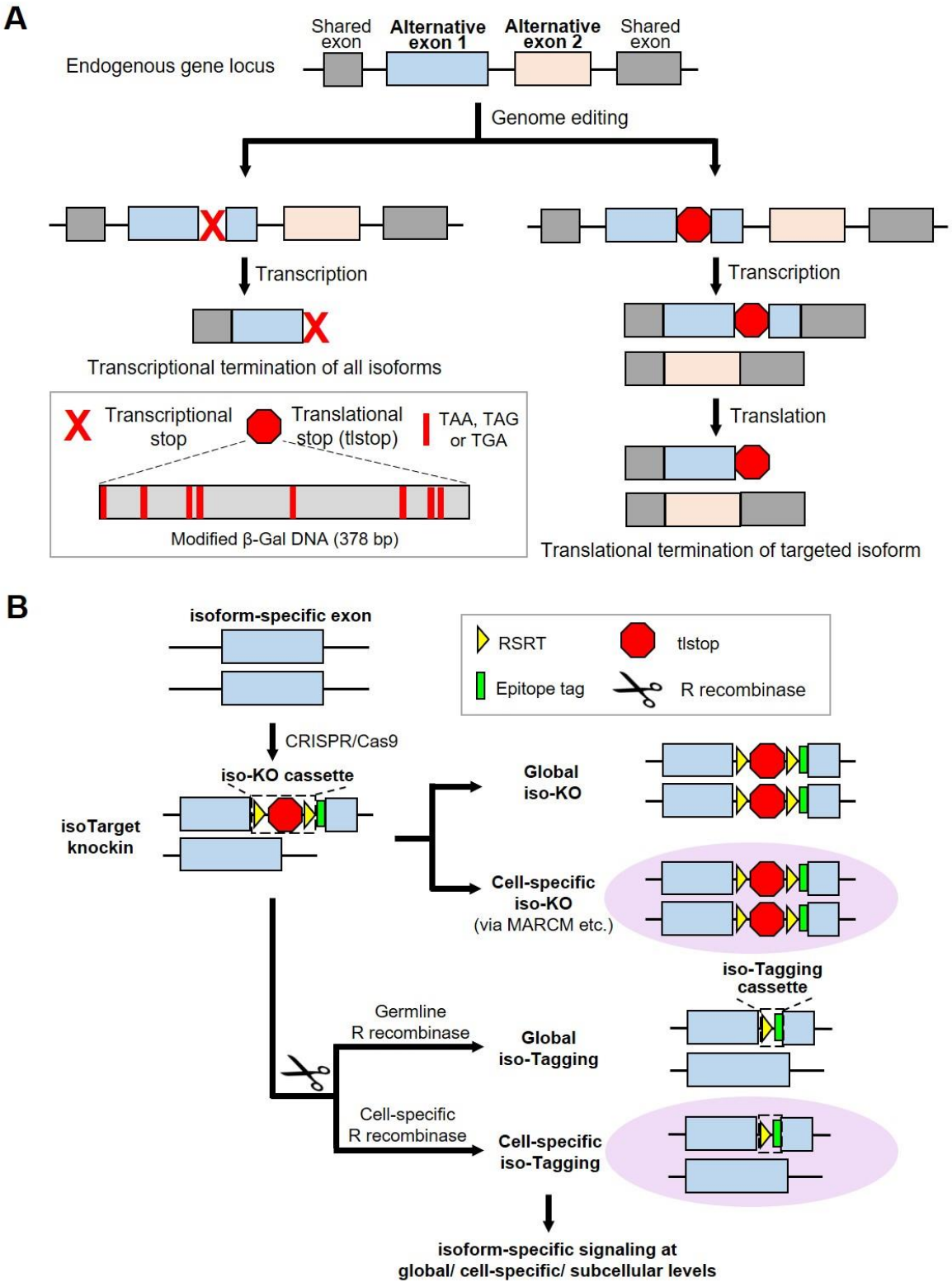
A
Shared exon
Alternative exon 1
Alternative exon 2
Shared exon
Endogenous gene locus
Genome editing
Transcription
Transcription
Transcriptional termination of all isoforms
Transcriptional stop
Translational stop (tlstop)
TAA, TAG or TGA
Modified β-Gal DNA (378 bp)
Translation
Translational termination of targeted isoform
B
isoform-specific exon
RSRT
tlstop
Epitope tag
R recombinase
CRISPR/Cas9
iso-KO cassette
isoTarget knockin
Global iso-KO
Cell-specific iso-KO (via MARCM etc.)
iso-Tagging cassette
Germline R recombinase
Global iso-Tagging
Cell-specific R recombinase
Cell-specific iso-Tagging
isoform-specific signaling at global/ cell-specific/ subcellular levels

Figure 2.1. Design of *isoTarget* and its application to studying the functional diversity of splicing isoforms.
(**A**) Introducing translational stops into alternative exons allows isoform-specific manipulations of the gene. Inserting the commonly used transcriptional stop cassette into alternative exon leads to the transcriptional termination of all isoforms downstream of the targeted exon (left branch). In order to truncate the targeted isoform, but not the transcription or translation of the other isoforms (right branch), we engineered a *translational stop* (*tlstop*) cassette by introducing multiple stop codons into the DNA sequence encoding a non-catalytic region of β-Gal (bottom left).
(**B**) Combining *tlstop* with other genetic methods for multi-purpose studies of the targeted splicing isoform. The *isoTarget* cassette, which consists of an RSRT site, a translational stop (*tlstop*), another RSRT site, and an epitope tag, is inserted into the targeted isoform exon by CRISPR/Cas9-mediated genome editing. The insertion generates a loss-of-function allele of either the targeted isoform or the entire gene, depending on the length of the *tlstop* cassette (see Figure S3F). Single cells that are homozygous for the targeted allele can be produced by genetic mosaic techniques, such as MARCM. The endogenous isoforms can be visualized in specific neurons by selective expression of R recombinase to remove the RSRT-*tlstop*-RSRT cassette. Expression of R recombinase in female germline cells leads to tagging of the isoform in all cells that express this isoform in the progeny ("global iso-tagging"). Expression of R recombinase in specific cell types or single cells leads to tagging of the isoform in those cells. In the iso-Tagged flies, upstream regulators and downstream effectors of specific isoforms can be identified through genetic, cell biological, and biochemical analyses.

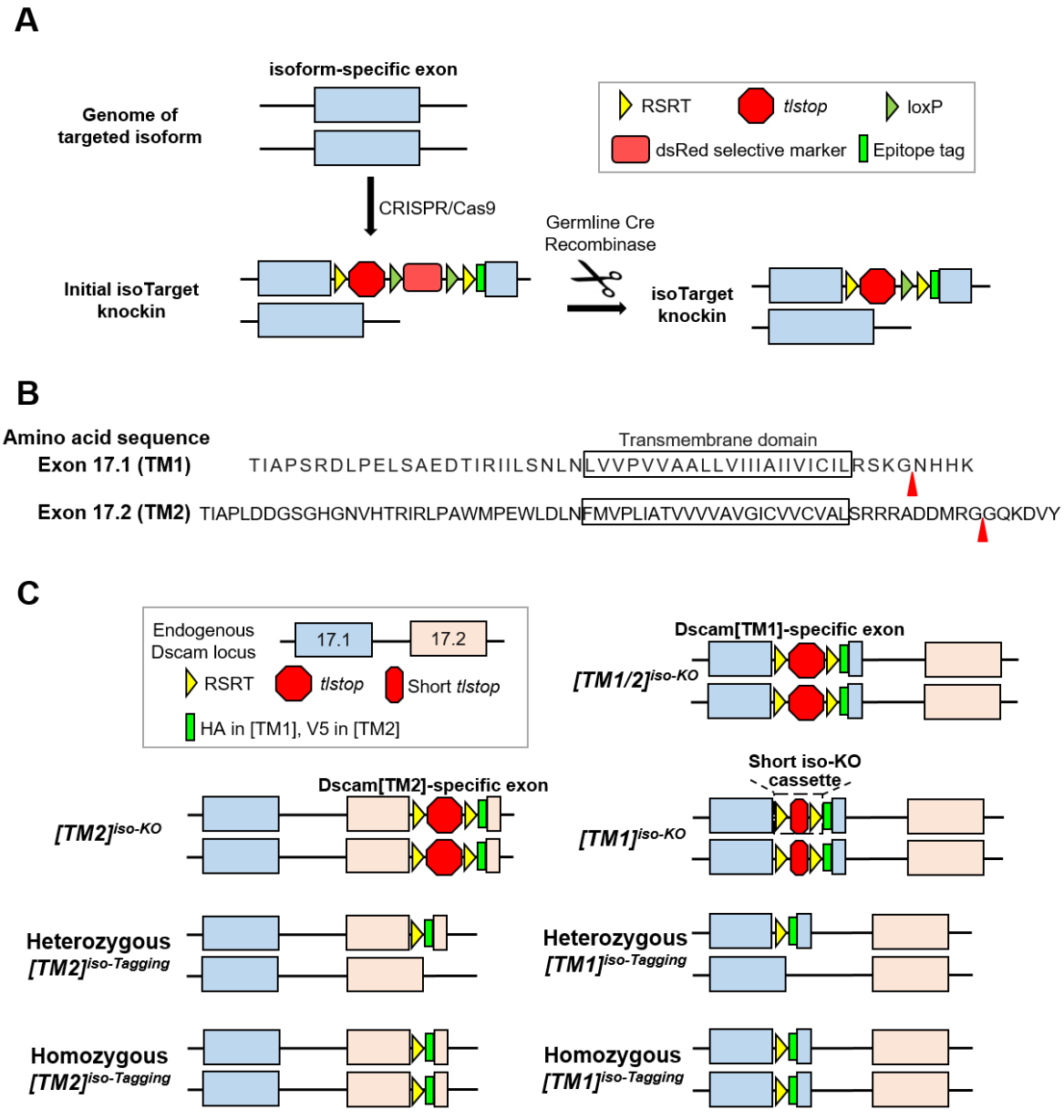
A
isoform-specific exon
Genome of targeted isoform
RSRT
tlstop
loxP
dsRed selective marker
Epitope tag
CRISPR/Cas9
Germline Cre Recombinase
Initial isoTarget knockin
isoTarget knockin
B
Amino acid sequence
Transmembrane domain
Exon 17.1 (TM1) TIAPSRDLPELSAEDTIRIILSNLNLVVPVVAALLVIIIAIIVICILRSKGNHHK
Exon 17.2 (TM2) TIAPLDDGSGHGNVHTRIRLPAWMPEWLDLNFMVPLIATVVVVAVGICVVCVALSRRRADDMRGGQKDVY
C
Endogenous Dscam locus
17.1
17.2
RSRT
tlstop
Short tlstop
HA in [TM1], V5 in [TM2]
Dscam[TM1]-specific exon
[TM1/2]iso-KO
Dscam[TM2]-specific exon
[TM2]iso-KO
Short iso-KO cassette
[TM1]iso-KO
Heterozygous [TM2]iso-Tagging
Heterozygous [TM1]iso-Tagging
Homozygous [TM2]iso-Tagging
Homozygous [TM1]iso-Tagging

Figure 2.2. The detailed design of the *isoTarget* cassette.
(**A**) At the core of the cassette is a *tlstop* that contains multiple termination codons to ensure the disruption of mRNA translation. To achieve cell-type-specific labeling of targeted isoforms through inducible site-specific recombination, the *tlstop* is flanked by two RSRT sites followed by an epitope tag. To facilitate the screening of animals with successful integration of the *isoTarget* cassette, a transgene expressing dsRed under the 3xP3 enhancer/Hsp70 promoter is inserted in between the *tlstop* and the second RSRT site. The dsRed transgene is flanked by two loxP sites, allowing the removing of the dsRed in the presence of Cre recombinase. The *isoTarget* cassette can be knocked into the exon encoding the targeted isoform by CRISPR/Cas9.
(**B**) The *isoTarget* insertion sites in Dscam[TM1] and [TM2] isoforms. Shown are the amino acid sequences encoded by the 17.1 (TM1) and 17.2 (TM2) exons. Red arrow heads indicate the insertion sites in the juxtamembrance regions.
(**C**) Application of *isoTarget* to studying Dscam isoforms. As shown later, iso-KO of [TM1] impairs both [TM1] and [TM2] expression, and is thus named $[TM1/2]^{iso\text{-}KO}$. We discovered a short *tlstop* cassette ("short iso-KO") that specifically knocks out [TM1], but not [TM2]. Iso-Tagging of Dscam[TM1] does not affect [TM1] functions. Iso-KO of [TM2] abolishes, while iso-Tagging preserves, Dscam[TM2] functions. Depending on the purpose of the experiment, Dscam[TM1] and [TM2] can be tagged either globally or specifically in targeted cell types.

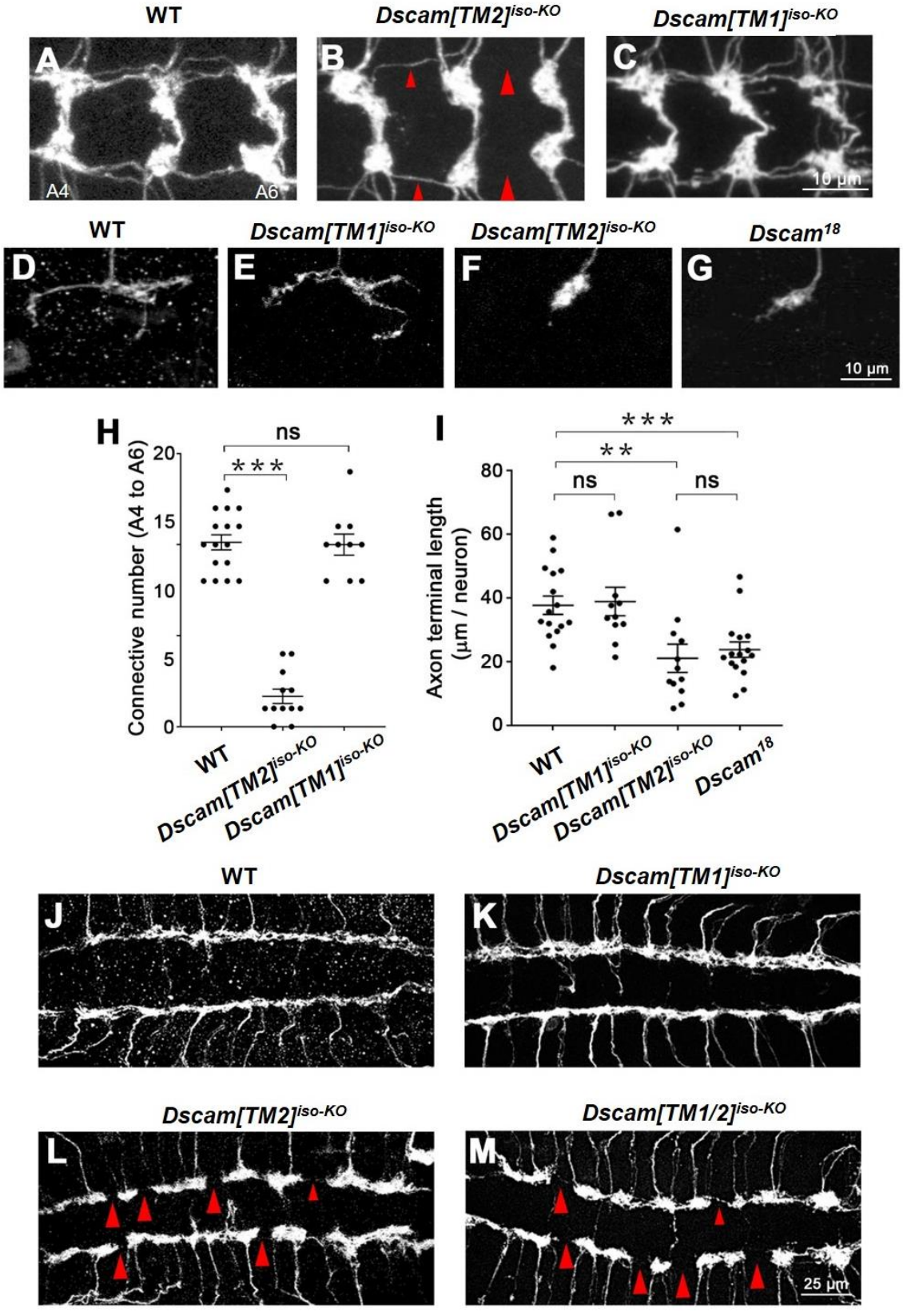
WT
Dscam[TM2]iso-KO
Dscam[TM1]iso-KO
A
B
C
A4
A6
10 µm
WT
Dscam[TM1]iso-KO
Dscam[TM2]iso-KO
Dscam18
D
E
F
G
10 µm
H
ns
***
Connective number (A4 to A6)
20
15
10
5
0
WT
Dscam[TM2]iso-KO
Dscam[TM1]iso-KO
I
***
**
ns
ns
Axon terminal length (µm / neuron)
80
60
40
20
0
WT
Dscam[TM1]iso-KO
Dscam[TM2]iso-KO
Dscam18
WT
Dscam[TM1]iso-KO
J
K
Dscam[TM2]iso-KO
Dscam[TM1/2]iso-KO
L
M
25 µm

Figure 2.3. *isoTarget* uncovers a specific role for the Dscam[TM2] isoform in axon terminal growth.
(**A-C**) Compared with WT (**A**), global *Dscam[TM2]*$^{iso\text{-}KO}$ (**B**), but not *Dscam[TM1]*$^{iso\text{-}KO}$ (**C**), impairs axon terminal growth in C4da neurons. The C4da-specific driver *ppk*-Gal4 was used to label all C4da axon terminals in the CNS. Shown are representative images of abdominal segment 4 to 6 (A4-A6). The large red arrowheads point to the sites where longitudinal axon tracts are broken, and the small arrowheads point to where the tracts are thinned.
(**D-G**) *Dscam[TM2]*, but not *[TM1]*, is required for the growth of axon terminals in single C4da neurons. The MARCM technique was used to generate single GFP-labeled C4da neurons that were homozygous of the indicated alleles. *Dscam[TM1]*$^{iso\text{-}KO}$ has no effect on axon terminal growth (**D** & **E**), while *Dscam[TM2]*$^{iso\text{-}KO}$ reduced the length of axon terminals to the same level as the loss of both isoforms (**F** & **G**).
(**H**) Quantification of the number of axon connectives (i.e., the longitudinal branches) from A4 to A6. Unless specified otherwise, mean ± SEM is shown in all figures, and the statistical tests are one-way ANOVA followed by Student's t test. *: $p < 0.05$; **: $p < 0.01$; ***: $p < 0.001$; ns: not significant ($p > 0.05$).
(**I**) Quantification of presynaptic terminal length in the C4da neuron ddaC.
(**J-M**) *Dscam[TM2]*, but not *[TM1]*, is required for the growth of axon terminals in C3da neurons. The longitudinal axon tracts of C3da neurons in the CNS remain intact in *Dscam[TM1]*$^{iso\text{-}KO}$ (**J** & **K**), but are disrupted in *Dscam[TM2]*$^{iso\text{-}KO}$ (**L**) or in mutants lacking both isoforms (**M**). The large red arrow heads point to the sites where longitudinal axon tracts are broken. The small red arrowheads point to the sites where longitudinal axon tracts are thinned.

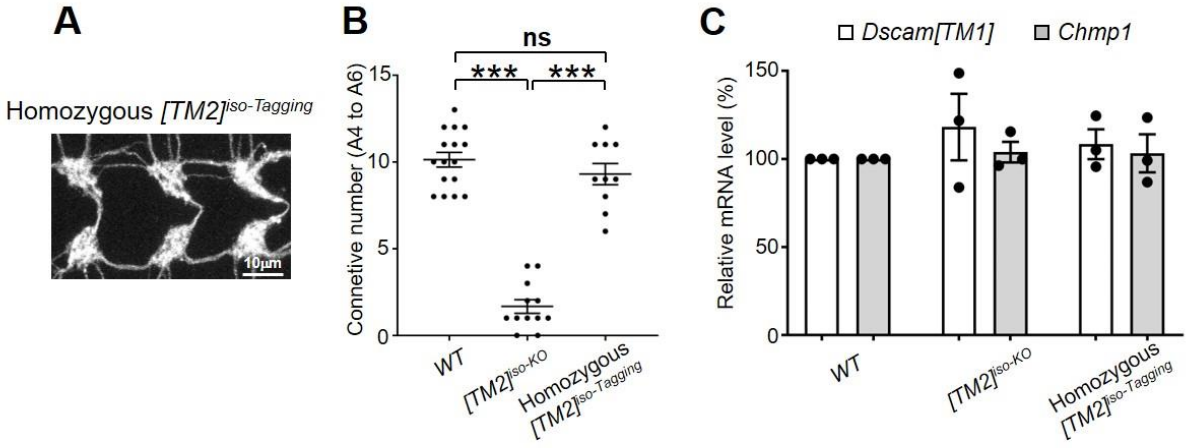

Figure 2.4. Validation of *isoTarget* in Dscam[TM2].
(**A**) *[TM2]*$^{iso\text{-}Tagging}$ does not affect [TM2] functions. As shown in Figure 2A and B, *[TM2]*$^{iso\text{-}KO}$ impairs axon terminal growth in C4da neurons. The axonal defect is completely rescued in homozygous global *[TM2]*$^{iso\text{-}Tagging}$ larvae generated by excision of the RSRT-tlstop-RSRT box from the iso-KO. Shown are the C4da axon terminals in A4-A6 segments.
(**B**) Quantification of the number of C4da axon connectives.
(**C**) Neither global *[TM2]*$^{iso\text{-}KO}$ nor homozygous global *[TM2]*$^{iso\text{-}Tagging}$ affect the mRNA levels of *Dscam[TM1]*. mRNAs from the whole CNS of 3rd instar larvae were used for reverse-transcription real-time PCR. The ΔCt value of [TM2] mRNA is normalized to that of *elav* gene as descried in the Experimental Procedure. *Chmp1* serves as the internal control. Each dot represents one independent experiment.

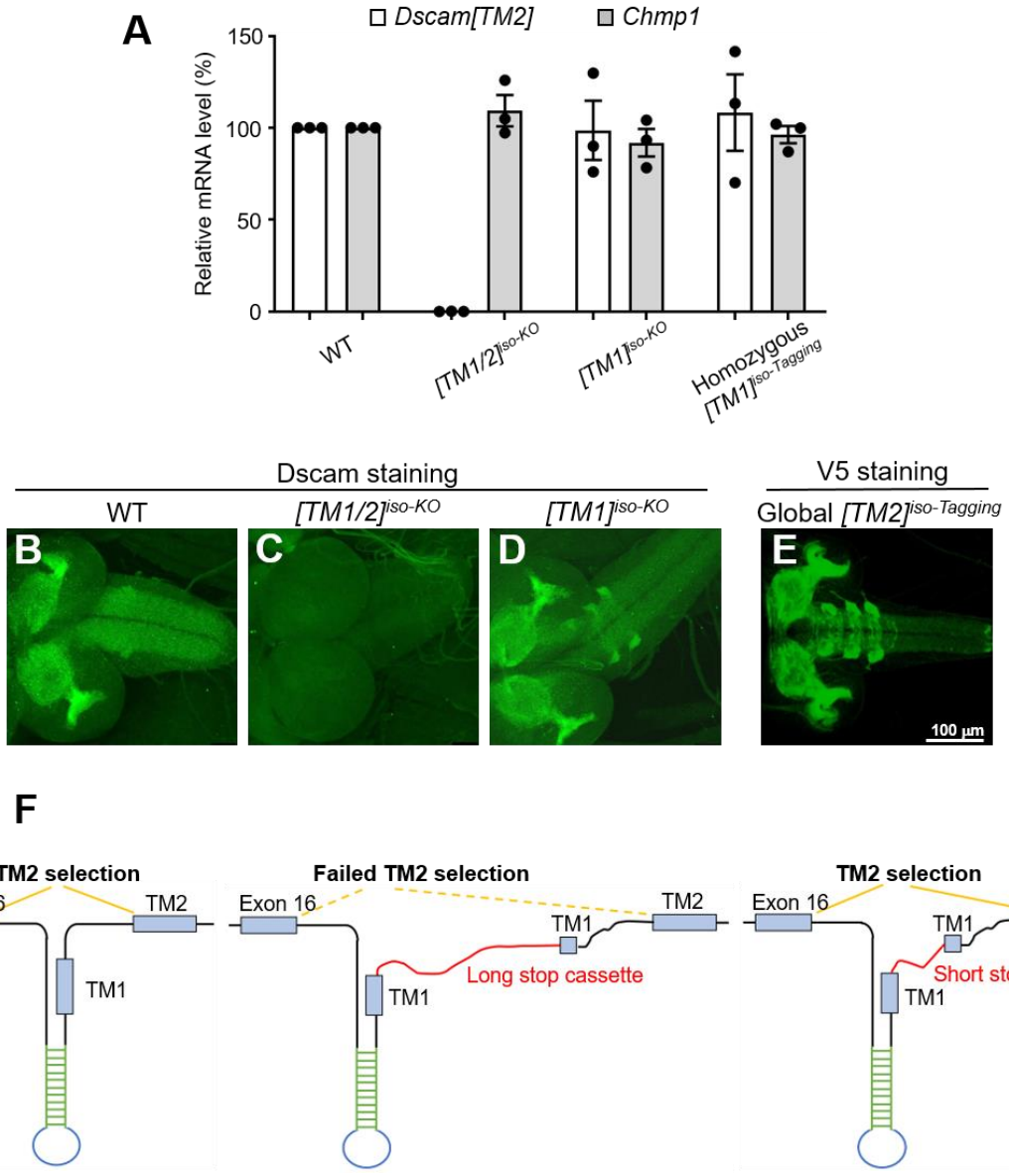
A
Dscam[TM2]
Chmp1
Relative mRNA level (%)
150
100
50
0
WT
[TM1/2]iso-KO
[TM1]iso-KO
Homozygous [TM1]iso-Tagging
Dscam staining
V5 staining
WT
[TM1/2]iso-KO
[TM1]iso-KO
Global [TM2]iso-Tagging
B
C
D
E
100 μm
F
TM2 selection
Exon 16
TM2
TM1
Failed TM2 selection
Long stop cassette
TM2 selection
Short stop cassette

Figure 2.5. Validation of *isoTarget* in Dscam[TM1] and the discovery of short *tlstop* cassette.

(**A**) *Dscam[TM2]* mRNA is undetectable in global *Dscam[TM1]* isoTarget flies resulted from the insertion of the original long *tlstop* cassette ("*[TM1/2]*$^{iso\text{-}KO}$"), but remains intact in global *Dscam[TM1] isoTarget* flies generated by the insertion of the short *tlstop* cassette ("*[TM1]*$^{iso\text{-}KO}$"). *Dscam[TM2]* mRNA level is not affected in homozygous global *[TM1]*$^{iso\text{-}Tagging}$ larvae. mRNAs from the whole CNS of 3rd instar larvae were used for reverse-transcription real-time PCR.

(**B**-**E**) Immunostaining of the CNS with an anti-Dscam antibody shows that while Dscam expression is abolished in global *Dscam[TM1/2]*$^{iso\text{-}KO}$ (**C**), it is detectable in global *Dscam[TM2]*$^{iso\text{-}KO}$ (**D**) and exhibits a pattern that is similar to endogenous Dscam[TM2] labeled by global [TM2]::V5 iso-Tagging (**E**).

(**F**) A schematic model of TM exon selection from *Dscam* pre-mRNA, based on a previous study (Anastassiou, Liu, and Varadan 2006). The complementary sequences (green) form a stem-loop, which is required for the selection of TM2 exon into *Dscam* mRNA. Inserting a long cassette into TM1 exon may create a long distance that eliminates TM2 exon selection.

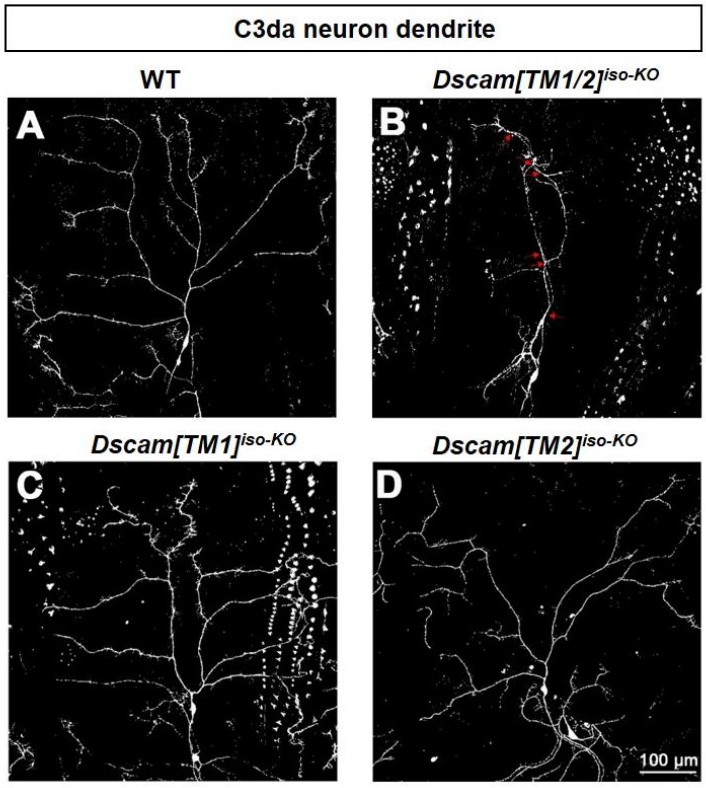
C3da neuron dendrite
WT
Dscam[TM1/2]iso-KO
A
B
Dscam[TM1]iso-KO
Dscam[TM2]iso-KO
C
D
100 μm

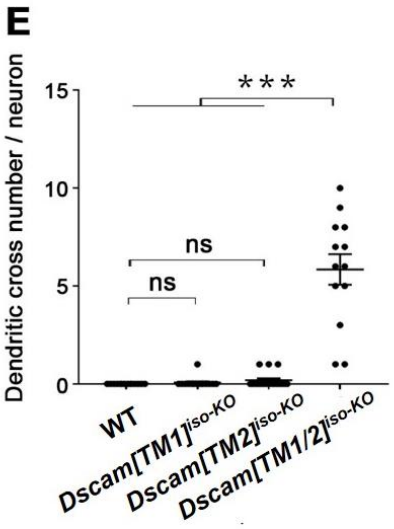
E
Dendritic cross number / neuron
15
10
5
0
***
ns
ns
WT
Dscam[TM1]iso-KO
Dscam[TM2]iso-KO
Dscam[TM1/2]iso-KO

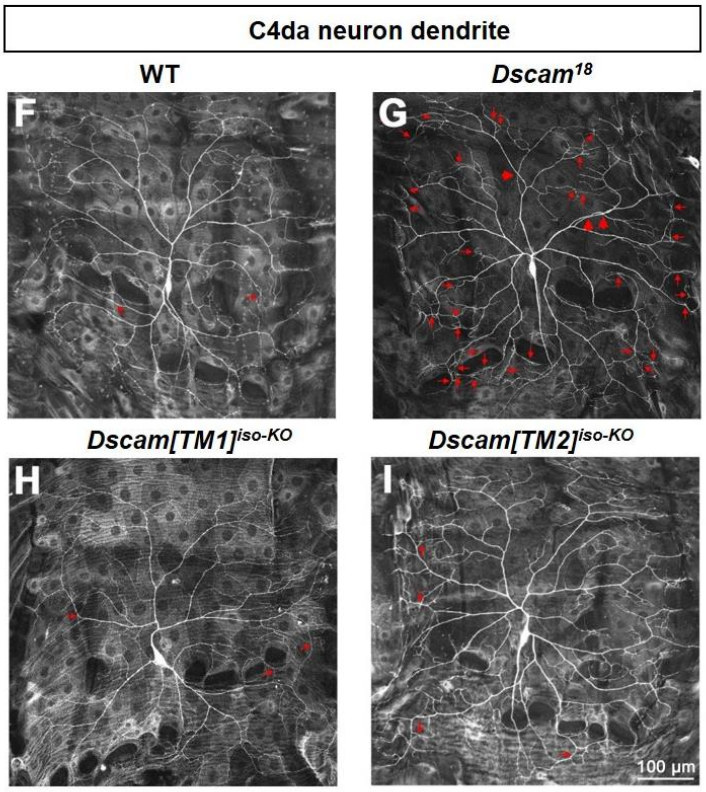
C4da neuron dendrite
WT
Dscam18
F
G
Dscam[TM1]iso-KO
Dscam[TM2]iso-KO
H
I
100 μm

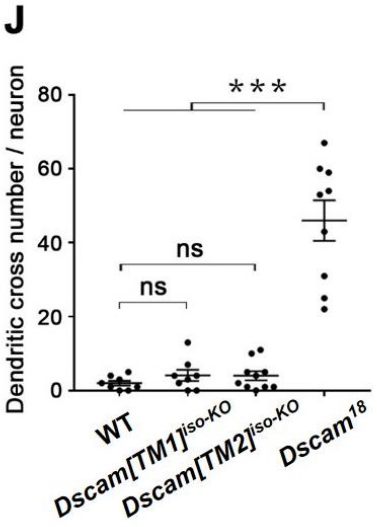
J
Dendritic cross number / neuron
80
60
40
20
0
***
ns
ns
WT
Dscam[TM1]iso-KO
Dscam[TM2]iso-KO
Dscam18

Figure 2.6. *isoTarget* uncovers redundant functions for Dscam[TM1] and [TM2] in dendrite self-avoidance.
(**A-D**) Dscam[TM1] and [TM2] function redundantly in mediating dendritic self-avoidance in C3da neuron. In 3rd instar larvae, C3da dendrites rarely fasciculate or intersect with each other in wild-type (WT) (**A**), while loss of both *Dscam[TM1]* and *[TM2]* isoforms (*Dscam[TM1/2]*$^{iso\text{-}KO}$) significantly impairs self-avoidance (**B**). Loss of either *Dscam[TM1]* (**C**) or *[TM2]* (**D**) does not affect dendritic self-avoidance. The red arrows point to dendritic crossing sites.
(**E**) Quantification of dendritic branch crossings in the C3da neuron ddaF.
(**F-I**) Dscam[TM1] and [TM2] function redundantly in mediating dendritic self-avoidance in C4da neurons. The MARCM technique was used. Small red arrows point to crossings of fine dendritic branches, and large red arrows point to crossings of major dendritic branches, which is only observed when both isoforms are lost.
(**J**) Quantification of dendritic branch crosses in the C4da neuron ddaC.

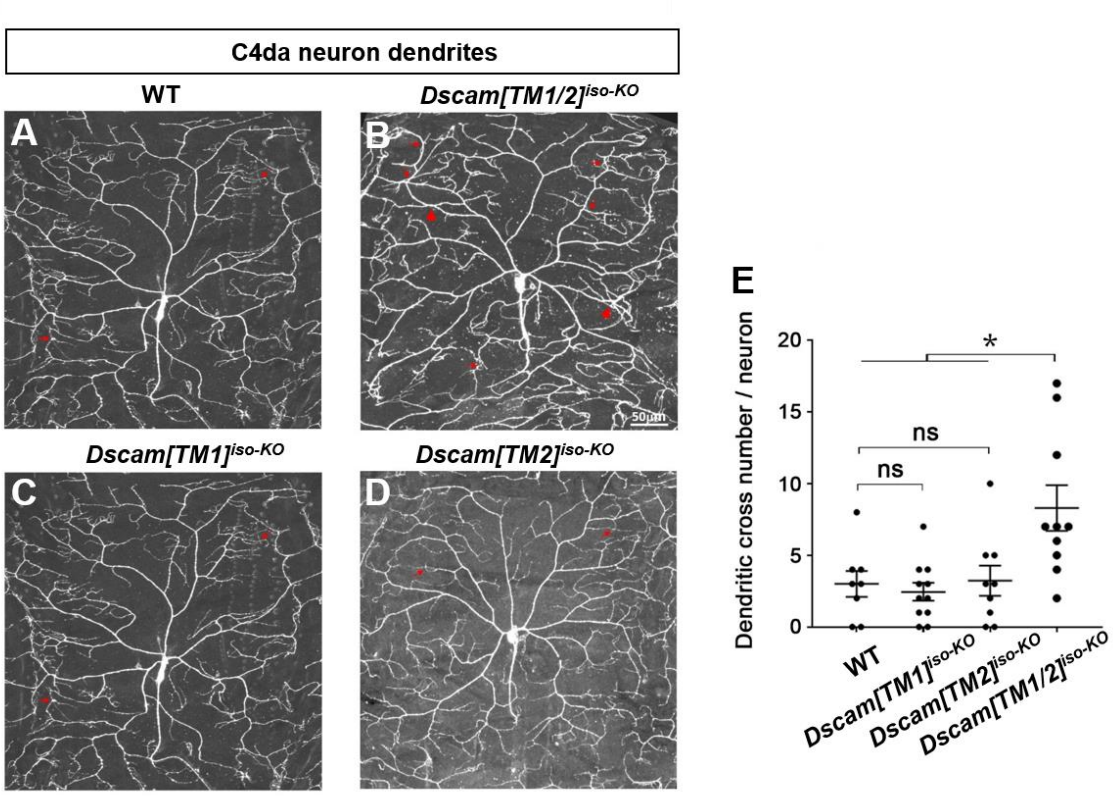

Figure 2.7. *Dscam[TM1]* and *[TM2]* function redundantly in mediating dendritic self-avoidance in C4da neurons.
(**A-D**) While *Dscam[TM1/2]*$^{iso\text{-}KO}$ (**B**) increases the crossing of dendritic branches in C4da neurons in 3rd instar larvae, neither *Dscam[TM1]*$^{iso\text{-}KO}$ nor *Dscam[TM2]*$^{iso\text{-}KO}$ impairs dendritic self-avoidance (**C** & **D**). Small red arrows point to crossings of fine dendritic branches, and large red arrows point to crossings of major dendritic branches, which is only observed when both isoforms are lost.
(**E**) Quantification of dendritic branch crosses in the C4da neuron ddaC.

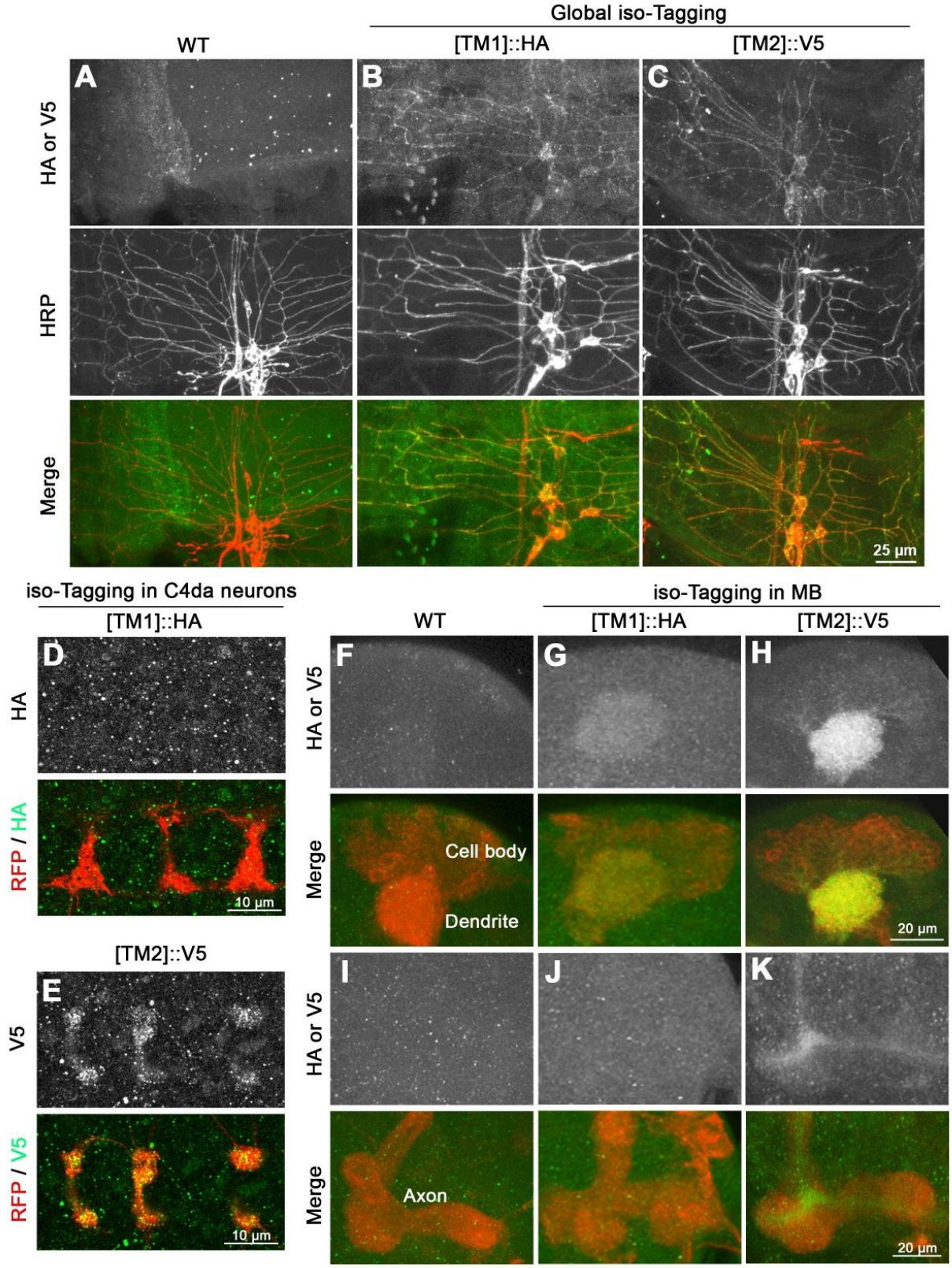
Global iso-Tagging
WT
[TM1]::HA
[TM2]::V5
A
B
C
HA or V5
HRP
Merge
25 µm
iso-Tagging in C4da neurons
[TM1]::HA
D
HA
RFP / HA
10 µm
[TM2]::V5
E
V5
RFP / V5
10 µm
iso-Tagging in MB
WT
[TM1]::HA
[TM2]::V5
F
G
H
HA or V5
Cell body
Dendrite
Merge
20 µm
I
J
K
HA or V5
Axon
Merge
20 µm

Figure 2.8. Using *isoTarget* to identify the subcellular localizations of endogenous Dscam isoforms.

(**A**-**C**) Both Dscam[TM1] and [TM2] are localized in the dendrites of larval PNS neurons. At early 2nd instar stage, compared with control (**A**), global iso-Tagging reveals the localization of endogenous [TM1] and [TM2] in the dendrites of PNS da neurons, which is double-labeled by the PNS neuron marker anti-HRP.

(**D** & **E**) iso-Tagging shows that endogenous Dscam[TM2], but not [TM1], is in the axon terminals of C4da neurons in early 2nd instar larvae. The C4da-specific driver *ppk*-Gal4 was used to tag endogenous Dscam[TM1] or [TM2] by driving the expression of UAS-R-recombinase and to label C4da axon terminals by driving the expression of UAS-mCD8::RFP.

(**F**-**H**) Both Dscam[TM1] and [TM2] are localized in the dendrites of CNS neurons. Iso-Tagging in mushroom body neurons shows that both endogenous [TM1] and [TM2] are present in MB calyx, which is a cluster of dendrites in 3rd instar larvae. The MB driver OK107-Gal4 was used to drive the expression of R recombinase for tagging endogenous Dscam[TM1] or [TM2] and the expression of mCD8::RFP for labeling MB morphology.

(**I**-**K**) Dscam[TM2], but not [TM1], is localized in MB axons. Compared to the WT control, endogenous Dscam[TM2], but not [TM1], is detected in the axon peduncles of MB in 3rd instar larvae.

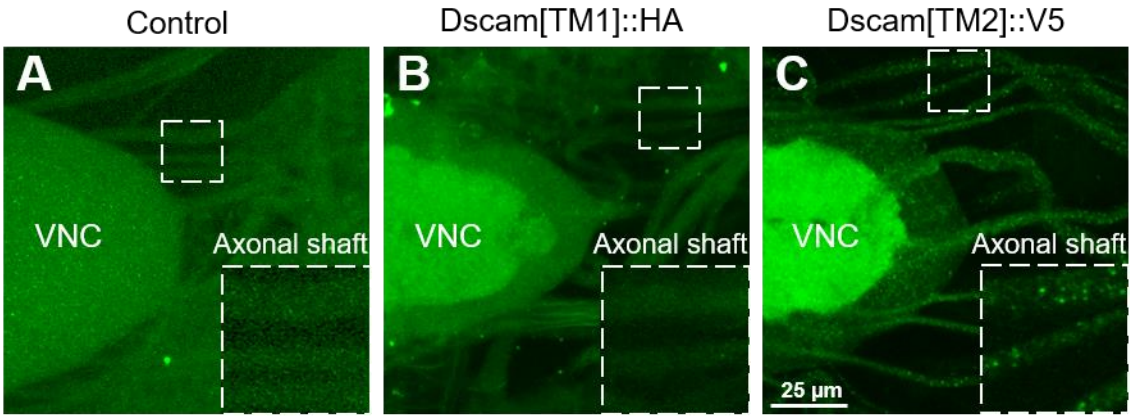

Figure 2.9. Endogenous Dscam[TM2], but not [TM1], is localized in axons connecting the CNS and PNS.
Endogenous Dscam[TM1] is observed in VNC neuropil region, but not in axonal shafts. By contrast, endogenous Dscam[TM2] is localized in axon shafts besides the VNC neuropil. The insets are magnified views of the boxed regions.

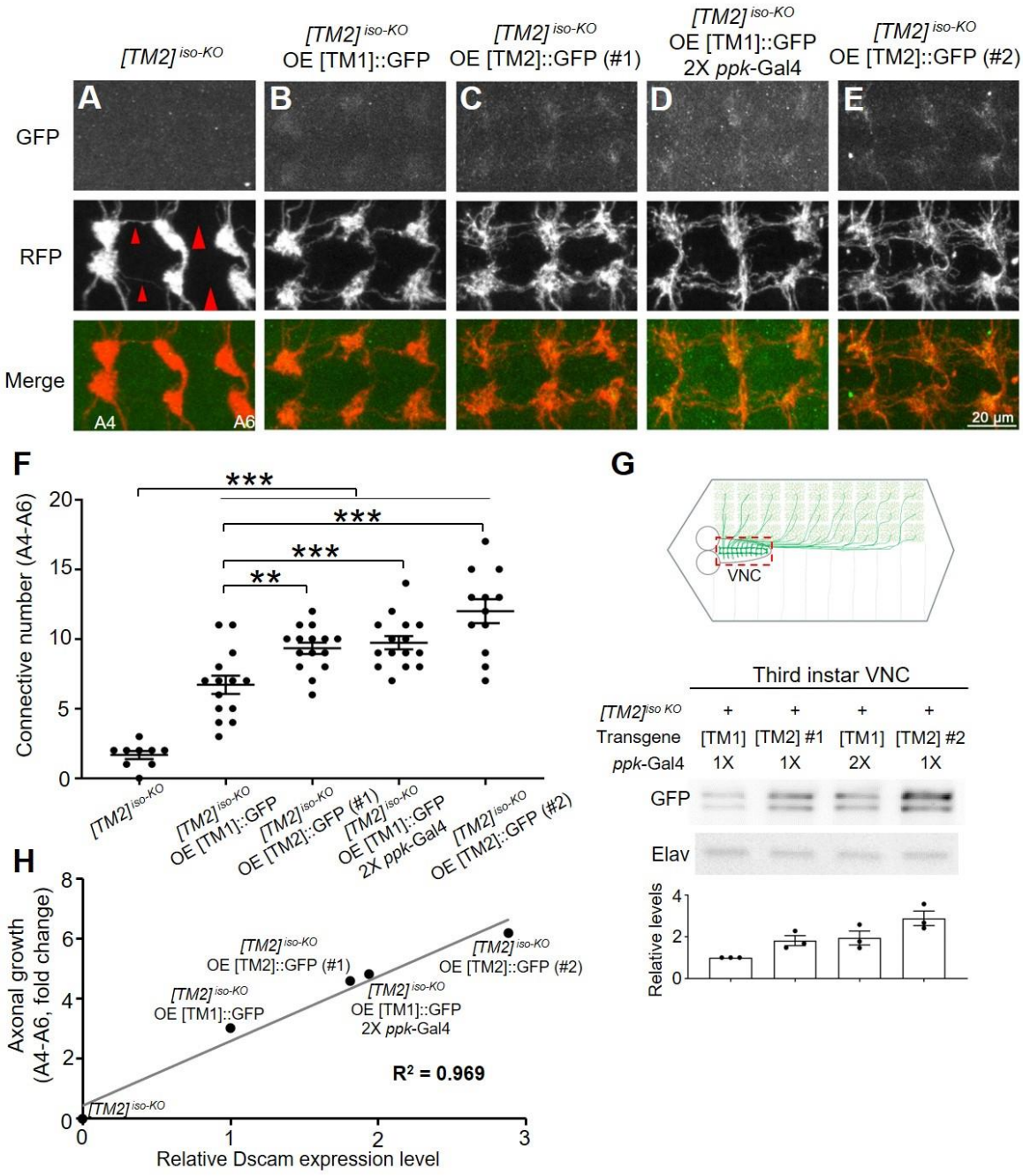
[TM2] iso-KO
[TM2] iso-KO OE [TM1]::GFP
[TM2] iso-KO OE [TM2]::GFP (#1)
[TM2] iso-KO OE [TM1]::GFP 2X ppk-Gal4
[TM2] iso-KO OE [TM2]::GFP (#2)
A
B
C
D
E
GFP
RFP
Merge
A4
A6
20 µm
F
Connective number (A4-A6)
***
***
***
**
G
VNC
Third instar VNC
[TM2]iso KO
Transgene
ppk-Gal4
[TM1] 1X
[TM2] #1 1X
[TM1] 2X
[TM2] #2 1X
GFP
Elav
Relative levels
H
Axonal growth (A4-A6, fold change)
Relative Dscam expression level
R² = 0.969

Figure 2.10. Dendrite-specific localization restrains endogenous Dscam[TM1] from functioning in axons.
(**A**) *Dscam[TM2]*$^{iso\text{-}KO}$ dramatically impairs the axon terminal growth in C4da neurons. The large red arrowheads point to the sites where longitudinal axon tracts are broken, and the small arrowheads point to where the tracts are thinned.
(**B**) Overexpression of a Dscam[TM1] transgene with a single copy of *ppk*-Gal4 leads to a low level of [TM1] in axon terminals and mitigates the axonal defect in [TM2] iso-KO.
(**C**) Overexpression of the Dscam[TM2]#1 transgene with a single copy of *ppk*-Gal4 also mitigates the axonal defect in [TM2] iso-KO.
(**D**) When the Dscam[TM1] transgene is driven by 2 copies of *ppk*-Gal4, it leads to higher levels of [TM1] in axon terminals than the overexpression driven by one copy of *ppk*-Gal4 and rescue effects that are comparable with [TM2] overexpression.
(**E**) Overexpression of the Dscam[TM2]#2 transgene with a single copy of *ppk*-Gal4 leads to higher levels and rescue effects than that of [TM1] in C4da axon terminals.
(**F**) Quantification of the number of C4da axon connectives in segments A4-A6.
(**G**) Quantitation of transgenic Dscam::GFP levels in C4da axon terminals. The experiments were done in *Dscam[TM2]*$^{iso\text{-}KO}$ larvae. As shown in the schematic (top, green drawings), UAS-Dscam::GFP transgenes were expressed in C4da neurons with the *ppk*-Gal4 driver. VNCs (indicated by the dashed red box in the top panel), which contained transgenic Dscam::GFP in C4da axon terminals, were dissected out from 3rd instar larvae for Western blotting. The bottom panel shows the Western blots of transgenic Dscam::GFP in the axon terminals of C4da neurons. The VNC lysates were used for Western blotting with anti-GFP and anti-Elav antibodies. The relative expression levels are GFP signals normalized by Elav signals. Each dot represents the result from one independent experiment. Overexpression of a [TM1] transgene resulted in a modest level of [TM1] in axon terminals, while two different [TM2] transgenes caused higher levels of [TM2] in axon terminals. Two copies of *ppk*-Gal4 increased the levels of [TM1] in axon terminals.
(**H**) The rescue of the axonal defect caused by loss of *Dscam* is proportional to the level of transgenic Dscam in C4da axon terminals, regardless of the isoform. The relative Dscam expression levels were determined by Western blotting of CNS lysates from larvae overexpressing [TM1]::GFP or [TM2]::GFP by *ppk*-Gal4 and plotted against the rescue effect of the transgene.

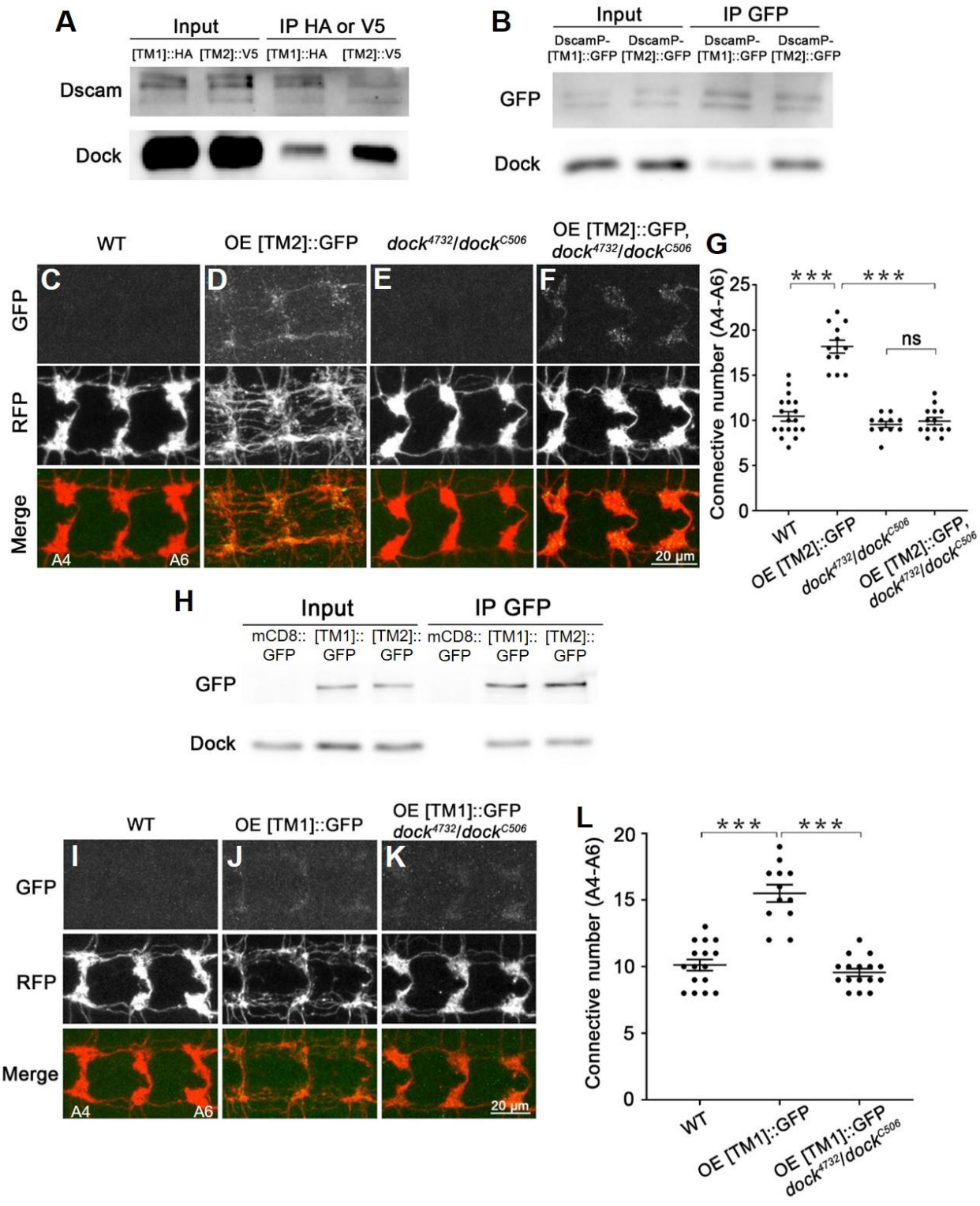
A
Input
IP HA or V5
[TM1]::HA
[TM2]::V5
[TM1]::HA
[TM2]::V5
Dscam
Dock
B
Input
IP GFP
DscamP-[TM1]::GFP
DscamP-[TM2]::GFP
DscamP-[TM1]::GFP
DscamP-[TM2]::GFP
GFP
Dock
WT
OE [TM2]::GFP
dock4732/dockC506
OE [TM2]::GFP, dock4732/dockC506
GFP
RFP
Merge
C
D
E
F
A4
A6
20 μm
G
Connective number (A4-A6)
***
***
ns
WT
OE [TM2]::GFP
dock4732/dockC506
OE [TM2]::GFP, dock4732/dockC506
H
Input
IP GFP
mCD8::GFP
[TM1]::GFP
[TM2]::GFP
mCD8::GFP
[TM1]::GFP
[TM2]::GFP
GFP
Dock
WT
OE [TM1]::GFP
OE [TM1]::GFP dock4732/dockC506
GFP
RFP
Merge
I
J
K
A4
A6
20 μm
L
Connective number (A4-A6)
***
***
WT
OE [TM1]::GFP
OE [TM1]::GFP dock4732/dockC506

Figure 2.11. Dscam[TM1] and [TM2] exhibit similar biochemical properties and cellular functions when they are localized in the same subcellular compartment.
(**A** & **B**) Dock preferentially interacts with endogenous Dscam[TM2] *in vivo*. (**A**) Brain lysates of larvae with global iso-Tagging of [TM1]::HA or [TM2]::V5 were immunoprecipitated by anti-HA or V5 beads, respectively, and immunoblotted with an anti-Dscam antibody that recognizes both [TM1] and [TM2] and an anti-Dock antibody. This experiment was repeated twice independently. (**B**) Brain lysates of larvae that expressed [TM1]::GFP or [TM2]::GFP through the endogenous *Dscam* promoter were immunoprecipitated by an anti-GFP antibody. The immunoprecipitates were immunoblotted with anti-GFP and anti-Dock antibodies. This experiment was repeated three times independently.
(**C**-**F**) Dscam[TM2] requires Dock to promote presynaptic terminal growth. Shown are representative images of A4-A6. Overexpressing a Dscam[TM2]::GFP transgene significantly promotes axonal growth in C4da neurons (**C** & **D**). While loss of *dock* does not affect C4da axon terminals (**E**), it completely abolishes the overgrowth caused by Dscam[TM2]::GFP overexpression (**F**).
(**G**) Quantification of the number of C4da axon connectives.
(**H**) Dock binds to [TM1] and [TM2] in similar affinity in cultured S2 cells. Lysates of S2 cells expressing mCD8::GFP, Dscam[TM1]::GFP or [TM2]::GFP were immunoprecipitated with an anti-GFP antibody. Inputs and immunoprecipitates were blotted by anti-GFP and anti-Dock antibodies. This experiment was repeated three times independently.
(**I**-**K**) Transgenic Dscam[TM1] requires Dock to promote presynaptic terminal growth. Compared to WT (**I**), overexpressing [TM1]::GFP transgene significantly promotes axonal growth in C4da neurons (**J**), which is completely abolished by loss of *dock* (**K**).
(**L**) Quantification of the number of C4da axon connectives from A4-A6.

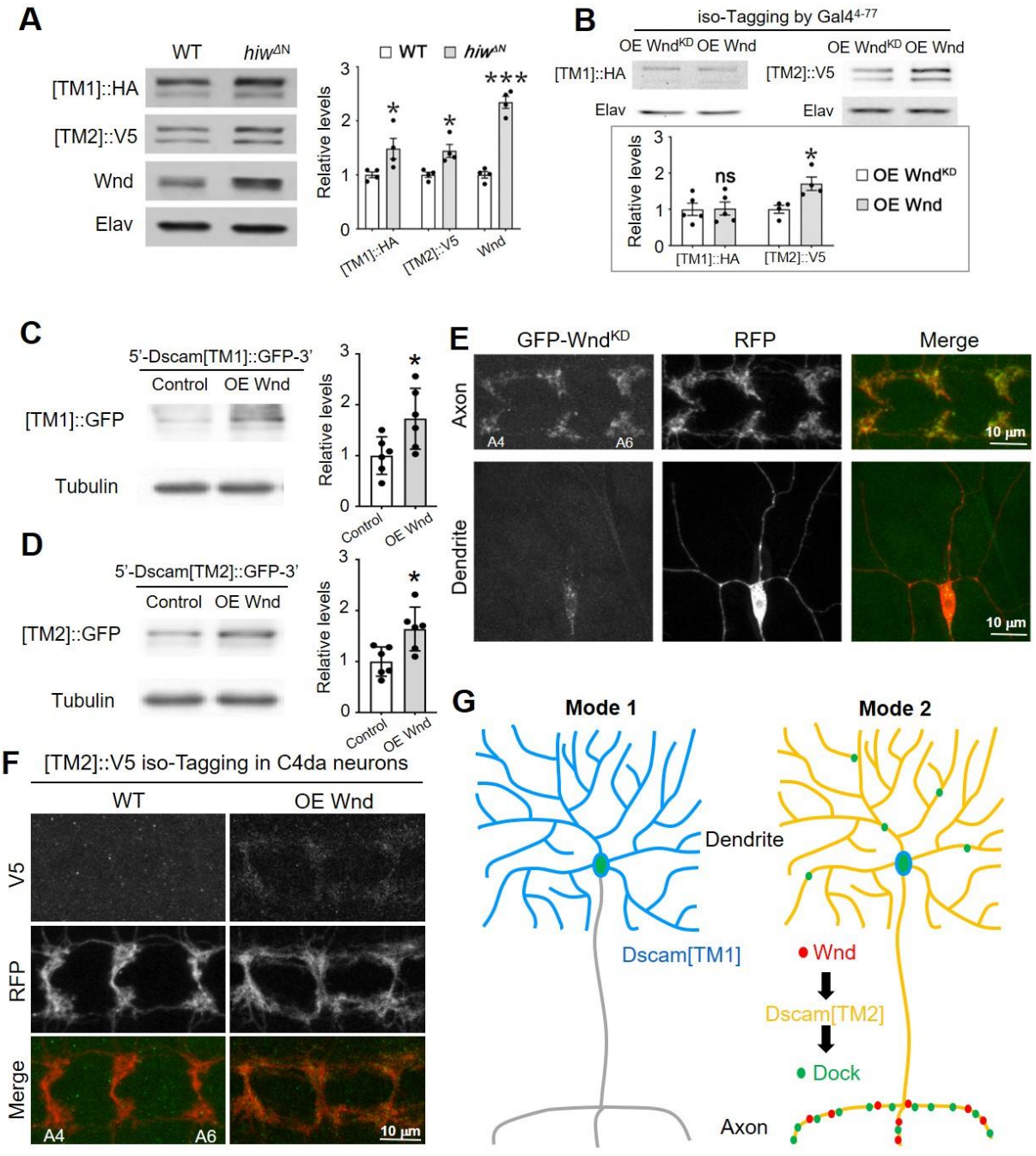
A
WT
hiwΔN
[TM1]::HA
[TM2]::V5
Wnd
Elav
Relative levels
[TM1]::HA
[TM2]::V5
Wnd
B
iso-Tagging by Gal4 4-77
OE WndKD OE Wnd
[TM1]::HA
[TM2]::V5
Elav
ns
OE WndKD
OE Wnd
C
5'-Dscam[TM1]::GFP-3'
Control
OE Wnd
[TM1]::GFP
Tubulin
D
5'-Dscam[TM2]::GFP-3'
[TM2]::GFP
E
GFP-WndKD
RFP
Merge
Axon
Dendrite
A4
A6
10 µm
F
[TM2]::V5 iso-Tagging in C4da neurons
WT
OE Wnd
V5
RFP
Merge
G
Mode 1
Mode 2
Dendrite
Dscam[TM1]
Wnd
Dscam[TM2]
Dock
Axon

Figure 2.12. Axonal enrichment of Wnd compartmentalizes Wnd-Dscam[TM2] signaling.
(**A**) Hiw suppresses the expression of both Dscam[TM1] and [TM2]. In the brains of 3rd instar larvae that were trans-heterozygotes of global iso-Tagging of [TM1]::HA and [TM2]::V5, loss of *hiw* (*hiw*$^{\Delta N}$) elevated the levels of both endogenous [TM1] and [TM2]. Left: Western blots; Right: quantification of Western blots. Each dot represents the result from one independent experiment.
(**B**) Overexpression of Wnd increases the levels of Dscam[TM2], but not that of [TM1]. Top: The Gal4$^{4\text{-}77}$, which is expressed in a small set of PNS neurons and a number of CNS neurons, was used to drive the expression of R recombinase for iso-Tagging and the overexpression of Wnd. Compared with a kinase-dead Wnd transgene (Wnd^{KD}), overexpressing Wnd does not affect endogenous Dscam[TM1] levels (left), but significantly increases Dscam[TM2] levels (right) in 3rd-instar larval brains. Bottom: quantification of Western blots. Each dot represents the result from one independent experiment.
(**C**) Overexpression of Wnd increases endogenous Dscam[TM2] levels in the presynaptic terminals of C4da neurons. At the 3rd instar larval stage, Dscam[TM2]::V5$^{iso\text{-}Tagging}$ is no longer detectable in C4da axon terminals. Overexpression of Wnd elevates the level of Dscam[TM2]::V5$^{iso\text{-}Tagging}$ in these terminals.
(**D, E**) Wnd similarly promotes [TM1] and [TM2] expression in cultured S2 cells. S2 cells are transfected with plasmids expressing Wnd and [TM1]::GFP or [TM2]::GFP with endogenous *Dscam* 5' and 3' UTR. Lysates of S2 cells were blotted by anti-GFP and anti-tublin antibodies. Each dot represents the result from one independent experiment.
(**F**) Wnd is enriched in axons. GFP-tagged kinase-dead Wnd (GFP::Wnd^{KD}) was expressed in C4da neurons by *ppk*-Gal4. mCD8::RFP was used to label the neurons. While GFP::Wnd^{KD} signal is enriched in axon terminals, little is observed in dendrites. Yellow arrows point to major dendritic branches.
(**G**) Subcellular localization expands the functional diversity of splicing isoforms via two different modes. In Mode 1, the localization of an isoform in a particular subcellular location (e.g., Dscam[TM1] in dendrites) restrains this isoform from functioning in other compartments. In Mode 2, the enrichment of the functional partners (e.g., Wnd and Dock) for a ubiquitously localized isoform (e.g., Dscam[TM2]) leads to isoform-specific subcellular signaling and functions.

Chapter 3

Dscam Gene Triplication Causes Neocortical Overinhibition in Down Syndrome

This chapter is modified after a research article that is under revision for publication with authors listed as Hao Liu, René N. Caballero-Florán, Tao Yang, Jacob M. Hull, Geng Pan, Ruonan Li, Macy Veling, Lori L. Isom, Kenneth Y. Kwan, Z. Josh Huang, Peter G. Fuerst, Paul M. Jenkins and Bing Ye.

3.1 Abstract

A growing number of molecules have been identified as regulators of inhibitory synapse development, but whether dysregulated expression of these molecules contribute to brain disorders is poorly understood. Here we show that Down syndrome cell adhesion molecule (Dscam) regulates the inhibition of neocortical pyramidal neurons (PyNs) in a level-dependent fashion. Loss of *Dscam* impairs inhibitory neuron development and function. In the Ts65Dn mouse model for Down syndrome, where Dscam is overexpressed, GABAergic innervation of cortical PyNs by chandelier and basket cells is increased. Genetic normalization of Dscam expression rescues the excessive GABAergic innervation and the increased inhibition of PyNs. These findings demonstrate excessive GABAergic innervation and inhibition in the neocortex of Down syndrome mouse model and identify Dscam overexpression as the cause. They also

implicate dysregulated Dscam levels as a potential pathogenic driver in related neurological disorders.

3.2 Introduction

GABAergic neurons mediate synaptic inhibition in the mammalian brain (Tremblay, Lee, and Rudy 2016; Lim et al. 2018), and altered GABAergic inhibition has emerged as a nexus of circuit dysfunction in a number of neurodevelopmental disorders (Chattopadhyaya and Cristo 2012; Ramamoorthi and Lin 2011). A growing number of molecules have been identified in GABAergic synapse formation and synaptic transmission (Ko, Choii, and Um 2015; Ramamoorthi and Lin 2011; Dalva, McClelland, and Kayser 2007; de Wit and Ghosh 2016; Krueger-Burg, Papadopoulos, and Brose 2017; Sudhof 2018). Intriguingly, copy number variations of these genes are commonly found in different neurological diseases (Ko, Choii, and Um 2015), suggesting that dysregulated expression of these genes might be a pathogenic driver. However, whether or not this is true remains largely unknown.

Down syndrome cell adhesion molecule (Dscam) is an evolutionarily conserved type I transmembrane protein (Yamakawa et al. 1998). In humans, *Dscam* gene is localized in the Down syndrome critical region on chromosome 21 (hCh21) (Yamakawa et al. 1998). We previously showed in *Drosophila* that Dscam protein levels determine the sizes of presynaptic terminals without requiring the ectodomain diversity of the *Drosophila Dscam* gene (Kim et al. 2013). Moreover, others reported that overexpression of Dscam impairs synaptic targeting and transmission in *Drosophila* (Cvetkovska et al. 2013; Lowe, Hodge, and Usowicz 2018). These findings suggest that dysregulated Dscam levels might contribute to neuronal defects in brain disorders. In fact, altered Dscam expression levels have been reported in multiple brain disorders, including Down syndrome (DS) (Saito et al. 2000), autism spectrum disorders (ASD) (O'Roak et al. 2014; Krumm et al. 2015; Turner et al. 2016), intractable epilepsy (Shen et al. 2011), bipolar disorder (Amano et al. 2008), and possibly Fragile X syndrome (Brown et al.

2001; Darnell et al. 2011; Kim et al. 2013; Cvetkovska et al. 2013). Although recent findings suggest a conserved role of *Dscam* in promoting presynaptic growth in vertebrates (Santos et al. 2018; Bruce et al. 2017), whether dysregulated Dscam expression results in neuronal defects in brain disorders remains unknown.

In this work, we sought to determine the effects of altered expression levels of Dscam in mouse models of DS, in which the *Dscam* gene is triplicated. Previous studies have shown that enhanced GABAergic inhibition impairs cognition in Ts65Dn mice (Fernandez et al. 2007; Colas et al. 2013b; Braudeau, Dauphinot, et al. 2011; Braudeau, Delatour, et al. 2011; Martinez-Cue et al. 2013), the most widely used DS animal model (Reeves et al. 1995; Rueda, Florez, and Martinez-Cue 2012). A series of studies have demonstrated excessive GABAergic inhibition in the hippocampus of Ts65Dn mice (Fernandez and Garner 2008; Kleschevnikov, Belichenko, Faizi, et al. 2012; Kleschevnikov, Belichenko, Gall, et al. 2012; Kleschevnikov et al. 2004; Costa and Grybko 2005; Siarey et al. 1997; Fernandez et al. 2007; Contestabile, Magara, and Cancedda 2017; Haydar and Reeves 2012; Chakrabarti et al. 2010). However, whether GABAergic signaling is altered in other brain regions and, if it is, what genes on hCh21 cause it, are poorly understood. Here, by combining recently developed genetic tools for sparse labeling and whole-cell patch-clamp, we found excessive GABAergic innervation and inhibition of PyNs by chandelier (ChC) and basket cells in the neocortex of Ts65Dn mice. Genetic normalization of Dscam expression levels rescued the presynaptic overgrowth and excessive synaptic transmission of GABAergic neurons. Consistently, loss of *Dscam* impaired ChC presynaptic terminals and reduced GABAergic inhibition of neocortical PyNs. In addition, we found that ChC axon terminal growth and synaptogenesis are coupled and positively correlated with neocortical Dscam levels in both wide-type and Ts65Dn mice. These findings uncover novel

molecular, cellular and synaptic mechanisms for DS brain disorders and highlight the critical role of Dscam levels in regulating neocortical inhibition. Dysregulated Dscam expression levels may be a common contributor to GABAergic dysfunctions in associated neurological diseases.

3.3 Results

Loss of *Dscam* impairs ChC presynaptic development in mice

To determine whether Dscam regulates GABAergic neuron development in the neocortex, we focused the analysis on ChCs for two reasons. First, ChCs are thought to be the most potent inhibitory neurons in the neocortex (DeFelipe 1999). Each ChC innervates roughly two hundred PyNs at their axon initial segments (AIS) (Blazquez-Llorca et al. 2015), where action potentials are generated (Szentagothai 1975b; Jones 1975). Second, the morphology of ChCs is relatively stereotypical and reliably quantifiable (Fazzari et al. 2010; Tai et al. 2014; Favuzzi et al. 2019; Yang et al. 2018). We specifically label single ChCs in the neocortex by crossing the Nkx2.1-CreER mouse line with the tdTomato reporter line Ai14 (Taniguchi, Lu, and Huang 2013)(Figure 3.1A). A single ChC extends only a few dendritic branches but several hundreds of presynaptic terminals, called axonal cartridges, each of which innervates one or two PyNs (Inan and Anderson 2014). The axonal cartridges and presynaptic boutons of single ChCs were quantified in a three-dimensional volume defined based on the position of ChC cell body (Figure 3.2). AIS-colocalized cartridges and presynaptic boutons were quantified, as off-target varicosities lack presynaptic markers and symmetric synaptic densities (Steinecke et al. 2017). The AIS was immunolabeled by an anti-phospho-IκB antibody (pIκB) (Taniguchi, Lu, and Huang 2013; Lu et al. 2017; Tai et al. 2014; Fazzari et al. 2010), which strongly correlates with the AIS labeled by ankyrin-G antibodies in the mouse neocortex (Buffington et al. 2012) (Figure 3.3). Quantification was performed in a double-blinded fashion to avoid experimenters' bias. The ChCs in the cortical layer II and III of the anterior cingulate cortex (ACC) were analyzed as the morphology of ChCs in this region is most stereotypical. Mice were analyzed on postnatal day 28 (P28), a time after ChC development is complete (Inan and Anderson 2014).

Similar to its role in presynaptic development in *Drosophila*, loss of Dscam significantly impeded the development of ChC presynaptic terminals (Figures 3.1B-E). Compared to heterozygous littermates, the number and length of individual cartridges were significantly reduced in Dscam-/- mice by 8% and 12%, respectively, so that the total cartridge length for each ChC was reduced by 23% (Figures 3.1C-E). Moreover, the numbers and sizes of presynaptic boutons were significantly reduced by 20% and 16%, respectively (Figures 3.1F-H). Interestingly, no difference was observed in the interbouton distance between these two groups (Figure 3.4A), indicating that Dscam does not regulate bouton density. These results demonstrate that Dscam is required for ChC presynaptic development in mice.

Loss of Dscam impaired GABAergic inhibition of PyNs

To determine whether defective GABAergic synaptogenesis caused by loss of Dscam impairs GABAergic synaptic transmission, whole-cell patch-clamp was applied to record PyNs in layers II/III of the ACC from acute neocortical brain slices. Consistent with impaired axonal growth and synaptogenesis in ChCs, we found that the average frequency of miniature inhibitory postsynaptic currents (mIPSCs) was ~35% less in Dscam-/- mice than that in heterozygous littermates (Figures 3.5A-B). In addition, the average amplitude of mIPSCs was 42% less, - suggesting that postsynaptic responses were impaired by loss of Dscam (Figures 3.5A and C). Similar changes were observed in the frequency and amplitude of spontaneous IPSC (sIPSCs) (Figures 3.5D-F).

Consistent with the reduced GABAergic transmission, we observed hyperactivity in neocortical PyNs, as indicated by c-fos expression levels (Herrera and Robertson 1996). There was 5-fold more c-fos-positive PyNs in Dscam-/- than in Dscam+/- mice (Figures 3.5G-H).

Taken together, these data suggest that Dscam is required for the normal level of inhibition of PyNs in the neocortex.

ChCs exhibit excessive presynaptic terminals and boutons in Ts65Dn mice

Next, we determined whether the presynaptic development of ChCs is altered in the Ts65Dn mouse model of DS, where Dscam is present in 3 copies (Reeves et al. 1995) and overexpressed (Figure 3.6). Compared to euploid littermates, the number and length of individual axonal cartridges were significantly increased in Ts65Dn mice by 28% and 11%, respectively (Figures 3.7A-C). The total cartridge length, which is the sum of individual cartridges in the quantified volume, was increased by 37% (Figure 3.7D). In addition, ChC showed a significant increase in both the number and size of synaptic boutons in Ts65Dn mice. The bouton number for each ChC is increased by 36% (Figures 3.7E-F). The average size of presynaptic boutons was enlarged by 21% (Figures 3.7E and G). The increased ChC presynaptic bouton number and size are consistent with previous reports of increased number of the puncta positive of vesicular GABA transporter proteins (VGAT) and enlarged inhibitory synapses in the neocortex of Ts65Dn mice (Kurt et al. 2000; Nosheny et al. 2015). The average interbouton distance between neighboring boutons showed a significant, though subtle, decrease in the trisomy mice (Figure 3.4B), suggesting a slight increase in bouton density. Altogether, by labeling and quantifying single interneurons in the ACC, we found excessive presynaptic terminals and boutons in Ts65Dn mice, which is opposite of what we observed in Dscam-/- mice.

Normalization of Dscam levels rescues ChC presynaptic overgrowth in Ts65Dn mice

Dscam is overexpressed in both the brains of DS patients and those of Ts65Dn mouse model of DS (Saito et al. 2000) (Figure 3.6). Previous studies in *Drosophila* have demonstrated that increased levels of Dscam lead to excessive growth of presynaptic terminals (Kim et al. 2013; Sterne, Kim, and Ye 2015b). To determine whether the overexpressed Dscam in Ts65Dn mice causes presynaptic overgrowth in ChCs, we normalized Dscam gene dosage in Ts65Dn mice by crossing female Ts65Dn mice with male Dscam+/- mice to obtain the Ts65Dn:Dscam+/+/- genotype (Figure 3.8A). This genetic scheme also yielded regular Ts65Dn littermates (Ts65Dn:Dscam+/+/+). In Ts65Dn mice with two copies of functional Dscam genes, the average levels of Dscam proteins were statistically indistinguishable from the euploid mice (Figure 3.8B).

Normalizing Dscam levels rescued ChC presynaptic overgrowth in Ts65Dn mice. Compared with Ts65Dn littermates, the ChC cartridge number, individual cartridge length and total cartridge length were reversed to levels indistinguishable from euploid in Ts65Dn:Dscam+/+/- mice (Figures 3.8C-F). In addition, the increased bouton number and bouton size were mostly rescued by normalizing Dscam expression (Figures 3.8G-I), while no change was observed in the interbouton distance (Figure 3.4B). These results demonstrate that ChC presynaptic terminal overgrowth is mainly caused by Dscam overexpression in Ts65Dn mice.

ChC axon terminal growth and synaptogenesis are positively coupled

Presynaptic terminal growth and synaptogenesis are concurrent processes for forming proper neuronal connections (Javaherian and Cline 2005). Little is known about whether and how these two events are orchestrated in mammalian GABAergic interneurons. The sparse

labeling of ChCs offers an opportunity to address these questions at the single-cell resolution. We examined the relationship between cartridge length and three morphological aspects of synaptic boutons, namely bouton number, size, and density (as reflected by the interbouton distance), in single ChCs. We found a strong correlation between the cartridge length and the bouton number of each ChC in both wild-type (euploid) ($R2 = 0.82$, $p < 10\text{-}7$) and Ts65Dn mice ($R2 = 0.79$, $p < 10\text{-}15$) (Figure 3.9A). Although Dscam positively regulated both cartridge length and bouton number (Fig. 3.1E, G and Fig. 3.8F, H), loss of Dscam did not impair their coupling ($R2 = 0.89$, $p < 10\text{-}8$) (Figure 3.9B). There was also a significant correlation between cartridge length and bouton size in both wild-type and Ts65Dn mice (Figure 3.9C), though it was weaker than that between cartridge length and bouton number. Loss of Dscam seemed to mildly impair the coupling between cartridge length and bouton size (Figure 3.9D). There was no correlation between cartridge length and bouton density in any of the genotypes tested (Figures 3.9E and F). Taken together, these results suggest that presynaptic terminal growth and synaptogenesis are positively coupled in ChC development.

ChC presynaptic cartridge length and synaptogenesis are proportional to neocortical Dscam levels

In *Drosophila*, Dscam levels determine the size of presynaptic arbors (Kim et al. 2013). Western blotting results suggested that Dscam levels in the neocortex exhibited individual variations in euploid, Ts65Dn, and Ts65Dn:Dscam+/+/- mice (Figure 3.8B and 3.10A). We plotted the neocortical Dscam level of each mouse, as assayed by western blotting, against the average cartridge length, bouton number, size or density in each mouse. We observed a strong correlation between Dscam levels and cartridge lengths, bouton number and bouton sizes in mice

(Figures 3.10B-D). In contrast, no correlation was found between Dscam levels and interbouton distance (Figure 3.10E), again supporting that bouton density is not regulated by Dscam (Figures 3.4A-B). The dosage-dependence highlights the importance of Dscam expression levels in regulating ChC presynaptic development.

Dscam overexpression increases the number of GABAergic synapses on PyN somas in Ts65Dn mice

Dscam is expressed in different subtypes of GABAergic neurons (Paul et al. 2017). Does its overexpression in Ts65Dn mice cause developmental defects in other types of GABAergic neurons? Basket cells are the most common cortical interneurons that preferentially innervate the somas of PyNs (Tremblay, Lee, and Rudy 2016; Lim et al. 2018). Because basket cell morphology is highly heterogeneous (Wang, Gupta, et al. 2002), we analyzed the GABAergic synapses formed by basket cells on PyN soma (i.e., perisomatic synapses), rather than quantifying the morphology of single basket cells as we did on ChCs. To visualize perisomatic GABAergic synapses, brain sections were triply labeled with anti-Bassoon (for presynaptic active zone) (Dieck et al. 1998), anti-VGAT (for presynaptic GABAergic boutons) (Chaudhry et al. 1998), and anti-GRASP1 (for PyN soma and proximal dendrites) (Ye et al. 2000). Most Bassoon+ puncta around a PyN soma were surrounded by or overlapped with VGAT signals (Figure 3.11A). We found that the average number of GABAergic synapses around each PyN soma—as indicated by Bassoon+ puncta that were either apposed to or overlapped with VGAT+ signals—was 20% more in Ts65dn neocortices than euploid controls (Figures 3.12A-B). Strikingly, normalizing Dscam expression level completely rescued the enhanced synaptogenesis

(Figures 3.12B-D). These data suggest that the overexpressed Dscam in Ts65Dn mice also increases the number of GABAergic synapses on PyN somas.

Normalizing Dscam levels rescues the excessive GABAergic synaptic transmission in the Ts65Dn neocortex

Previous studies in Ts65Dn neocortices have demonstrated enhanced GABAergic neurogenesis (Chakrabarti et al. 2010), increased numbers of GABAergic synapses (Nosheny et al. 2015), and enlargement of these synapses (Kurt et al. 2000). However, whether GABAergic synaptic transmission in the neocortex is increased in these mice remains to be determined. Our finding that the overexpressed Dscam in Ts65Dn mice increased GABAergic synaptogenesis in the neocortex prompted us to test this possibility.

We examined GABAergic synaptic transmission in acute neocortical brain slices, using the whole-cell patch-clamp technique to record from PyNs in layers II/III of the ACC. We found that mIPSC frequency was increased by ~63% in Ts65Dn mice compared to euploid littermates (Figures 3.12E-F). These results suggest an increase in presynaptic neurotransmitter release and align well with our findings of enhanced synaptogenesis in ChCs and basket cells (Figures 3.7E-G and 3.12A-D). By contrast, we found no difference in mIPSC amplitudes between euploid littermates and Ts65Dn mice (Figures 3.12E, G), suggesting that postsynaptic responses may not be affected by the trisomy. Consistent with the role of Dscam in the excessive synaptogenesis in Ts65Dn mice (Figures 3.8G-I), normalizing Dscam expression prevented the increase in mIPSC frequency in these mice (Figure 3.12E-F), suggesting that the overexpressed Dscam causes excessive GABAergic synaptic transmission in the Ts65Dn neocortex. Similar changes in the

frequency, but not amplitude, were observed in spontaneous inhibitory postsynaptic currents (sIPSCs) among euploid, Ts65Dn, and Ts65Dn:Dscam+/+/- mice (Figure 3.12H-J).

Notably, normalizing Dscam levels did not rescue the increased parvalbumin-expressing (PV+) neuron density in the ACC region of Ts65Dn mice (Figures 3.13A-B). Consistently, the number of PV+ neurons was unaffected by loss of Dscam (Figures 3.13C-D). Thus, the overexpressed Dscam in the Ts65Dn neocortex causes excessive GABAergic synaptic transmission by increasing the number of GABAergic synapses without affecting the number of PV+ GABAergic neurons.

3.4 Discussion

In this study, we provide evidence for the important role of Dscam expression levels in the pathogenesis of brain disorders in DS. We show that Dscam overexpression leads to prominent presynaptic overgrowth in ChCs and basket cells. The hyperinnervation and excessive GABAergic inhibition of PyNs in Ts65Dn were rescued by normalizing the Dscam levels. The converse phenotypes were observed in Dscam loss-of-function mutant mice. The sensitivity of GABAergic synapse development and function to Dscam expression levels suggest that dysregulated Dscam expression may underlie GABAergic dysfunction in neurological disorders that exhibit abnormal Dscam expression, including DS, ASDs, intractable epilepsy, bipolar disorders and, possibly, Fragile X syndrome.

Dscam expression levels determine presynaptic terminal sizes in mammalian neurons

The stereotypical morphology of ChCs axon arbors and presynaptic terminals are advantageous for quantitative assessment (Fazzari et al. 2010; Tai et al. 2014). Moreover, recent advances in genetic labeling of ChCs have allowed sparse labeling of single ChCs for quantifying presynaptic terminals at single-cell resolution (Taniguchi, Lu, and Huang 2013; Wang et al. 2019). By taking advantage of this system, we show in this study that Dscam overexpression causes presynaptic overgrowth of ChCs in the neocortex. Notably, ChC cartridge length and synaptogenesis are proportional to neocortical Dscam expression levels, suggesting the sensitivity of ChC development to Dscam levels. Thus, this work supports a conserved role of Dscam in regulating presynaptic terminal growth in *Drosophila* and mice.

The coupling between presynaptic terminal growth and synaptogenesis in ChCs

Among the different types of GABAergic neurons, ChCs are thought to be the most powerful inhibitory neurons in the neocortex (DeFelipe 1999). These neurons form unique axo-axonic GABAergic synapses that selectively innervate PyNs at their AIS, where action potentials are generated (Szentagothai 1975b; Jones 1975); each ChC innervates roughly two hundred PyNs (Blazquez-Llorca et al. 2015). Impaired ChC presynaptic growth is present in individuals with epilepsy and schizophrenia, both of which are thought to be caused, in part, by disrupted GABAergic signaling (DeFelipe 1999; Woo et al. 1998; Nakazawa et al. 2012; Lewis et al. 2012; Lewis 2014). Recent studies demonstrate that deleting Erbb4, a schizophrenia-associated gene, in ChCs causes a schizophrenia-like phenotype in mice, indicating a causal relationship between ChC defects and schizophrenia (Del Pino et al. 2013; Yang et al. 2018). In addition to ErbB4, Neuregulin 1, DOCK7, Fgf13 and L1CAM have also been found to regulate the synapse formation between ChCs and PyNs (Fazzari et al. 2010; Tai et al. 2014; Favuzzi et al. 2019; Tai et al. 2019).

In the present study, detailed investigation of the cartridge growth and synaptogenesis at single-cell resolution uncovered several interesting features of ChC development. First, presynaptic cartridge growth is strongly associated with bouton number and, to a lesser extent, bouton size (Figure 3.9A-D). This observation supports the synaptotropic model proposing that synaptogenesis stabilizes axonal arbor growth in neurodevelopment (Cline and Haas 2008). Second, the factors that regulate cartridge growth and synaptogenesis are not necessarily the factors coupling these two processes. Although Dscam regulates both cartridge growth and bouton number, the coupling of these two processes remains intact in mice that are deficient of Dscam function, suggesting that Dscam is not the coupling factor. Identifying and distinguishing

coupling factors from regulators is an important step toward a mechanistic understanding of ChC development.

Dscam overexpression leads to excessive neocortical inhibition in DS mouse model

Overproliferation of GABAergic neurons caused by triplication of Olig1 and Olig2 contributes to excessive GABAergic signaling in the hippocampus (Chakrabarti et al. 2010; Contestabile, Magara, and Cancedda 2017; Haydar and Reeves 2012). However, several lines of evidence suggest that heterogeneous etiology may exist in DS brain disorders such that different brain regions exhibit distinct molecular, cellular, and physiological defects. For example, mIPSC frequency is increased in the dentate gyrus, but not the CA1 region, of the hippocampus in adult Ts65Dn mice (Chakrabarti et al. 2010; Kleschevnikov, Belichenko, Gall, et al. 2012). In contrast to the large body of literature on GABAergic signaling in the hippocampus of DS animal models, very little is known about whether GABAergic signaling is altered in the neocortex. Previous studies showed that the sizes of synaptic boutons and inhibitory synapses are enlarged in the neocortex of Ts65Dn mice, suggesting possible alterations in GABAergic synaptic functions in the neocortex (Belichenko et al. 2009; Kurt et al. 2000; Belichenko et al. 2004). In the present study, we demonstrate that GABAergic inhibition of neocortical PyNs is excessive in Ts65Dn mice and that Dscam overexpression plays a key role in this process.

Our results support the notion that alterations in GABAergic signaling in DS brains are region-specific. Normalizing Dscam expression reverses both increased mIPSC and sIPSC rates in neocortical PyNs (Figures 3.12E-J), while normalizing Olig1 and Olig2 expression specifically corrects sIPSC frequency in hippocampal CA1 (Chakrabarti et al. 2010). In addition, the effects of Dscam unlikely originate from mitotic proliferation for several reasons. Firstly,

Dscam is expressed in differentiating neurons but not mitotic progenitors (Yamakawa et al. 1998; Larsen and Callaway 2006; Mayer et al. 2018; Mi et al. 2018). Secondly, our results show that normalizing Dscam levels does not rescue the increased density of parvalbumin-expressing (PV+) neurons in the ACC region of Ts65Dn mice (Figures 3.13A-B). Consistently, the number of cortical PV+ neurons was not affected in Dscam knock out mice (Figures 3.13C-D).

Taken together, our findings suggest that the overexpressed Dscam in Ts65Dn mice causes presynaptic overgrowth and enhances neocortical GABAergic inhibition. They also suggest that systemic screening of hCh21 genes in *Drosophila* might be an effective approach to identify candidate genes that drive the pathogenesis of DS diseases.

3.5 Future directions

Cell-autonomous function of Dscam in GABAergic neurons

An important question is whether Dscam functions cell-autonomously to promote presynaptic growth in GABAergic neurons. Previous studies in *Drosophila* sensory neurons and gain-of-function studies in mouse retinal ganglion cells suggest a cell-autonomous role of Dscam in promoting axonal growth (Kim et al. 2013; Bruce et al. 2017). However, using Nkx2.1-CreER mouse line for genetic deletion of Dscam in single ChCs is challenging. Due to the weak Cre activity in Nkx2.1-CreER mouse line, administration of tamoxifen cannot guarantee the deletion of target genes in all or vast majority of cells in floxed mice. Immunostaining or in-situ hybridization is required to confirm the deletion. However, available anti-Dscam antibodies are not conducive for immunostaining in neocortices (Saito et al. 2000)(data not shown). Moreover, the experimental procedures for in situ hybridization are not compatible with morphological studies of ChCs by immunostaining.

To address this question, one may use Lhx6-Cre, a strong mouse Cre line that targets both ChCs and basket cells at early developing stages (Kimura et al. 1999; Grigoriou et al. 1998; Del Pino et al. 2013). Crossing Lhx6-Cre with one copy of Dscam floxed mice will enable normalizing Dscam expression levels in GABAergic neurons in the Ts65Dn background. By combining immunostaining for morphological assays and patch-clamp recordings for functional readout, one would be able to interrogate whether Dscam cell-autonomously regulates synaptogenesis and synaptic transmission in GABAergic neurons.

Targeting Dscam signaling for treating DS

This work has demonstrated a critical role of Dscam overexpression in the pathogenesis of the brain disorders in DS. However, *Dscam* encodes IgG-domain transmembrane proteins, which is difficult to be targeted by chemical compounds. To date, most FDA-approved chemical drugs target kinases to specifically inhibit their activities. In this perspective, the downstream effector of Dscam--Abelson tyrosine kinase (ABL)—is a promising target as FDA has approved multiple ABL inhibitors with high specificity and safety profiles. Particularly, our lab has shown that treating *Drosophila* larvae with ABL inhibitors rescues Dscam overexpression phenotype in promoting pain-sensing neuron overgrowth (Sterne, Kim, and Ye 2015a). In the future, it will be important to determine whether the high Dscam levels in DS mouse models cause hyperactivity of ABL tyrosine kinase and whether delivering ABL inhibitors, such as nilotinib, rescues the GABAergic dysfunctions. These studies will provide critical insights into the feasibility of post-natal treatment of DS brain disorders with ABL inhibitors, including intellectual disability and hypersensitivity to pain.

The role of dysregulated Dscam levels in other brain disorders

Altered Dscam expression levels have been associated with many brain disorders, including DS, ASD, intractable epilepsy and bipolar disorder (Saito et al. 2000; Amano et al. 2008; Shen et al. 2011; O'Roak et al. 2014; Krumm et al. 2015; Turner et al. 2016), and possibly Fragile X syndrome (Brown et al. 2001; Darnell et al. 2011; Kim et al. 2013; Cvetkovska et al. 2013). The present work has established a causal relationship between dysregulated Dscam levels and the developmental and functional defects of GABAergic neurons. The dose-dependent function of Dscam suggests that dysregulated Dscam levels may be a common pathogenic driver of GABAergic dysfunctions in related neurological diseases. For example, genetic analyses have

revealed multiple disruptive single-nucleotide variants (SNVs) and copy number variants (CNVs) in Dscam gene in idiopathic ASD individuals, which raises the possibility of altered Dscam expression levels (Turner et al. 2016; Krumm et al. 2015; O'Roak et al. 2014; Wang et al. 2016). Given the regulation of GABAergic signaling by Dscam levels discovered in the present study and the established role of impaired GABAergic signaling in ASD (Cellot and Cherubini 2014), one may hypothesize that reduced Dscam expression causes impaired GABAergic signaling in ASD. In support of this, some ASD individuals with CNV of deleted enhancer region in Dscam show nonfebrile seizures (Turner et al. 2016), a symptom also found in mice with deficient Dscam function (Fuerst et al. 2008). It is thus important to examine Dscam levels in post-mortem samples of autistic individuals and determine whether altered Dscam expression causes GABAergic dysfunctions in ASD mouse models.

3.6 Author contribution

H.L. and B.Y. conceived the project and designed the experiments. H.L. performed mouse breeding, drug delivery, western blotting, immunostaining, and data analysis. R.C.F, J.M.H, and G.P. performed electrophysiology recordings and analysis. T.Y., R.L. and M.V. assisted on mouse breeding and immunostaining. J.Z.H. and P.F. provided Nkx2.1-CreER and *Dscam*^{2j} mice, respectively. B.Y. supervised the project. H.L., R.C.F., L.L.I., K.Y.K, P.M.J., and B.Y. wrote the paper.

3.7 Materials and methods

Mice breeding and tamoxifen administration

Age-matched littermates were used for all experiments. Ts65Dn (Ts(17(16))65Dn) was purchased from Jackson Laboratory (Stock No: 005252) and maintained by crossing with C57BL/C3H F1 hybrid males.

For labeling single ChCs in Ts65Dn mice, Ts65Dn females were crossed with Nkx2.1-CreER+/-, Ai14-/-, Dscam+/- male mice of mixed C57BL/C3H background to obtain euploid, Ts65Dn and Ts65Dn: Dscam+/+/- littermates with Nkx2.1-CreER+/-, Ai14+/- transgenes. Tamoxifen (Sigma, T5648-1G), dissolved in corn oil, was delivered to P0 pups by intraperitoneal injection at the dosage of 80 mg/kg body weight. Pseudodam was prepared in advance to lactate the pups as the pups were often discarded by Ts65Dn dam after the drug delivery. For labeling single ChCs in Dscam2j mice, female Dscam+/- mice of C3H background were crossed with Nkx2.1-CreER+/-, Ai14-/-, Dscam+/- male mice of mixed C57BL/C3H background to obtain Dscam+/- and Dscam-/- pups with Nkx2.1-CreER+/-, Ai14+/- transgenes. Tamoxifen was delivered to P0 pups as above. Strong pups were sacrificed at P0 to keep the litter size 4-5 to increase the surviving rate of Dscam-/- pups. Nkx2.1-CreER+/-, Ai14-/-, Dscam+/- male mice were removed from the cage before female laboring as the male adults is likely to attack and sacrifice Dscam-/- pups.

For electrophysiology recordings, Ts65Dn females were crossed with C3H Dscam+/- male mice to obtain euploid, Ts65Dn and Ts65Dn: Dscam+/+/- littermates. C3H Dscam+/- mice were interbred to obtain Dscam+/- and Dscam-/- pups for recordings.

PCR genotyping was performed on purified tail tips at least 2 times to confirm the genotype according to the protocol by Jackson Laboratory. All work involving mice was approved by the University of Michigan Institutional Animal Care and Use Committee (IACUC) and in

accordance with the National Research Council Guide for the Care and Use of Laboratory Animals (NIH).

Tissue processing

P28 mice were euthanized by CO2 and immediately followed by intracardial infusion of 4% paraformaldehyde (PFA) with 4% sucrose in 1x PBS. The brains were then removed and post-fixed in 4% PFA overnight at 4 °C, followed by incubation in 30% sucrose (wt/vol) for at least 1 day. The brains were embedded in the OCT compound (Fisher HealthCare), frozen in -20 °C overnight and then sectioned to 100 μm-thick slices with a Leica CM3050S cryostat. Sectioned brain slices were kept in 1x PBS containing 0.05% sodium azide at 4 °C until immunostaining.

Immunohistochemistry

For ChC and AIS staining, coronal brain sections (100 μm) were blocked with 8% BSA in PBST (1x PBS + 0.1% Triton x-100) containing 0.05 % sodium azide at 37°C for 1 hour, and then incubated with the following primary antibodies in the blocking solution at 37°C overnight: anti-mCherry (AB0081; 1:300; SICGEN) for neuronal morphology and anti-phospho-Iκβ-α (14D4 rabbit monoclonal antibody; 1:500; Cell Signaling) for labeling the AIS. After washing 3 time (1 hour each time) at 37°C in PBST, brain slices were incubated with the following secondary antibodies in the blocking solution at 37°C overnight: donkey anti-goat-rhodamine RX (RRX) (705-297-003; 1:300; Jackson ImmunoResearch), donkey anti-rabbit-AlexaFluor 488 (711-545-152; 1:300; Jackson ImmunoResearch). After washing 3x for a total of 1 hour at 37°C in PBST, the slices were mounted in sRIMS (Yang et al. 2014).

The procedure for staining of GABAergic neurons and PyNs was the same as above, except that antibody incubations were done at room temperature and different primary antibodies were used. Primary antibodies used were anti-parvalbumin (PVG213; 1:1,000, Swant Inc), anti-CAMKIIα (6G9; 1:5,000, LSBio). Secondary antibodies used were donkey anti-goat-RRX (705-297-003; 1:500; Jackson ImmunoResearch) and donkey anti-mouse-AlexaFluor 488 (715-545-150; 1:500; Jackson ImmunoResearch).

For staining perisomatic GABAergic synapses, antigen retrieval was conducted in 10 μM sodium citrate for 20 min at 95°C (Nelson et al. 2019). After a brief rinse in PBS, the slices were blocked in blocking buffer (1x PBS, 0.3% Triton x-100, 3% normal donkey serum, 0.05 % sodium azide) for 1 hour at room temperature (RT), and then incubated with the following primary antibodies in the blocking solution at 4°C overnight: mouse anti-Bassoon (SAP7F407; 1:1,000; ENZO), G.P. anti-VGAT (131 004; 1:1,000; Synaptic System), rabbit anti-GRASP1 (1:2,000) (Ye et al. 2000). After washing 3 time (20 mins each time) at RT in PBST, brain slices were incubated with the following secondary antibodies in the blocking solution at RT 3 hours: donkey anti-mouse-AlexaFluor 488 (715-545-150; 1:300; Jackson ImmunoResearch), donkey anti-G.P.-RRX (706-295-148; 1:300; Jackson ImmunoResearch), donkey anti-rabbit- AlexaFluor 647 (711-605-152; 1:300; Jackson ImmunoResearch),. The slices were mounted for imaging after washing 3x for a total of 1 hour at RT in PBST.

The procedure for c-fos staining was as described previously (Flak et al. 2017). Briefly, brain sections were washed three times (10-min each) with 1x PBS, and then treated sequentially with the following solutions: 2% H2O2, 0.3% NaOH/1x PBS for 20 min, 1x PBS for 5 min twice, 0.3% glycine/1x PBS for 10 min, 1x PBS for 5 min twice, 0.03% SDS/1x PBS for 10 min, and 1x PBS for 5 min twice. The brain sections were then blocked in 3% normal donkey serum/0.1%

Triton X-100/1x PBS for 1 hr, and subsequently incubated overnight in blocking solution that contained anti-c-Fos antibody (#2250; 1:2000 cell signaling). The sections were washed in 1x PBS for three 20-min washes, and incubated with biotinylated secondary antibody (711-066-152; 1:200; Jackson Immunoresearch) in blocking solution for 2 hours. After washing in 1x PBS for three 10-min washes, the sections were processed for ABC amplification (PK-6100; 1:500 in PBS dilution; Vector Laboratories) for 1 hour, washed in 1x PBS for 10 min three times, incubated in 0.05% diaminobenzidine (DAB)/0.015% H2O2/1x PBS for 3 min, and then washed in 1x PBS for 10 min three times.

Image acquisition and quantitative analysis

All images were acquired from layer II/III of the ACC in the mouse neocortex by using a Leica SP5 confocal microscope equipped with a resonant scanner, except the samples for perisomatic GABAergic synapses (see below). For ChCs imaging, different fluorescence channels were imaged sequentially with the pinhole set at airy 1. A 63x objective lens with a numerical aperture of 1.4 was used. Confocal image stacks were collected with 100 continuous optical sections at 0.3-μm z-steps. The cell body was positioned around the middle of the 30-μm in depth. Before quantification, the image stacks were maximally projected along the z-axis. A region of 120 μm (length) x 80 μm (width) with the cell body in the top middle was set for quantification. Cartridges and boutons that colocalized with AIS were quantified by the NeuroLucida software (MBF Bioscience). Cartridge/bouton number was defined as the number of cartridges/boutons within this region. Cartridge length was defined as the distance from the first bouton that colocalized with AIS to the last one colocalized with AIS in that cartridge. Bouton size was defined as the length of the bouton in parallel to the AIS. We quantified the sizes of boutons in

the 10 cartridges nearest to the cell body. Interbouton distance was defined as the distance between two neighboring boutons.

Samples for perisomatic GABAergic synapses were imaged on a Leica SP8 confocal microscope with a 63x objective lens (NA 1.4). For each PyN, a single confocal image was taken at the z-position where PyN cell body occupied the most area. Images were deconvoluted with the Huygens software (Scientific Volume Imaging). Perisomatic VGAT+ and Bassoon+ puncta were quantified in defined PyN soma regions, as shown in Figure 6B, by the NeuroLucida software (MBF Bioscience).

For c-fos and parvabumin imaging, a 20x objective lens with a NA of 1.4 was used. The z-steps were 1 μm. Five optical sections were maximally projected before quantification. Three fields were imaged for each mouse. Cells were counted in a defined area (252.4 μm × 200 μm) for each field manually with the assistance of the NeuroLucida software.

To eliminate experimenter's bias, these experiments were carried out in double-blind fashion. Two double-blind methods were used. First, the images acquired by the primary experimenter (H.L.) was coded and randomized by the second lab member (R.L. or M.V.). After the primary experimenter quantified the data, the data were decoded for statistical analysis. ChCs from 2 littermates were quantified in this method. Second, the mouse brains from the primary experimenter (H.L.) were coded and randomized by the second lab member (R.L. or M.V.). The second lab member sent the encoded mouse brains to the third lab member (T.Y.) for sectioning. After the primary experimenter immunostained and quantified the encoded brain sections, the data were decoded for a final statistical analysis. ChCs from 3 littermates and the c-fos, parvabumin and basket cell synapse quantifications were performed in this method.

Western blotting

Mouse neocortices were removed immediately after PFA perfusion. Similar volumes of tissues were homogenized in SDS sample buffer and loaded for electrophoresis. The proteins were transferred to PVDF membranes and blocked with 5% milk (wt/vol) for 1 h at room temperature. The blots were incubated overnight at 4 °C with goat anti Dscam (AF3666, 1:500, R&D systems) and mouse anti-tubulin (12G10, 1:5,000, DSHB). After washing, blots were incubated for 2 h with HRP-conjugated secondary antibodies and developed by chemiluminescence (Catalog# 32106, Pierce). Quantification was performed using ImageJ.

Electrophysiology recordings and analysis

Electrophysiological recordings of spontaneous and miniature inhibitory postsynaptic currents were performed as described previously (Nelson et al. 2018). Brains were obtained from euploid, Ts65Dn, and Ts65Dn/Dscam+/+/- mice at around P28. The animals were decapitated under isoflurane and USP anesthesia, and the brain was quickly removed from the skull and placed in 4°C slicing solution containing (in mM) 62.5 NaCl, 2.5 KCl, 1.25 KH_2PO_4, 26 $NaHCO_3$, 5 $MgCl_2$, 0.5$CaCl_2$, 20 glucose and 100 sucrose (pH maintained at 7.4 by saturation with 95% O_2 + 5%CO_2). Coronal brain slices (300-350 µm thick) containing layers II/III of the ACC neocortex were cut with a microtome (VF-300, Compresstome). The slices were then transferred to a holding chamber and maintained at room temperature in artificial cerebrospinal fluid (ACSF) containing (in mM) 125 NaCl, 2.9 KCl, 1.25 KH_2PO_4, 26 $NaHCO_3$, 1 $MgCl_2$, 2 $CaCl_2$ and 20 glucose, pH 7.4 (with 95% O_2 and 5% CO_2 bubbling through the solution) for at least 1 hour prior to recording. After equilibration, individual slices were transferred to the recording chamber continuously perfused with ACSF (1-2 mL/min). Recording micropipettes were pulled

from borosilicate glass capillaries (1.5 mm O.D. Harvard Apparatus) for a final resistance of 3-6 MΩ and filled with a solution containing (in mM) 135 CsCl, 4 NaCl, mM GTP, Mg-ATP, 0.5 CaCl2, 5 EGTA and 10 HEPES. The signals were recorded with an Axoclamp 700B amplifier (Axon Instruments, Union City, CA). Voltage clamp recordings were obtained from neurons in layers II/III of the ACC region; the cells in these brain regions were identified using a Nikon Eclipse FN-1 microscope with a 40x water-immersion objective and a DAGE MTI IR-1000 video camera. Neurons were visualized using IR-DIC to evaluate their orientation and morphology. Whole-cell patch-clamp recordings for cells with a high cell resistance (greater than 8 GΩ before break-in). sIPSC and mIPSC recordings in voltage-clamp configuration were acquired at 2 kHz fixing the voltage at -70 mV. The IPSCs were recorded in the presence of the NMDA receptor antagonist DL-2-amino-5-phosphonopentanoic acid (AP-5) at 50 mM and the AMPA/kainite antagonist 6-cyano-7-nitroquinoxaline-2,3-dione (CNQX) at 10 µM. For measurement of mIPSCs, 1 µM tetrodotoxin (TTX) was added to the perfusion solution to block synaptic responses dependent on the AP. Access resistance was monitored throughout the experiment and experiments were canceled if changes greater than 20% occurred. Peak events were identified automatically using Minianalysis (Synaptosoft Inc.) and visually monitored to exclude erroneous noise. The frequency, amplitude and distribution of events were analyzed. One euploid neuron (1 out of 20) with mIPSC frequency 8.9 Hz was defined as an outlier by the Grubbs' test and removed from quantification. Mean values were compared using the Student’s t-test. Data are presented as mean ± SEM.

Statistical analysis

Data are presented as mean ± SEM. Comparisons of mean differences between groups were performed by one way ANOVA followed by Student's t-test. $P < 0.05$ was considered to be statistically significant. For all quantification, *: $p < 0.05$; **: $p < 0.01$; ***: $p < 0.001$; ns: not significant ($p > 0.05$).

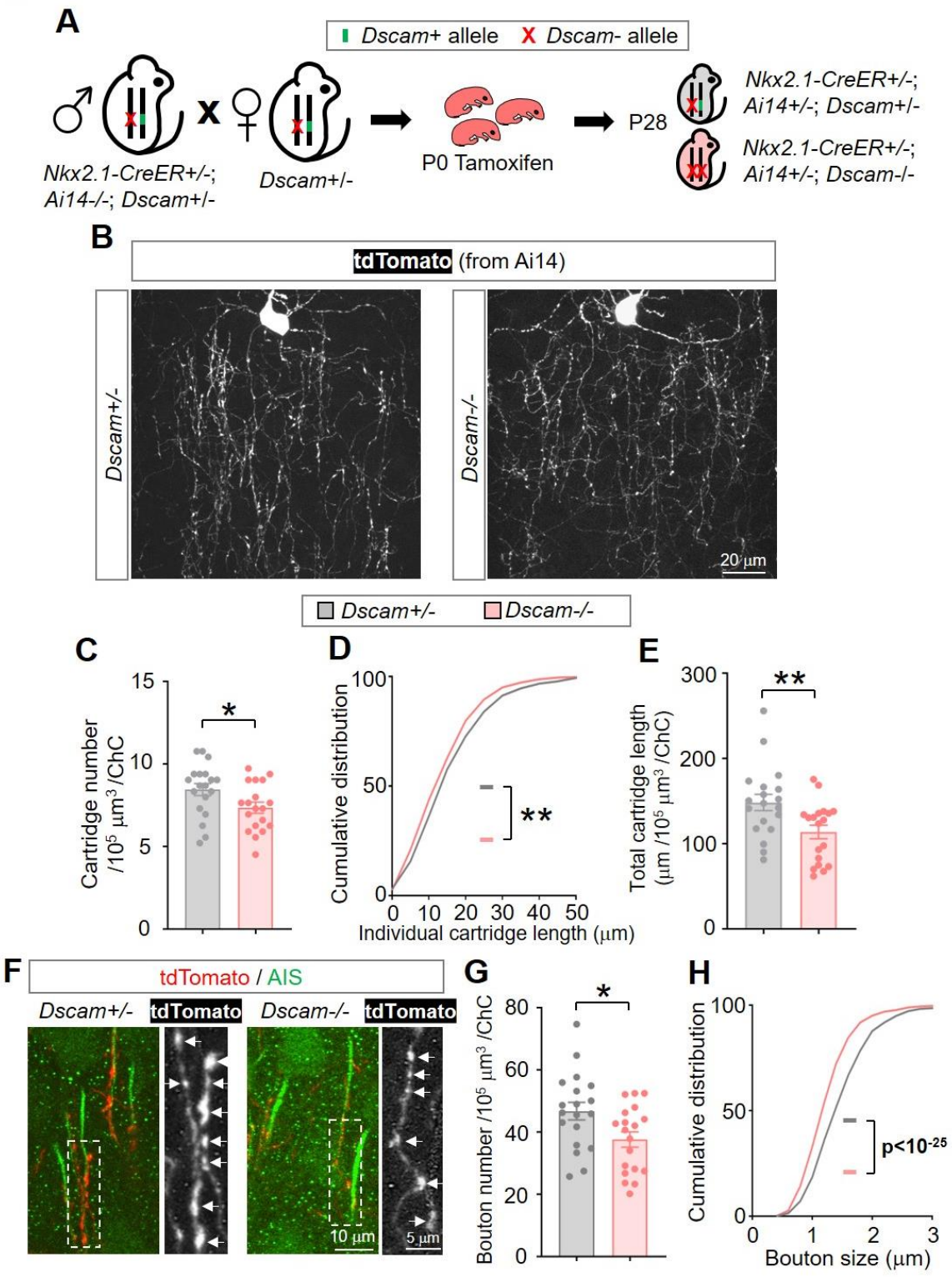
A
Dscam+ allele
Dscam- allele
Nkx2.1-CreER+/-; Ai14-/-; Dscam+/-
Dscam+/-
P0 Tamoxifen
P28
Nkx2.1-CreER+/-; Ai14+/-; Dscam+/-
Nkx2.1-CreER+/-; Ai14+/-; Dscam-/-
B
tdTomato (from Ai14)
Dscam+/-
Dscam-/-
20 µm
Dscam+/-
Dscam-/-
C
Cartridge number /10^5 µm^3 /ChC
D
Cumulative distribution
Individual cartridge length (µm)
E
Total cartridge length (µm /10^5 µm^3 /ChC)
F
tdTomato / AIS
Dscam+/-
tdTomato
Dscam-/-
tdTomato
10 µm
5 µm
G
Bouton number /10^5 µm^3 /ChC
H
Cumulative distribution
p<10^-25
Bouton size (µm)

Figure 3.1. Loss of *Dscam* impairs the growth of ChC axon cartridges and boutons.
(**A**) A schematic of the procedure that produced the mice for the experiments.
(**B**) Representative images of single ChCs in layer II/III of anterior cingulate cortex (ACC). Shown are ChCs of *Dscam*$^{2j/+}$ (+/-, left) and *Dscam*$^{2j/2j}$ (-/-, right) mice at P28. All ChC images in this paper are from this brain region of P28 mice. Scale bar, 20 μm.
(**C-E**) Quantification of axon cartridge number (C), length (D) and the total cartridge length (E). For each ChC, all axon cartridges (~15-40) innervating the AIS of PyNs in a volume of 120 μm (length) x 80 μm (width) x 30 μm (thickness) with the ChC cell body in the top middle were analyzed. 4-6 ChCs were analyzed for each mouse, and 4 *Dscam*+/- and 4 *Dscam*-/- mice were analyzed. Each dot in (C) and (E) represents one ChC. Sample numbers in (B) and (D) are 19 for *Dscam*+/- and 19 for *Dscam*-/-. In (D), cumulative plots show the distributions of cartridge length. Sample numbers are 462 for *Dscam*+/- and 402 for *Dscam*-/-. . Unless specified, mean ± SEM is shown in the figures, and the statistical tests are one-way ANOVA followed by Student's t test. *: $p < 0.05$; **: $p < 0.01$; ***: $p < 0.001$; ns: not significant ($p > 0.05$).
(**F**) Representative images of ChC axon cartridges innervating the AIS of PyNs. Cartridges of single ChCs were labeled with tdTomato (Red). The AIS of PyNs were labeled by anti-phospho-IκB (pIκB, Green). The arrows point to presynaptic boutons of ChCs in the boxed regions.
(**G-H**) Quantification of bouton number (G) and size (H). For each ChC, all boutons (38~194) in axon cartridges that innervate AIS in the defined volume (Figure S1) were analyzed for bouton numbers; boutons (31~84) in the 10 cartridges nearest to the cell body were analyzed for bouton sizes. 4-6 ChCs were analyzed in each mouse. 4 *Dscam*+/- and 4 *Dscam*-/- mice were analyzed. In (G), each dot represents one ChC, N: 19 for *Dscam*+/- and *Dscam*-/-. In (H), accumulative plots show the distributions of bouton size. N: 1079 for *Dscam*+/- and 1004 for *Dscam*-/-.

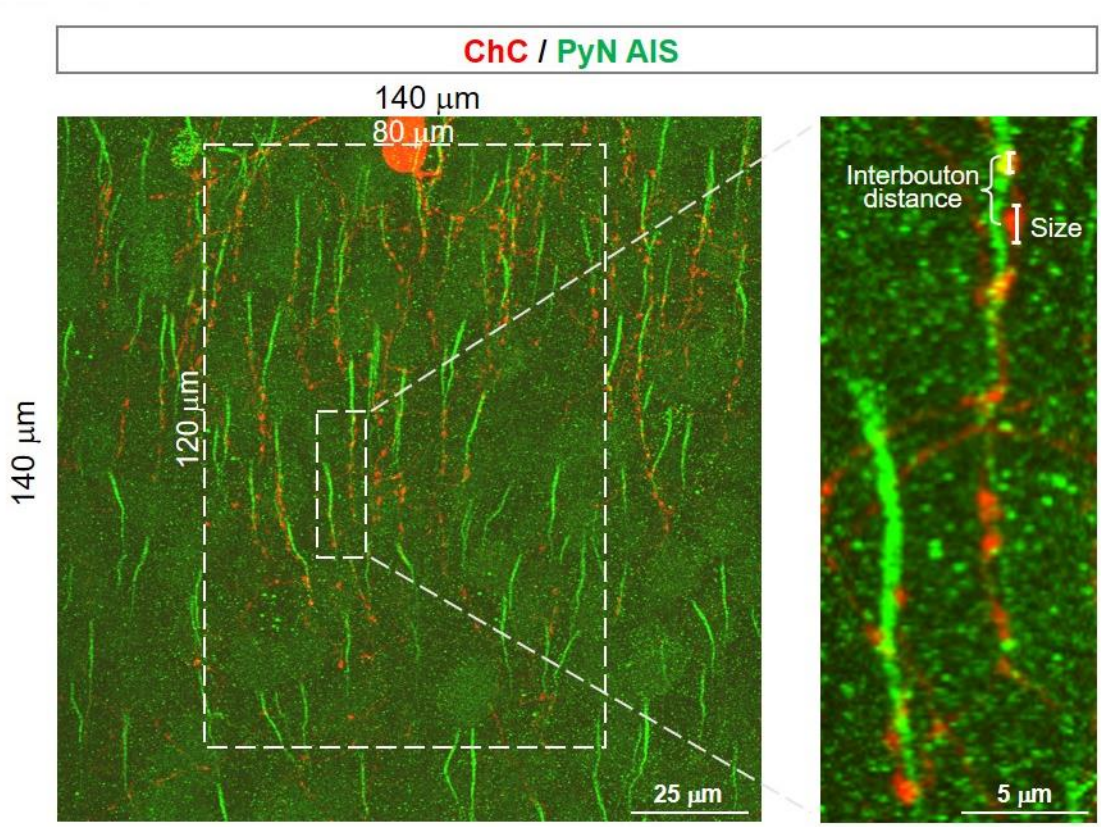

Figure 3.2. Quantification of ChC axon terminals and boutons.
ChCs were sparsely labeled by tdTomato (red), and axon initial segments of PyNs were labeled by immunostaining with anti-phospho-IκB (Green). Confocal image stacks (0.3 μm z-steps for 100 steps) were maximally projected along the z-axis. A region of 120 μm (length) x 80 μm (width) with the cell body in the top middle was quantified. Cartridges and boutons that colocalized with AIS were quantified. Cartridge number was defined as the number of cartridges within this region. Cartridge length was defined as the distance from the first to the last bouton that colocalizes with the AIS in that cartridge. Bouton size is defined as the length of bouton in parallel to AIS. Interbouton distance is defined as the distance between two neighboring boutons.

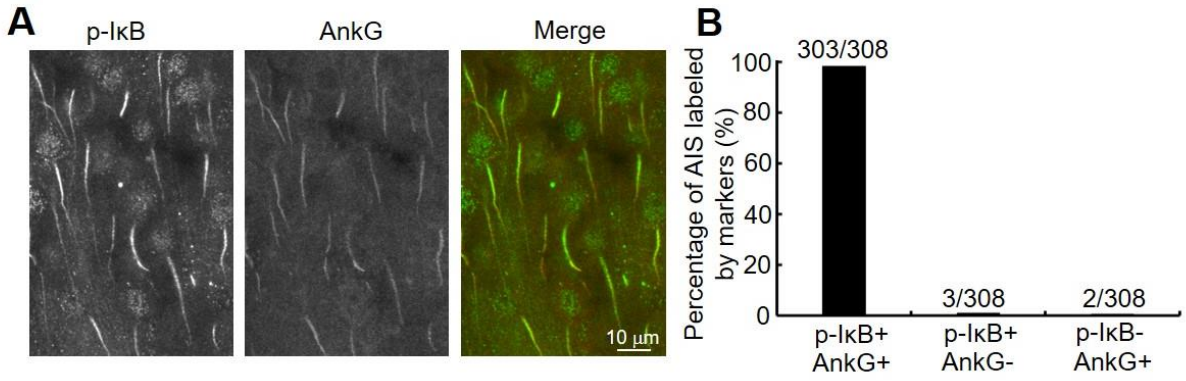

Figure 3.3. phospho-IκB and AnkG shows equal fidelity in labeling neocortical AIS.
(**A**) AIS in layer II/III ACC was co-labeled by phospho-IκB (green) and AnkG (red). Shown are maximal projection of confocal image stacks (1 μm z-steps X 7 steps).
(**B**) Quantification of the percentage of AIS that is labeled by phospho-IκB and/or AnkG. 308 AIS were quantified, among which 303 were co-labeled by phospho-IκB and AnkG.

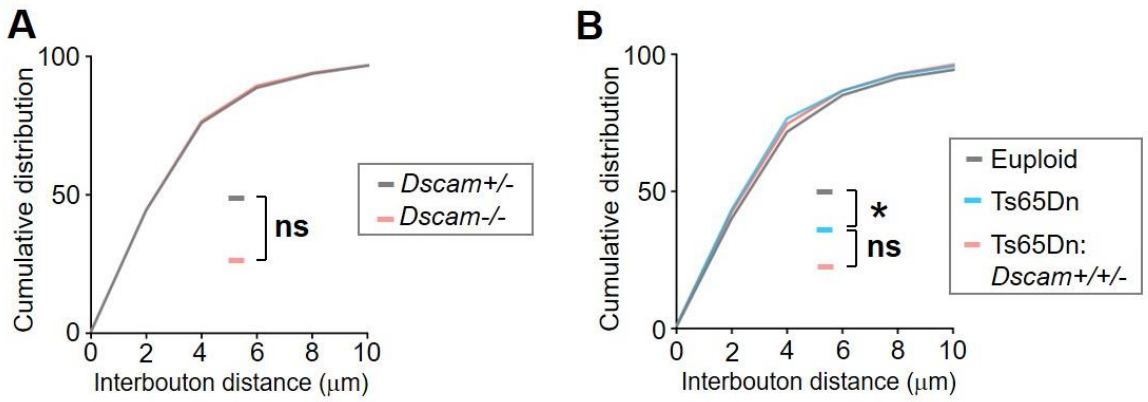

Figure 3.4. Dscam does not regulate bouton density.
For each ChC, all boutons (38~194) in axon cartridges that innervate AIS in the defined volume were analyzed for bouton density (indicated by interbouton distance); 4-6 ChCs were analyzed for each mouse. The accumulative plots show the distributions of bouton density. (A) 4 *Dscam*+/- and 4 *Dscam*-/- mice were analyzed. n: 2073 for *Dscam*+/- and 1640 for *Dscam*-/-. (B) 4 euploid, 5 Ts65Dn, and 4 Ts65Dn:*Dscam*+/+/- mice were analyzed. n: 2214 for euploid, 3189 for Ts65Dn and 1912 for Ts65Dn:*Dscam*+/+/-.

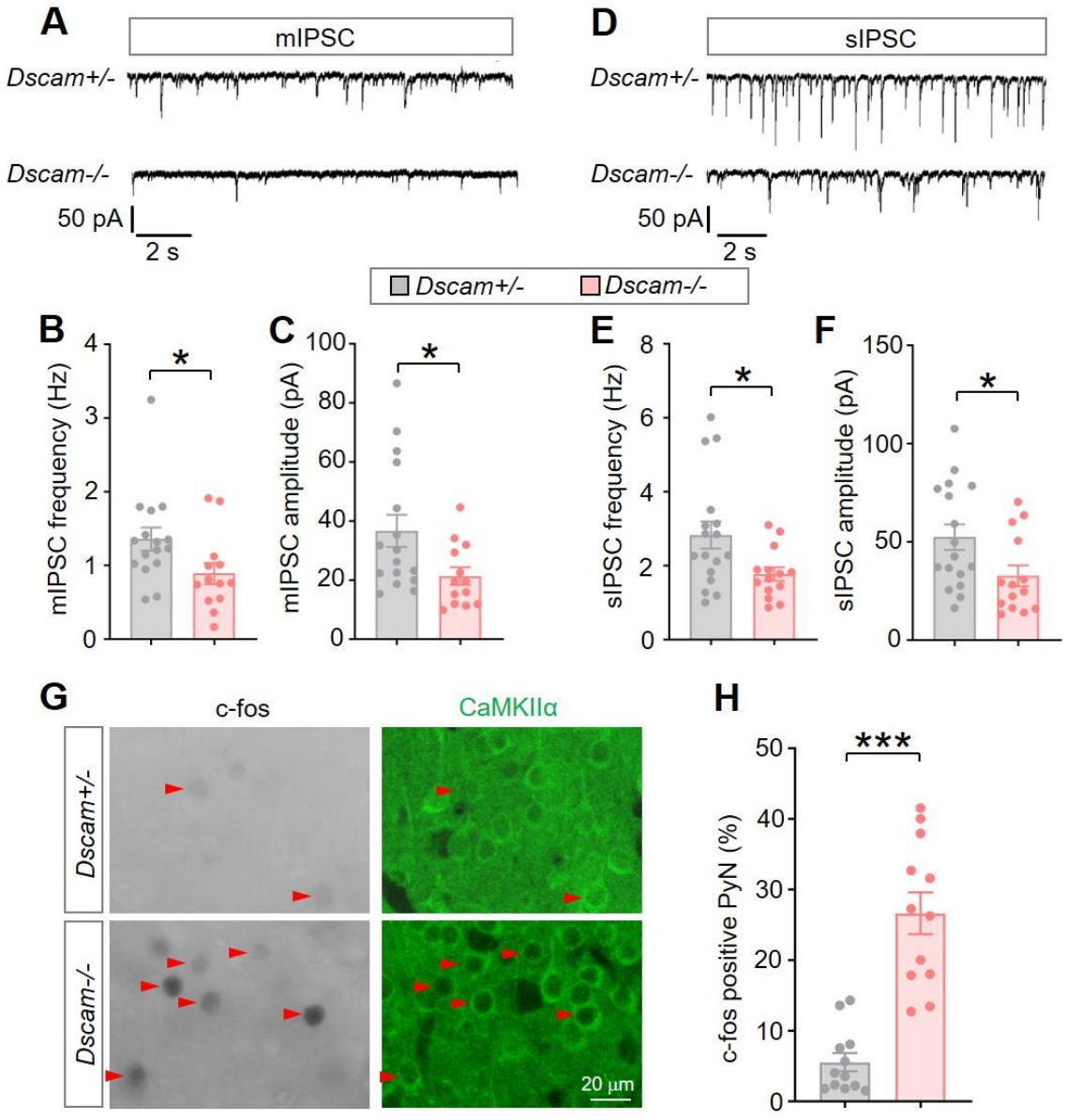
A
mIPSC
Dscam+/-
Dscam-/-
50 pA
2 s
D
sIPSC
Dscam+/-
Dscam-/-
50 pA
2 s
Dscam+/-
Dscam-/-
B
mIPSC frequency (Hz)
C
mIPSC amplitude (pA)
E
sIPSC frequency (Hz)
F
sIPSC amplitude (pA)
G
c-fos
CaMKIIα
Dscam+/-
Dscam-/-
20 μm
H
c-fos positive PyN (%)

Figure 3.5. Loss of *Dscam* impairs GABAergic inhibition of neocortical PyNs.
(**A**) Representative traces of mIPSCs from PyNs in layer II/III of ACC in *Dscam*+/- and *Dscam*-/- brain slices.
(**B-C**) Quantification of mIPSC frequency (B) and amplitude (C). 3-5 PyNs were recorded for each mouse. 5 *Dscam*+/- and 4 *Dscam*-/- mice were analyzed. N: 16 for *Dscam*+/-, and 13 for *Dscam*-/-.
(**D**) Representative traces of sIPSCs from PyNs in layer II/III of ACC in *Dscam*+/- and *Dscam*-/- brain slices.
(**E-F**) Quantification of sIPSC frequency (E) and amplitude (F). 3~5 PyNs were recorded for each mouse. 5 *Dscam*+/- and 4 *Dscam*-/- mice were analyzed. N: 17 for *Dscam*+/-, 14 for *Dscam*-/-.
(**G**) Representative images of c-fos levels in $Dscam^{+/-}$ and $Dscam^{-/-}$ mice. C-fos levels reflect neuronal activity. Anti-CaMKIIα immunostaining marks PyNs. The red arrowheads point to the PyNs with detectable c-fos immunostaining. Images were acquired from layer II/III of the ACC at P28.
(**H**) c-fos levels are increased in $Dscam^{-/-}$ mice. The graph shows the percentage of the percentage of c-fos-positive PyNs in total PyNs. Each dot represents the value in one randomly selected field for imaging. Three fields were imaged in each mouse. 4 *Dscam*+/- and 4 *Dscam*-/- mice were analyzed.

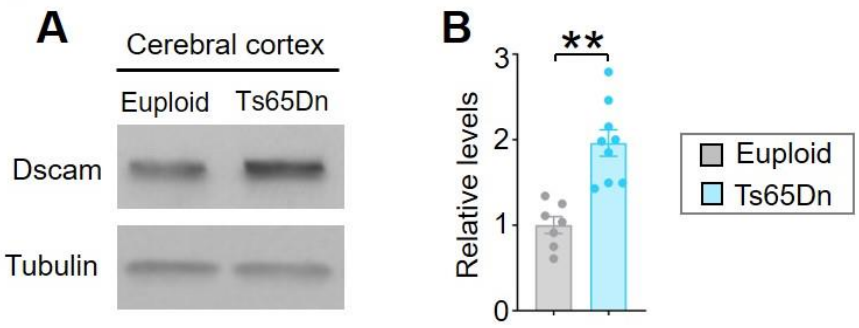

Figure 3.6. Dscam expression level is increased in Ts65Dn neocortices.
Representative western blots (A) and quantifications (B) of neocortical samples from euploid, Ts65Dn mice. Sample numbers are n=7 for euploid, 9 for Ts65Dn.

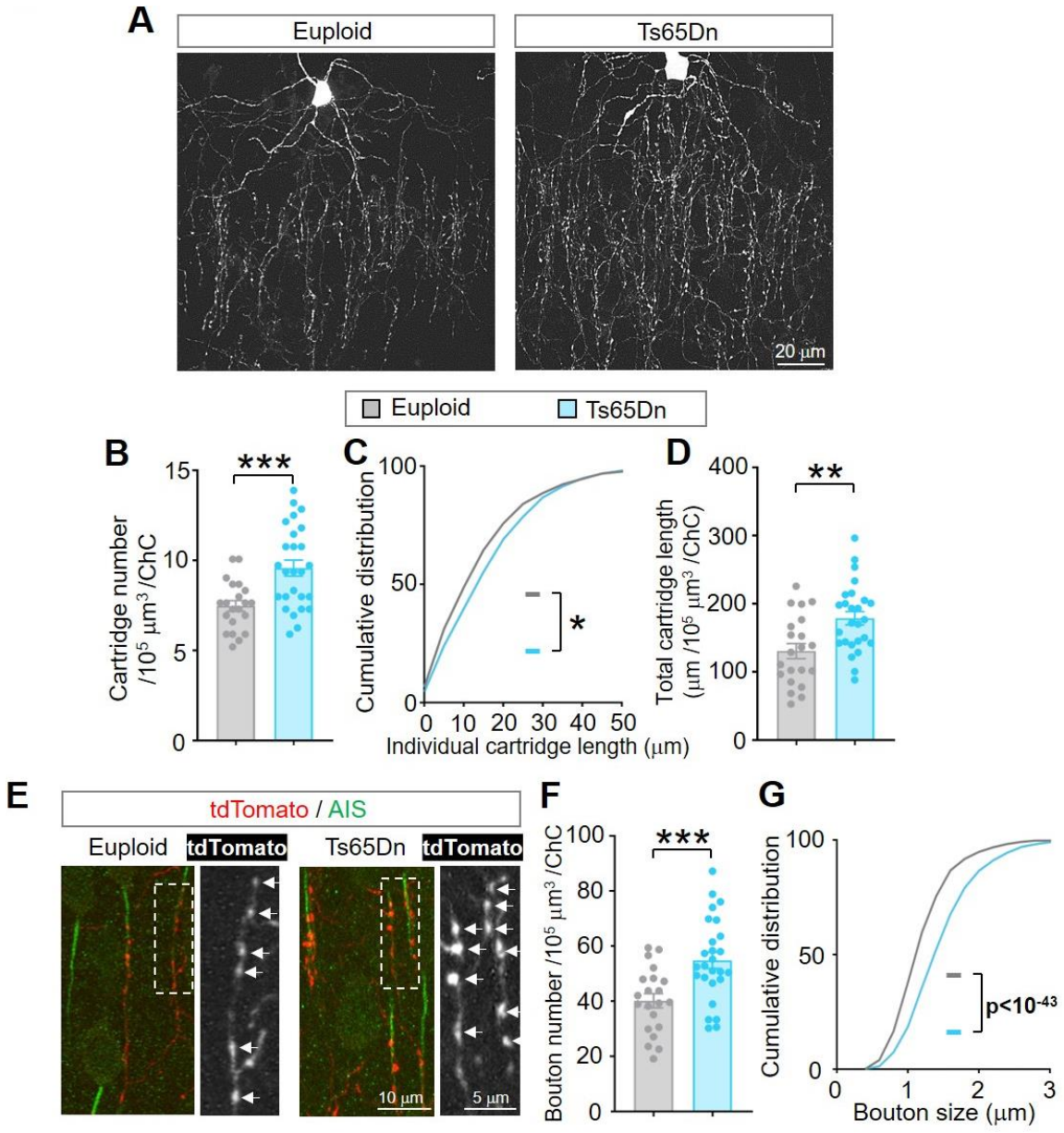
A
Euploid
Ts65Dn
20 µm
Euploid
Ts65Dn
B
***
Cartridge number /10⁵ µm³ /ChC
15
10
5
0
C
Cumulative distribution
100
50
0
0 10 20 30 40 50
Individual cartridge length (µm)
*
D
**
Total cartridge length (µm /10⁵ µm³ /ChC)
400
300
200
100
0
E
tdTomato / AIS
Euploid
tdTomato
Ts65Dn
tdTomato
10 µm
5 µm
F
***
Bouton number /10⁵ µm³ /ChC
100
80
60
40
20
0
G
Cumulative distribution
100
50
0
0 1 2 3
Bouton size (µm)
p<10-43

Figure 3.7. ChC axonal terminals and presynaptic boutons are overgrown in Ts65Dn mice.
(**A**) Representative images of single ChCs in wild-type (euploid, left) and Ts65Dn (right) mice at P28. Scale bar, 20 μm.
(**B-D**) Quantification of axon cartridge number (B), length (C) and the total cartridge length (D). Each dot in (B) and (D) represents one ChC. Sample number (n): 21 for euploid and 26 for Ts65Dn. In (C), cumulative plots show the distributions of cartridge length, n=452 for euploid, 717 for Ts65Dn. Sample numbers are shown in the figure.
(**E**) Representative images of ChC axon cartridges innervating the AIS of PyNs. Cartridges of single ChCs were labeled with tdTomato. The AIS of PyNs were labeled by anti-phospho-IκB (pIκB). The arrows point to presynaptic boutons of ChCs in the boxed regions.
(**F-G**) Quantification of bouton number (F) and size (G). 4-6 ChCs were analyzed for each mouse. 4 euploid and 5 Ts65Dn mice were analyzed. In (F), each dot represents one ChC, N: 21 for euploid and 26 for Ts65Dn. In (G), accumulative plots show the distributions of bouton size, n=1149 for euploid, 1655 for Ts65Dn.

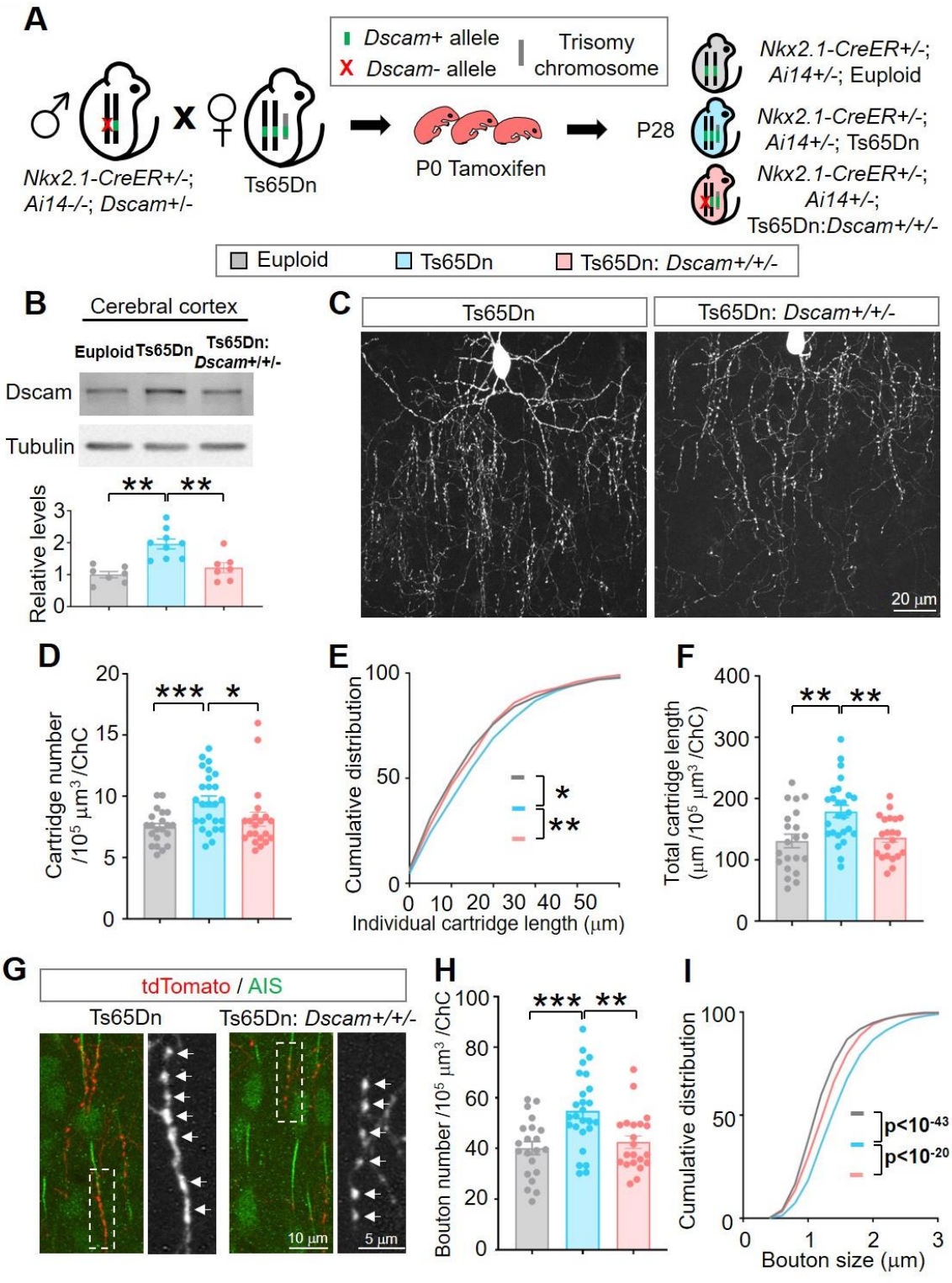
A
Dscam+ allele
Dscam- allele
Trisomy chromosome
Nkx2.1-CreER+/-; Ai14-/-; Dscam+/-
Ts65Dn
P0 Tamoxifen
P28
Nkx2.1-CreER+/-; Ai14+/-; Euploid
Nkx2.1-CreER+/-; Ai14+/-; Ts65Dn
Nkx2.1-CreER+/-; Ai14+/-; Ts65Dn:Dscam+/+/-
Euploid
Ts65Dn
Ts65Dn: Dscam+/+/-
B
Cerebral cortex
Euploid
Ts65Dn
Ts65Dn: Dscam+/+/-
Dscam
Tubulin
Relative levels
C
Ts65Dn
Ts65Dn: Dscam+/+/-
20 µm
D
Cartridge number /10^5 µm^3 /ChC
E
Cumulative distribution
Individual cartridge length (µm)
F
Total cartridge length (µm /10^5 µm^3 /ChC)
G
tdTomato / AIS
Ts65Dn
Ts65Dn: Dscam+/+/-
10 µm
5 µm
H
Bouton number /10^5 µm^3 /ChC
I
Cumulative distribution
p<10^-43
p<10^-20
Bouton size (µm)

Figure 3.8. Normalizing Dscam expression rescues the overgrowth of ChC axon cartridges and presynaptic boutons in Ts65Dn mice.
(**A**) A schematic of the procedure that produced the mice for the experiments.
(**B**) Dscam overexpression is normalized to the euploid level in Ts65Dn mice by introducing one *Dscam* mutant allele. Shown are representative western blots (top) and quantifications (bottom) of neocortical samples from euploid, Ts65Dn, and Ts65Dn:*Dscam*+/+/-. Sample numbers are indicated in the bars.
(**C**) Representative images of single ChCs in layer II/III of the ACC. Shown are ChCs of Ts65Dn (left) and Ts65Dn with *Dscam* allele normalized (Ts65Dn:*Dscam*+/+/-, right) mice at P28. Scale bar, 20 μm.
(**D-F**) Quantification of axon cartridge number (D), length (E) and the total cartridge length (F). 4-6 ChCs were analyzed for each mouse; 4 euploid, 5 Ts65Dn, and 4 Ts65Dn:*Dscam*+/+/- mice were analyzed. Sample numbers are 21 for euploid, 26 for Ts65Dn, and 21 for Ts65Dn:*Dscam*+/+/- in (D) and (F). In (E), n=452 for euploid, 717 for Ts65Dn and 491 for Ts65Dn:*Dscam*+/+/-.
(**G**) Representative images of ChC cartridges innervating the AIS of PyNs. The arrows point to presynaptic boutons of ChCs in the boxed region.
(**H-I**) Quantification of bouton number (H) and size (I). 4-6 ChCs were analyzed for each mouse, and 4 euploid, 5 Ts65Dn, and 4 Ts65Dn:*Dscam*+/+/- mice were analyzed. In (H), each dot represents one ChC, N: 21 for euploid, 26 for Ts65Dn, and 21 for Ts65Dn:*Dscam*+/+/-. In (I), accumulative plots show the distributions of bouton size, n=1149 for euploid, 1655 for Ts65Dn and 1209 for Ts65Dn:*Dscam*+/+/-.

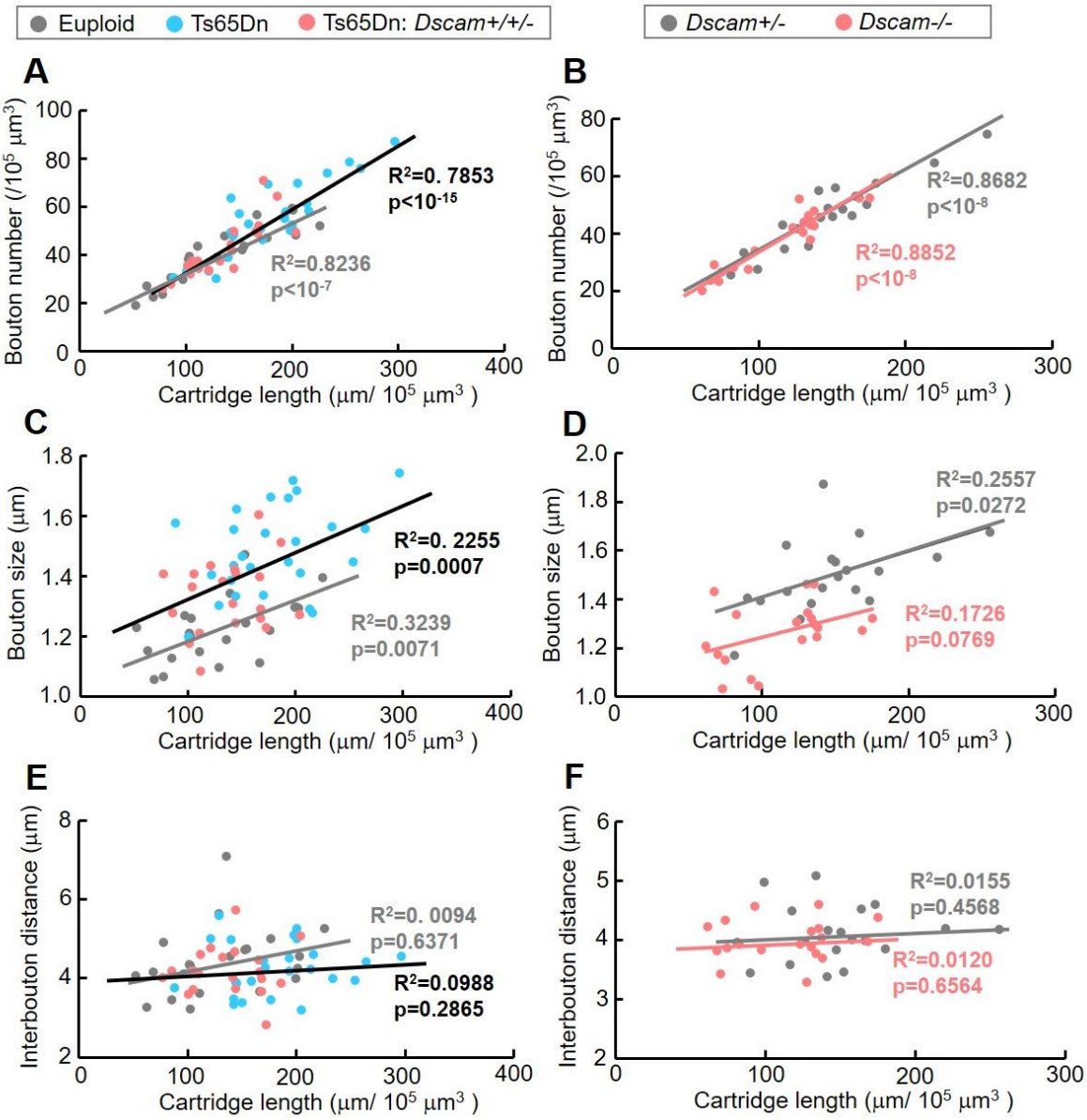
Euploid
Ts65Dn
Ts65Dn: Dscam+/+/-
Dscam+/-
Dscam-/-
A
Bouton number (/10^5 µm^3)
R²=0. 7853
p<10^-15
R²=0.8236
p<10^-7
Cartridge length (µm/ 10^5 µm^3)
B
Bouton number (/10^5 µm^3)
R²=0.8682
p<10^-8
R²=0.8852
p<10^-8
Cartridge length (µm/ 10^5 µm^3)
C
Bouton size (µm)
R²=0. 2255
p=0.0007
R²=0.3239
p=0.0071
Cartridge length (µm/ 10^5 µm^3)
D
Bouton size (µm)
R²=0.2557
p=0.0272
R²=0.1726
p=0.0769
Cartridge length (µm/ 10^5 µm^3)
E
Interbouton distance (µm)
R²=0. 0094
p=0.6371
R²=0.0988
p=0.2865
Cartridge length (µm/ 10^5 µm^3)
F
Interbouton distance (µm)
R²=0.0155
p=0.4568
R²=0.0120
p=0.6564
Cartridge length (µm/ 10^5 µm^3)

Figure 3.9. Coupling between presynaptic terminal growth and synaptogenesis in ChC development.
(**A**) ChC cartridge length and bouton number are strongly correlated in both euploid and Ts65Dn genetic backgrounds. Each dot presents one ChC. 4-6 ChCs were analyzed for each mouse. 4 euploid, 5 Ts65Dn, 4 Ts65Dn:*Dscam*+/+/- mice were analyzed. n=21 for euploid (gray dots), 26 for Ts65Dn (blue dots), 21 Ts65Dn:*Dscam*+/+/- (coral dots). R^2 and p are calculated for linear regression. The gray line indicates the trend line for gray dots, while the black line is that for blue and coral dots.
(**B**) ChC cartridge length and bouton number are strongly correlated in *Dscam*+/- and *Dscam*-/- mice. Each dot presents one ChC. 4–6 ChCs were analyzed for each mouse. 4 *Dscam*+/- and 4 *Dscam*-/- mice were analyzed. N: 19 for *Dscam*+/- (gray dots) and 19 for *Dscam*-/- (coral dots).
(**C**) ChC cartridge length and bouton size show weak, yet significant, correlation in euploid and Ts65Dn background. Each dot presents one ChC.
(**D**) The correlation between cartridge length and bouton number is impaired in $Dscam^{-/-}$ mice. Each dot presents one ChC. R^2 is small in both $Dscam^{+/-}$ and $Dscam^{-/-}$ mice, suggesting that linear regression only explains a small fraction of the samples. The correction is insignificant in $Dscam^{-/-}$ mice ($p > 0.05$).
(**E-F**) ChC cartridge length and interbouton distance shows no significant correlation between any two genotypes tested. Each dot presents one ChC.

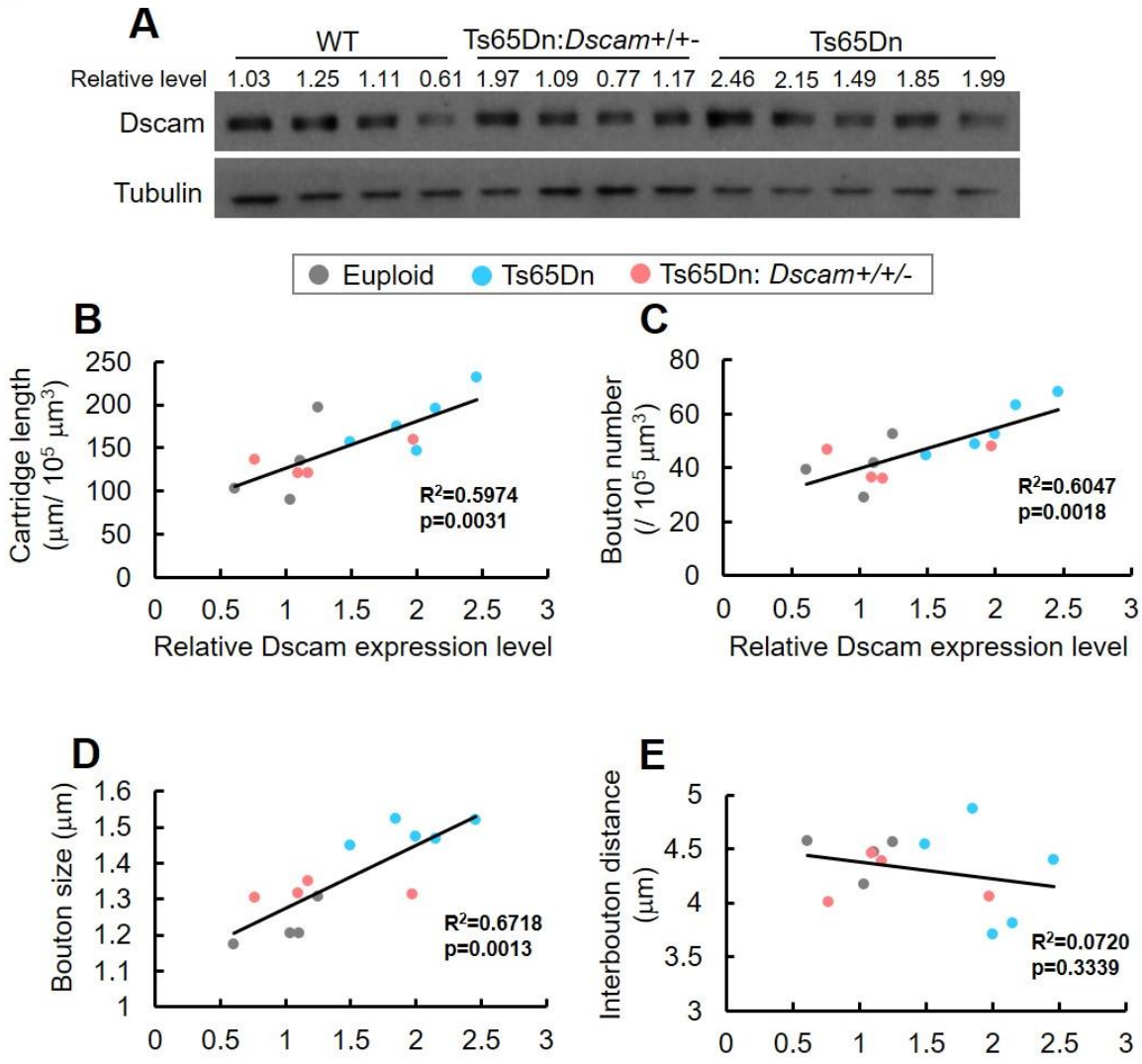

Figure 3.10. Dscam regulates ChC cartridge length and synaptogenesis in a dosage-dependent manner.

(**A**) Western blots showing Dscam levels in the neocortex. The mouse neocortex was taken immediately after perfusion.

(**B-E**) The correlation analyses between Dscam expression level and ChC cartridge length (B), bouton number (C), bouton size (D) or interbouton distance (E). In (B), the Dscam level of a mouse is plotted against the mean of the total cartridge length in the volume specified in Supplementary Fig. 1 in this mouse. The average cartridge length is the calculated as the average value of 4-6 ChCs sampled in each mouse. 4 euploid, 5 Ts65Dn, and 4 Ts65Dn:*Dscam*+/+/- mice were analyzed. N: 21 euploid (black dots), 26 Ts65Dn (red dots), and 21 Ts65Dn:*Dscam*+/+/- (green dots). R^2 and p are calculated for linear regression.

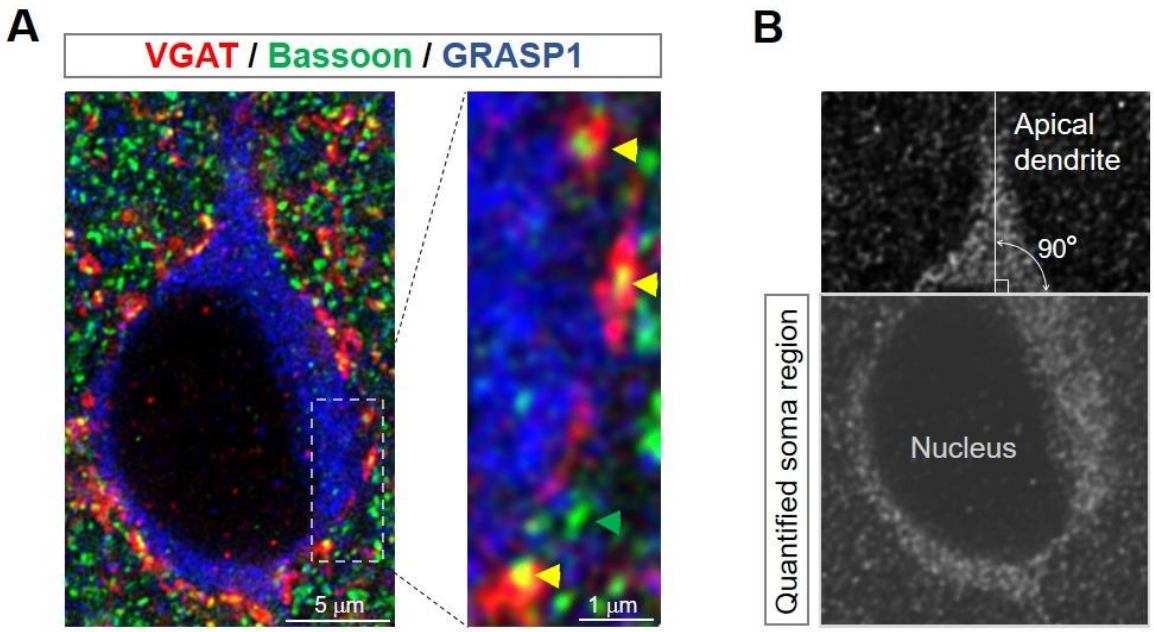

Figure 3.11. Quantification of perisomatic GABAergic synapses on PyNs.
(**A**) Representative confocal image of a PyN in layer II/III in the ACC. The soma is labeled by anti-GRASP1 (blue). The presynaptic active zones are labeled by anti-Bassoon (green). The GABA vesicles in presynaptic terminals of GABAergic neurons are labeled by anti-VGAT (red). The perisomatic Bassoon+ puncta that are apposed to or overlap with VGAT+ puncta were quantified as GABAergic synapses (yellow arrowhead). The green arrowhead indicates the VGAT-independent perisomatic Bassoon+ puncta.
(**B**) To define the soma region for quantifying perisomatic GABAergic synapses, we drew a line that is both perpendicular to the apical dendrite and tangent to the edge of the PyN nucleus, and then quantified GABAergic synapses in the GRASP1+ area below the line.

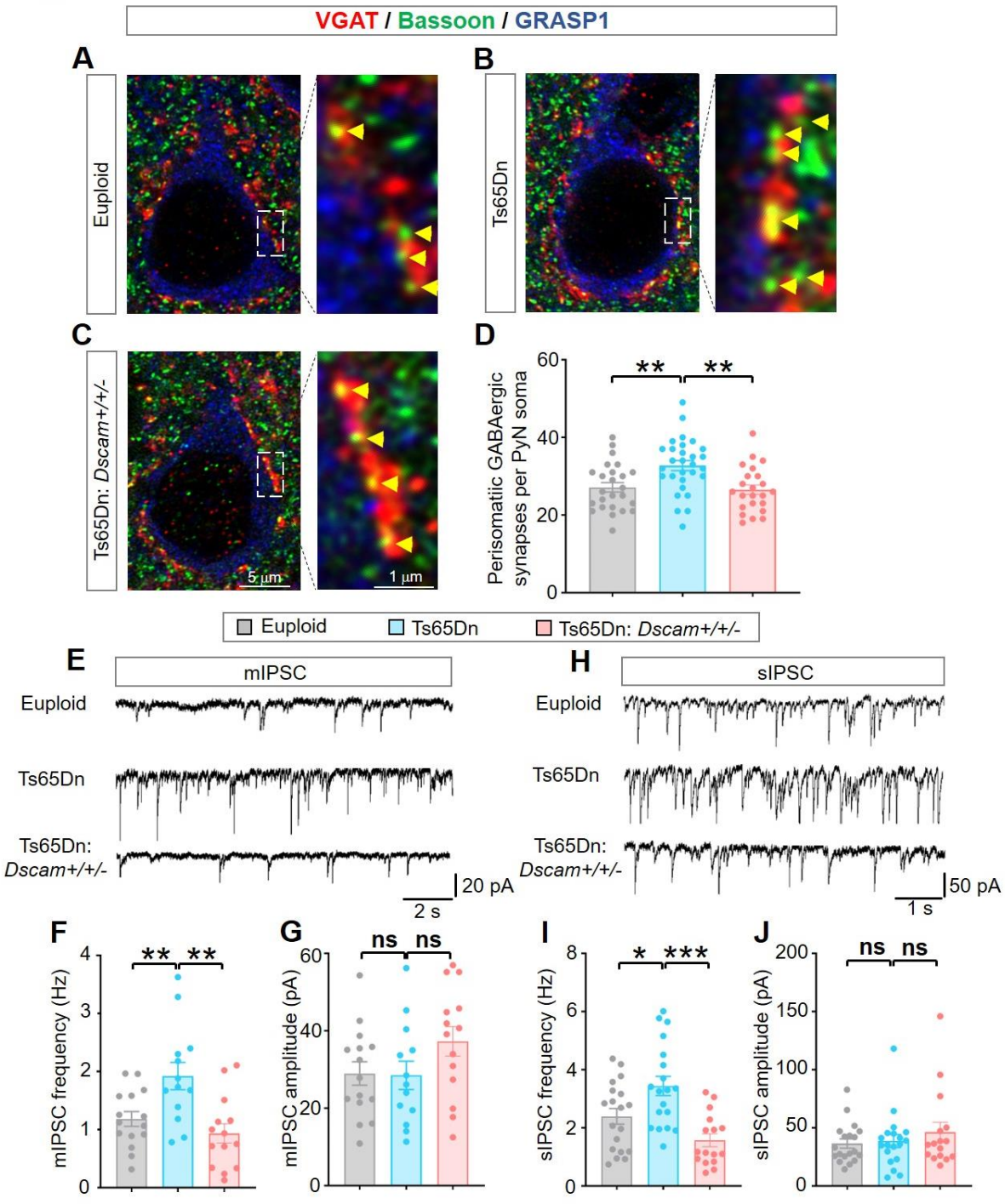
VGAT / Bassoon / GRASP1
A
Euploid
B
Ts65Dn
C
Ts65Dn: Dscam+/+/-
5 µm
1 µm
D
Perisomatic GABAergic synapses per PyN soma
**
**
Euploid
Ts65Dn
Ts65Dn: Dscam+/+/-
E
mIPSC
Euploid
Ts65Dn
Ts65Dn: Dscam+/+/-
20 pA
2 s
H
sIPSC
Euploid
Ts65Dn
Ts65Dn: Dscam+/+/-
50 pA
1 s
F
mIPSC frequency (Hz)
** **
G
mIPSC amplitude (pA)
ns ns
I
sIPSC frequency (Hz)
* ***
J
sIPSC amplitude (pA)
ns ns

Figure 3.12. Normalizing Dscam levels rescues the increased synaptogenesis in basket cells and the enhanced GABAergic synaptic transmission in Ts65Dn neocortex.
(**A-C**) Representative images of perisomatic GABAergic synapses innervating PyNs in layer II/III ACC of euploid (wild-type), Ts65Dn, and Ts65Dn:*Dscam*+/+/-. Scale bar, 5 μm. Right side is the magnified views of the regions boxed by dotted lines. Scale bar, 1 μm. The soma and proximal dendrites of PyNs were labeled by GRASP1. Yellow arrow head point to GABAergic synapses as indicated by Bassoon+ puncta that are either apposed to or overlapped with VGAT+ puncta.
(**D**) Quantification of the number of perisomatic GABAergic synapses per PyN. 5-7 PyNs were analyzed for each mouse; 4 euploid, 5 Ts65Dn, and 4 Ts65Dn:*Dscam*+/+/- mice were analyzed. Sample numbers are 24 for euploid, 29 for Ts65Dn, and 23 for Ts65Dn:*Dscam*+/+/-.
(**E**) Representative traces of mIPSCs from PyNs in layer II/III of ACC in euploid, Ts65Dn, and Ts65Dn:*Dscam*+/+/- brain slices.
(**F-G**) Quantification of mIPSC frequency (F) and amplitude (G). 2-4 PyNs were recorded for each mouse. 6 euploid control, 6 Ts65Dn, and 6 Ts65Dn:*Dscam*+/+/- were analyzed. N: 15 for euploid, 13 for Ts65Dn, and 14 Ts65Dn:*Dscam*+/+/-.
(**H**) Representative traces of sIPSCs from PyNs in layer II/III of ACC in euploid, Ts65Dn and Ts65Dn:*Dscam*+/+/- brain slices.
(**I-J**) Quantification of sIPSC frequency (I) and amplitude (J). 2~4 PyNs were recorded for each mouse. 6 euploid, 7 Ts65Dn, and 6 Ts65Dn:*Dscam*+/+/- mice were analyzed. N: 19 for euploid, 19 for Ts65Dn, and 16 Ts65Dn:*Dscam*+/+/-.

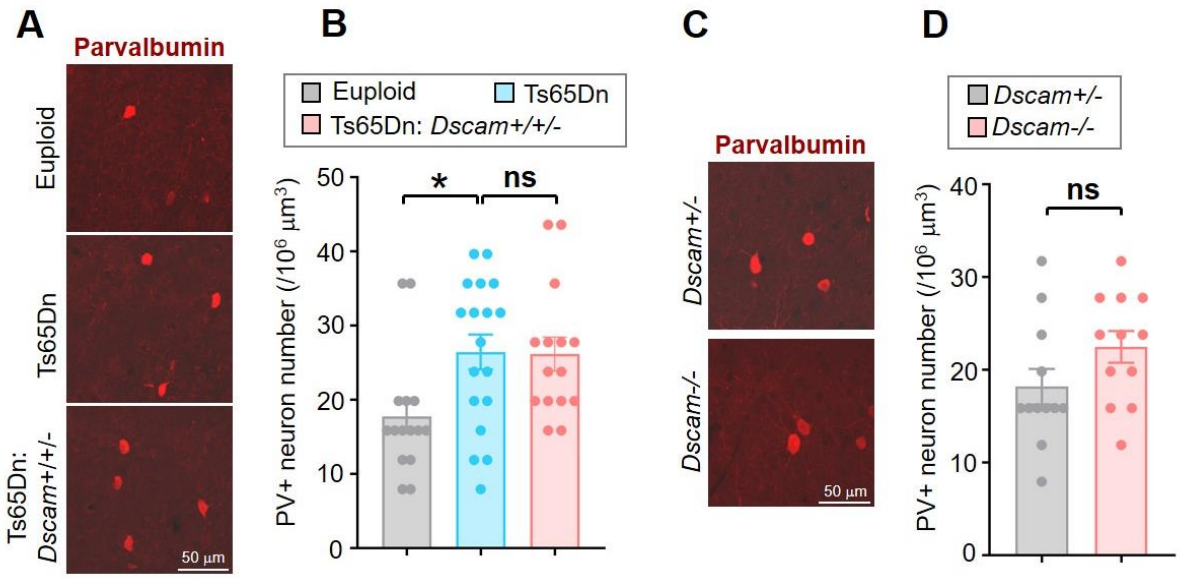

Figure 3.13. Dscam does not regulate the number of GABAergic neurons in the neocortex. (**A-B**) Dscam overexpression in Ts65Dn mice does not affect the number of GABAergic neurons in the neocortex. Brain sections from P28 mice were immunostained with anti-parvalbumin (PV). Representative images are shown in (A), and quantifications of the density of PV+ neurons are shown in (B). Each dot represents the value from one imaging field that is 252.4 µm (width) x 200 µm (length) x 5 µm (thickness). Images were collected from layer II/III of the ACC. Three fields in each mouse were randomly selected for imaging. 5 euploid, 6 Ts65Dn, and 5 Ts65Dn:*Dscam*+/+/- mice were analyzed.
(**C-D**) Loss of *Dscam* does not affect the number of GABAergic neurons in the ACC. Representative images and quantifications are shown in (C) and (D), respectively. 4 *Dscam*+/- and 4 *Dscam*-/- mice were analyzed.

BIBLIOGRAPHY

Altafaj, X., M. Dierssen, C. Baamonde, E. Marti, J. Visa, J. Guimera, M. Oset, J. R. Gonzalez, J. Florez, C. Fillat, and X. Estivill. 2001. 'Neurodevelopmental delay, motor abnormalities and cognitive deficits in transgenic mice overexpressing Dyrk1A (minibrain), a murine model of Down's syndrome', *Hum Mol Genet*, 10: 1915-23.

Amano, K., K. Yamada, Y. Iwayama, S. D. Detera-Wadleigh, E. Hattori, T. Toyota, K. Tokunaga, T. Yoshikawa, and K. Yamakawa. 2008. 'Association study between the Down syndrome cell adhesion molecule (DSCAM)gene and bipolar disorder', *Psychiatric Genetics*, 18: 1-10.

Anastassiou, D., H. Liu, and V. Varadan. 2006. 'Variable window binding for mutually exclusive alternative splicing', *Genome Biol*, 7: R2.

Bando, J. K., S. Gilfillan, C. Song, K. G. McDonald, S. C. Huang, R. D. Newberry, Y. Kobayashi, D. S. J. Allan, J. R. Carlyle, M. Cella, and M. Colonna. 2018. 'The Tumor Necrosis Factor Superfamily Member RANKL Suppresses Effector Cytokine Production in Group 3 Innate Lymphoid Cells', *Immunity*, 48: 1208-19 e4.

Banker, G. 2018. 'The Development of Neuronal Polarity: A Retrospective View', *J Neurosci*, 38: 1867-73.

Baralle, F. E., and J. Giudice. 2017. 'Alternative splicing as a regulator of development and tissue identity', *Nature Reviews Molecular Cell Biology*, 18: 437-51.

Belichenko, P. V., A. M. Kleschevnikov, E. Masliah, C. Wu, R. Takimoto-Kimura, A. Salehi, and W. C. Mobley. 2009. 'Excitatory-inhibitory relationship in the fascia dentata in the Ts65Dn mouse model of Down syndrome', *J Comp Neurol*, 512: 453-66.

Belichenko, P. V., E. Masliah, A. M. Kleschevnikov, A. J. Villar, C. J. Epstein, A. Salehi, and W. C. Mobley. 2004. 'Synaptic structural abnormalities in the Ts65Dn mouse model of Down Syndrome', *J Comp Neurol*, 480: 281-98.

Blazquez-Llorca, L., A. Woodruff, M. Inan, S. A. Anderson, R. Yuste, J. DeFelipe, and A. Merchan-Perez. 2015. 'Spatial distribution of neurons innervated by chandelier cells', *Brain Struct Funct*, 220: 2817-34.

Braudeau, J., L. Dauphinot, A. Duchon, A. Loistron, R. H. Dodd, Y. Herault, B. Delatour, and M. C. Potier. 2011. 'Chronic Treatment with a Promnesiant GABA-A alpha5-Selective Inverse Agonist Increases Immediate Early Genes Expression during Memory Processing in Mice and Rectifies Their Expression Levels in a Down Syndrome Mouse Model', *Adv Pharmacol Sci*, 2011: 153218.

Braudeau, J., B. Delatour, A. Duchon, P. L. Pereira, L. Dauphinot, F. de Chaumont, J. C. Olivo-Marin, R. H. Dodd, Y. Herault, and M. C. Potier. 2011. 'Specific targeting of the GABA-A receptor alpha5 subtype by a selective inverse agonist restores cognitive deficits in Down syndrome mice', *J Psychopharmacol*, 25: 1030-42.

Brown, V., P. Jin, S. Ceman, J. C. Darnell, W. T. O'Donnell, S. A. Tenenbaum, X. Jin, Y. Feng, K. D. Wilkinson, J. D. Keene, R. B. Darnell, and S. T. Warren. 2001. 'Microarray identification

of FMRP-associated brain mRNAs and altered mRNA translational profiles in fragile X syndrome', *Cell*, 107: 477-87.
Bruce, F. M., S. Brown, J. N. Smith, P. G. Fuerst, and L. Erskine. 2017. 'DSCAM promotes axon fasciculation and growth in the developing optic pathway', *Proc Natl Acad Sci U S A*, 114: 1702-07.
Buffington, S. A., J. M. Sobotzik, C. Schultz, and M. N. Rasband. 2012. 'I kappa B alpha is not required for axon initial segment assembly', *Molecular and Cellular Neuroscience*, 50: 1-9.
Caceres, A., B. Ye, and C. G. Dotti. 2012. 'Neuronal polarity: demarcation, growth and commitment', *Current Opinion in Cell Biology*, 24: 547-53.
Castells-Nobau, A., I. Eidhof, M. Fenckova, D. B. Brenman-Suttner, J. M. Scheffer-de Gooyert, S. Christine, R. L. Schellevis, K. van der Laan, C. Quentin, L. van Ninhuijs, F. Hofmann, R. Ejsmont, S. E. Fisher, J. M. Kramer, S. J. Sigrist, A. F. Simon, and A. Schenck. 2019. 'Conserved regulation of neurodevelopmental processes and behavior by FoxP in Drosophila', *PLoS One*, 14.
Cellot, G., and E. Cherubini. 2014. 'GABAergic signaling as therapeutic target for autism spectrum disorders', *Frontiers in Pediatrics*, 2.
Chakrabarti, L., T. K. Best, N. P. Cramer, R. S. Carney, J. T. Isaac, Z. Galdzicki, and T. F. Haydar. 2010. 'Olig1 and Olig2 triplication causes developmental brain defects in Down syndrome', *Nat Neurosci*, 13: 927-34.
Chao, H. T., H. Chen, R. C. Samaco, M. Xue, M. Chahrour, J. Yoo, J. L. Neul, S. Gong, H. C. Lu, N. Heintz, M. Ekker, J. L. Rubenstein, J. L. Noebels, C. Rosenmund, and H. Y. Zoghbi. 2010. 'Dysfunction in GABA signalling mediates autism-like stereotypies and Rett syndrome phenotypes', *Nature*, 468: 263-9.
Chattopadhyaya, B., and G. D. Cristo. 2012. 'GABAergic circuit dysfunctions in neurodevelopmental disorders', *Front Psychiatry*, 3: 51.
Chaudhry, F. A., R. J. Reimer, E. E. Bellocchio, N. C. Danbolt, K. K. Osen, R. H. Edwards, and J. Storm-Mathisen. 1998. 'The vesicular GABA transporter, VGAT, localizes to synaptic vesicles in sets of glycinergic as well as GABAergic neurons', *Journal of Neuroscience*, 18: 9733-50.
Chen, B. E., M. Kondo, A. Garnier, F. L. Watson, R. Puettmann-Holgado, D. R. Lamar, and D. Schmucker. 2006. 'The molecular diversity of Dscam is functionally required for neuronal wiring specificity in Drosophila', *Cell*, 125: 607-20.
Chen, Y., O. Akin, A. Nern, C. Y. Tsui, M. Y. Pecot, and S. L. Zipursky. 2014. 'Cell-type-specific labeling of synapses in vivo through synaptic tagging with recombination', *Neuron*, 81: 280-93.
Cline, Hollis, and Kurt Haas. 2008. 'The regulation of dendritic arbor development and plasticity by glutamatergic synaptic input: a review of the synaptotrophic hypothesis', *J Physiol*, 586: 1509-17.
Colas, D., B. Chuluun, D. Warrier, M. Blank, D. Z. Wetmore, P. Buckmaster, C. C. Garner, and H. C. Heller. 2013a. 'Short-term treatment with the GABAA receptor antagonist pentylenetetrazole produces a sustained pro-cognitive benefit in a mouse model of Down's syndrome', *Br J Pharmacol*, 169: 963-73.
———. 2013b. 'Short-term treatment with the GABAA receptor antagonist pentylenetetrazole produces a sustained pro-cognitive benefit in a mouse model of Down's syndrome', *British Journal of Pharmacology*, 169: 963-73.
Collins, C. A., Y. P. Wairkar, S. L. Johnson, and A. DiAntonio. 2006. 'Highwire restrains synaptic growth by attenuating a MAP kinase signal', *Neuron*, 51: 57-69.

Connolly, J. B., I. J. Roberts, J. D. Armstrong, K. Kaiser, M. Forte, T. Tully, and C. J. O'Kane. 1996. 'Associative learning disrupted by impaired Gs signaling in Drosophila mushroom bodies', *Science*, 274: 2104-7.
Contestabile, A., S. Magara, and L. Cancedda. 2017. 'The GABAergic Hypothesis for Cognitive Disabilities in Down Syndrome', *Frontiers in cellular neuroscience*, 11: 54.
Costa, A. C., and M. J. Grybko. 2005. 'Deficits in hippocampal CA1 LTP induced by TBS but not HFS in the Ts65Dn mouse: a model of Down syndrome', *Neurosci Lett*, 382: 317-22.
Cvetkovska, V., A. D. Hibbert, F. Emran, and B. E. Chen. 2013. 'Overexpression of Down syndrome cell adhesion molecule impairs precise synaptic targeting', *Nat Neurosci*, 16: 677-82.
Dalva, M. B., A. C. McClelland, and M. S. Kayser. 2007. 'Cell adhesion molecules: signalling functions at the synapse', *Nature Reviews Neuroscience*, 8: 206-20.
Darnell, J. C., S. J. Van Driesche, C. Zhang, K. Y. Hung, A. Mele, C. E. Fraser, E. F. Stone, C. Chen, J. J. Fak, S. W. Chi, D. D. Licatalosi, J. D. Richter, and R. B. Darnell. 2011. 'FMRP stalls ribosomal translocation on mRNAs linked to synaptic function and autism', *Cell*, 146: 247-61.
DasGupta, S., C. H. Ferreira, and G. Miesenbock. 2014. 'FoxP influences the speed and accuracy of a perceptual decision in Drosophila', *Science*, 344: 901-04.
De la Torre, R., S. De Sola, M. Pons, A. Duchon, M. M. de Lagran, M. Farre, M. Fito, B. Benejam, K. Langohr, J. Rodriguez, M. Pujadas, J. C. Bizot, A. Cuenca, N. Janel, S. Catuara, M. I. Covas, H. Blehaut, Y. Herault, J. M. Delabar, and M. Dierssen. 2014. 'Epigallocatechin-3-gallate, a DYRK1A inhibitor, rescues cognitive deficits in Down syndrome mouse models and in humans', *Mol Nutr Food Res*, 58: 278-88.
de Wit, J., and A. Ghosh. 2016. 'Specification of synaptic connectivity by cell surface interactions', *Nat Rev Neurosci*, 17: 22-35.
DeFelipe, J. 1999. 'Chandelier cells and epilepsy', *Brain*, 122 (Pt 10): 1807-22.
Del Pino, I., C. Garcia-Frigola, N. Dehorter, J. R. Brotons-Mas, E. Alvarez-Salvado, M. Martinez de Lagran, G. Ciceri, M. V. Gabaldon, D. Moratal, M. Dierssen, S. Canals, O. Marin, and B. Rico. 2013. 'Erbb4 deletion from fast-spiking interneurons causes schizophrenia-like phenotypes', *Neuron*, 79: 1152-68.
Desai, C. J., P. A. Garrity, H. Keshishian, S. L. Zipursky, and K. Zinn. 1999. 'The Drosophila SH2-SH3 adapter protein Dock is expressed in embryonic axons and facilitates synapse formation by the RP3 motoneuron', *Development*, 126: 1527-35.
Dieck, S. T., L. Sanmarti-Vila, K. Langnaese, K. Richter, S. Kindler, A. Soyke, H. Wex, K. H. Smalla, U. Kampf, J. T. Franzer, M. Stumm, C. C. Garner, and E. D. Gundelfinger. 1998. 'Bassoon, a novel zinc-finger CAG/glutamine-repeat protein selectively localized at the active zone of presynaptic nerve terminals', *Journal of Cell Biology*, 142: 499-509.
Ehrhardt, C., M. Schmolke, A. Matzke, A. Knoblauch, C. Will, V. Wixler, and S. Ludwig. 2006. 'Polyethylenimine, a cost-effective transfection reagent', *Signal Transduction*, 6: 179–84.
Fan, X. P., J. P. Labrador, H. Hing, and G. J. Bashaw. 2003. 'Slit stimulation recruits Dock and Pak to the roundabout receptor and increases Rac activity to regulate axon repulsion at the CNS midline', *Neuron*, 40: 113-27.
Favuzzi, E., R. Deogracias, A. Marques-Smith, P. Maeso, J. Jezequel, D. Exposito-Alonso, M. Balia, T. Kroon, A. J. Hinojosa, F. Maraver E, and B. Rico. 2019. 'Distinct molecular programs regulate synapse specificity in cortical inhibitory circuits', *Science*, 363: 413-17.
Fazzari, P., A. V. Paternain, M. Valiente, R. Pla, R. Lujan, K. Lloyd, J. Lerma, O. Marin, and B. Rico. 2010. 'Control of cortical GABA circuitry development by Nrg1 and ErbB4 signalling', *Nature*, 464: 1376-80.

Fernandez, F., and C. C. Garner. 2008. 'Episodic-like memory in Ts65Dn, a mouse model of Down syndrome', *Behavioural brain research*, 188: 233-7.
Fernandez, F., W. Morishita, E. Zuniga, J. Nguyen, M. Blank, R. C. Malenka, and C. C. Garner. 2007. 'Pharmacotherapy for cognitive impairment in a mouse model of Down syndrome', *Nat Neurosci*, 10: 411-3.
Flak, J. N., D. Arble, W. Pan, C. Patterson, T. Lanigan, P. B. Goforth, J. Sacksner, M. Joosten, D. A. Morgan, M. B. Allison, J. Hayes, E. Feldman, R. J. Seeley, D. P. Olson, K. Rahmouni, and M. G. Myers. 2017. 'A leptin-regulated circuit controls glucose mobilization during noxious stimuli', *Journal of Clinical Investigation*, 127: 3103-13.
Forsthoefel, D. J., E. C. Liebl, P. A. Kolodziej, and M. A. Seeger. 2005. 'The Abelson tyrosine kinase, the Trio GEF and Enabled interact with the Netrin receptor Frazzled in Drosophila', *Development*, 132: 1983-94.
Fotaki, V., M. Dierssen, S. Alcantara, S. Martinez, E. Marti, C. Casas, J. Visa, E. Soriano, X. Estivill, and M. L. Arbones. 2002. 'Dyrk1A haploinsufficiency affects viability and causes developmental delay and abnormal brain morphology in mice', *Mol Cell Biol*, 22: 6636-47.
Fuerst, P. G., A. Koizumi, R. H. Masland, and R. W. Burgess. 2008. 'Neurite arborization and mosaic spacing in the mouse retina require DSCAM', *Nature*, 451: 470-U8.
Garcia-Cerro, S., P. Martinez, V. Vidal, A. Corrales, J. Florez, R. Vidal, N. Rueda, M. L. Arbones, and C. Martinez-Cue. 2014. 'Overexpression of Dyrk1A Is Implicated in Several Cognitive, Electrophysiological and Neuromorphological Alterations Found in a Mouse Model of Down Syndrome', *PLoS One*, 9.
Gardiner, K., Y. Herault, I. T. Lott, S. E. Antonarakis, R. H. Reeves, and M. Dierssen. 2010. 'Down syndrome: from understanding the neurobiology to therapy', *J Neurosci*, 30: 14943-5.
Garrity, P. A., Y. Rao, I. Salecker, J. McGlade, T. Pawson, and S. L. Zipursky. 1996. 'Drosophila photoreceptor axon guidance and targeting requires the dreadlocks SH2/SH3 adapter protein', *Cell*, 85: 639-50.
Goyal, G., J. Zheng, E. Adam, G. Steffes, M. Jain, K. Klavins, and T. Hummel. 2019. 'Sphingolipid-dependent Dscam sorting regulates axon segregation', *Nat Commun*, 10: 813.
Gratz, S. J., F. P. Ukken, C. D. Rubinstein, G. Thiede, L. K. Donohue, A. M. Cummings, and K. M. O'Connor-Giles. 2014. 'Highly specific and efficient CRISPR/Cas9-catalyzed homology-directed repair in Drosophila', *Genetics*, 196: 961-71.
Grigoriou, M., A. S. Tucker, P. T. Sharpe, and V. Pachnis. 1998. 'Expression and regulation of Lhx6 and Lhx7, a novel subfamily of LIM homeodomain encoding genes, suggests a role in mammalian head development', *Development*, 125: 2063-74.
Grueber, W. B., L. Y. Jan, and Y. N. Jan. 2002. 'Tiling of the Drosophila epidermis by multidendritic sensory neurons', *Development*, 129: 2867-78.
Grueber, W. B., and Y. N. Jan. 2004. 'Dendritic development: lessons from Drosophila and related branches', *Curr Opin Neurobiol*, 14: 74-82.
Grueber, W. B., B. Ye, A. W. Moore, L. Y. Jan, and Y. N. Jan. 2003. 'Dendrites of distinct classes of Drosophila sensory neurons show different capacities for homotypic repulsion', *Current Biology*, 13: 618-26.
Grueber, W. B., B. Ye, C. H. Yang, S. Younger, K. Borden, L. Y. Jan, and Y. N. Jan. 2007. 'Projections of Drosophila multidendritic neurons in the central nervous system: links with peripheral dendrite morphology', *Development*, 134: 55-64.

Grun, D., M. Kirchner, N. Thierfelder, M. Stoeckius, M. Selbach, and N. Rajewsky. 2014. 'Conservation of mRNA and protein expression during development of C. elegans', *Cell Rep,* 6: 565-77.
Gu, P., J. Gong, Y. Shang, F. Wang, K. T. Ruppell, Z. Ma, A. E. Sheehan, M. R. Freeman, and Y. Xiang. 2019. 'Polymodal Nociception in Drosophila Requires Alternative Splicing of TrpA1', *Curr Biol,* 29: 3961-73 e6.
Gutierrez, H., L. Kisiswa, G. W. O'Keeffe, M. J. Smithen, S. Wyatt, and A. M. Davies. 2013. 'Regulation of neurite growth by tumour necrosis superfamily member RANKL', *Open Biol,* 3: 120150.
Hamdan, H., B. C. Lim, T. Torii, A. Joshi, M. Konning, C. Smith, D. J. Palmer, P. Ng, C. Leterrier, J. A. Oses-Prieto, A. L. Burlingame, and M. N. Rasband. 2019. 'Mapping Axon Initial Segment Structure and Function by Multiplexed Proximity Biotinylation', *Molecular & Cellular Proteomics,* 18: S29-S29.
Hammerle, B., C. Elizalde, and F. J. Tejedor. 2008. 'The spatio-temporal and subcellular expression of the candidate Down syndrome gene Mnb/Dyrk1A in the developing mouse brain suggests distinct sequential roles in neuronal development', *Eur J Neurosci,* 27: 1061-74.
Hammerle, B., E. Vera-Samper, S. Speicher, R. Arencibia, S. Martinez, and F. J. Tejedor. 2002. 'Mnb/Dyrk1A is transiently expressed and asymmetrically segregated in neural progenitor cells at the transition to neurogenic divisions', *Developmental Biology,* 246: 259-73.
Han, G. S., and G. M. Carman. 2010. 'Characterization of the human LPIN1-encoded phosphatidate phosphatase isoforms', *J Biol Chem,* 285: 14628-38.
Haydar, T. F., and R. H. Reeves. 2012. 'Trisomy 21 and early brain development', *Trends Neurosci,* 35: 81-91.
Heisenberg, M. 2003. 'Mushroom body memoir: From maps to models', *Nature Reviews Neuroscience,* 4: 266-75.
Herculano-Houzel, S. 2009. 'The human brain in numbers: a linearly scaled-up primate brain', *Front Hum Neurosci,* 3: 31.
Herrera, D. G., and H. A. Robertson. 1996. 'Activation of c-fos in the brain', *Prog Neurobiol,* 50: 83-107.
Hing, H., J. Xiao, N. Harden, L. Lim, and S. L. Zipursky. 1999. 'Pak functions downstream of Dock to regulate photoreceptor axon guidance in Drosophila', *Cell,* 97: 853-63.
Hsouna, A., Y. S. Kim, and M. F. VanBerkum. 2003. 'Abelson tyrosine kinase is required to transduce midline repulsive cues', *J Neurobiol,* 57: 15-30.
Huang, Z. J., and A. Paul. 2019. 'The diversity of GABAergic neurons and neural communication elements', *Nat Rev Neurosci,* 20: 563-72.
Hughes, M. E., R. Bortnick, A. Tsubouchi, P. Baumer, M. Kondo, T. Uemura, and D. Schmucker. 2007. 'Homophilic Dscam interactions control complex dendrite morphogenesis', *Neuron,* 54: 417-27.
Hwang, R. Y., L. Zhong, Y. Xu, T. Johnson, F. Zhang, K. Deisseroth, and W. D. Tracey. 2007. 'Nociceptive neurons protect Drosophila larvae from parasitoid wasps', *Curr Biol,* 17: 2105-16.
Inan, M., and S. A. Anderson. 2014. 'The chandelier cell, form and function', *Curr Opin Neurobiol,* 26: 142-8.
Jan, Y. N., and L. Y. Jan. 2010. 'Branching out: mechanisms of dendritic arborization', *Nat Rev Neurosci,* 11: 316-28.
Javaherian, A., and H. T. Cline. 2005. 'Coordinated motor neuron axon growth and neuromuscular synaptogenesis are promoted by CPG15 in vivo', *Neuron,* 45: 505-12.

Jones, E. G. 1975. 'Varieties and distribution of non-pyramidal cells in the somatic sensory cortex of the squirrel monkey', *J Comp Neurol*, 160: 205-67.
Joshi, K., L. Shen, A. Michaeli, M. Salter, G. Thibault-Messier, S. Hashmi, J. H. Eubanks, M. A. Cortez, and O. C. Snead. 2016. 'Infantile spasms in down syndrome: Rescue by knockdown of the GIRK2 channel', *Ann Neurol*, 80: 511-21.
Kamiyama, D., R. McGorty, R. Kamiyama, M. D. Kim, A. Chiba, and B. Huang. 2015. 'Specification of Dendritogenesis Site in Drosophila aCC Motoneuron by Membrane Enrichment of Pak1 through Dscam1', *Dev Cell*, 35: 93-106.
Kelemen, O., P. Convertini, Z. Zhang, Y. Wen, M. Shen, M. Falaleeva, and S. Stamm. 2013. 'Function of alternative splicing', *Gene*, 514: 1-30.
Kim, J. H., X. Wang, R. Coolon, and B. Ye. 2013. 'Dscam expression levels determine presynaptic arbor sizes in Drosophila sensory neurons', *Neuron*, 78: 827-38.
Kim, S. E., B. Coste, A. Chadha, B. Cook, and A. Patapoutian. 2012. 'The role of Drosophila Piezo in mechanical nociception', *Nature*, 483: 209-12.
Kimura, N., M. Ueno, K. Nakashima, and T. Taga. 1999. 'A brain region-specific gene product Lhx6.1 interacts with Ldb1 through tandem LIM-domains', *Journal of Biochemistry*, 126: 180-87.
Kleschevnikov, A. M., P. V. Belichenko, M. Faizi, L. F. Jacobs, K. Htun, M. Shamloo, and W. C. Mobley. 2012. 'Deficits in cognition and synaptic plasticity in a mouse model of Down syndrome ameliorated by GABAB receptor antagonists', *J Neurosci*, 32: 9217-27.
Kleschevnikov, A. M., P. V. Belichenko, J. Gall, L. George, R. Nosheny, M. T. Maloney, A. Salehi, and W. C. Mobley. 2012. 'Increased efficiency of the GABAA and GABAB receptor-mediated neurotransmission in the Ts65Dn mouse model of Down syndrome', *Neurobiol Dis*, 45: 683-91.
Kleschevnikov, A. M., P. V. Belichenko, A. J. Villar, C. J. Epstein, R. C. Malenka, and W. C. Mobley. 2004. 'Hippocampal long-term potentiation suppressed by increased inhibition in the Ts65Dn mouse, a genetic model of Down syndrome', *J Neurosci*, 24: 8153-60.
Ko, J., G. Choii, and J. W. Um. 2015. 'The balancing act of GABAergic synapse organizers', *Trends Mol Med*, 21: 256-68.
Konopaske, G. T., R. A. Sweet, Q. Wu, A. Sampson, and D. A. Lewis. 2006. 'Regional specificity of chandelier neuron axon terminal alterations in schizophrenia', *Neuroscience*, 138: 189-96.
Krueger-Burg, D., T. Papadopoulos, and N. Brose. 2017. 'Organizers of inhibitory synapses come of age', *Curr Opin Neurobiol*, 45: 66-77.
Krueger, D. D., L. P. Tuffy, T. Papadopoulos, and N. Brose. 2012. 'The role of neurexins and neuroligins in the formation, maturation, and function of vertebrate synapses', *Curr Opin Neurobiol*, 22: 412-22.
Krumm, N., T. N. Turner, C. Baker, L. Vives, K. Mohajeri, K. Witherspoon, A. Raja, B. P. Coe, H. A. Stessman, Z. X. He, S. M. Leal, R. Bernier, and E. E. Eichler. 2015. 'Excess of rare, inherited truncating mutations in autism', *Nat Genet*, 47: 582-8.
Kuo, C. T., L. Y. Jan, and Y. N. Jan. 2005. 'Dendrite-specific remodeling of Drosophila sensory neurons requires matrix metalloproteases, ubiquitin-proteasome, and ecdysone signaling', *Proc Natl Acad Sci U S A*, 102: 15230-5.
Kurt, M. A., D. C. Davies, M. Kidd, M. Dierssen, and J. Florez. 2000. 'Synaptic deficit in the temporal cortex of partial trisomy 16 (Ts65Dn) mice', *Brain Res*, 858: 191-7.

Kurup, N., and Y. Jin. 2016. 'Neural circuit rewiring: insights from DD synapse remodeling', *Worm*, 5: e1129486.
Kurup, N., D. Yan, A. Goncharov, and Y. Jin. 2015. 'Dynamic microtubules drive circuit rewiring in the absence of neurite remodeling', *Curr Biol*, 25: 1594-605.
Kurup, N., D. Yan, K. Kono, and Y. Jin. 2017. 'Differential regulation of polarized synaptic vesicle trafficking and synapse stability in neural circuit rewiring in Caenorhabditis elegans', *PLoS Genet*, 13: e1006844.
Lakso, M., B. Sauer, B. Mosinger, Jr., E. J. Lee, R. W. Manning, S. H. Yu, K. L. Mulder, and H. Westphal. 1992. 'Targeted oncogene activation by site-specific recombination in transgenic mice', *Proc Natl Acad Sci U S A*, 89: 6232-6.
Larsen, D. D., and E. M. Callaway. 2006. 'Development of layer-specific axonal arborizations in mouse primary somatosensory cortex', *J Comp Neurol*, 494: 398-414.
Lawton, K. J., T. L. Wassmer, and D. L. Deitcher. 2014. 'Conserved role of Drosophila melanogaster FoxP in motor coordination and courtship song', *Behavioural Brain Research*, 268: 213-21.
Lee, H., U. Engel, J. Rusch, S. Scherrer, K. Sheard, and D. Van Vactor. 2004. 'The microtubule plus end tracking protein Orbit/MAST/CLASP acts downstream of the tyrosine kinase Abl in mediating axon guidance', *Neuron*, 42: 913-26.
Lee, J. A., A. Damianov, C. H. Lin, M. Fontes, N. N. Parikshak, E. S. Anderson, D. H. Geschwind, D. L. Black, and K. C. Martin. 2016. 'Cytoplasmic Rbfox1 Regulates the Expression of Synaptic and Autism-Related Genes', *Neuron*, 89: 113-28.
Lee, T., and L. Luo. 1999. 'Mosaic analysis with a repressible cell marker for studies of gene function in neuronal morphogenesis', *Neuron*, 22: 451-61.
Lee, Y., and D. C. Rio. 2015. 'Mechanisms and Regulation of Alternative Pre-mRNA Splicing', *Annu Rev Biochem*, 84: 291-323.
Lerch, J. K., F. Kuo, D. Motti, R. Morris, J. L. Bixby, and V. P. Lemmon. 2012. 'Isoform Diversity and Regulation in Peripheral and Central Neurons Revealed through RNA-Seq', *PLoS ONE*, 7.
Lewis, D. A. 2011. 'The chandelier neuron in schizophrenia', *Dev Neurobiol*, 71: 118-27.
———. 2014. 'Inhibitory neurons in human cortical circuits: substrate for cognitive dysfunction in schizophrenia', *Curr Opin Neurobiol*, 26: 22-6.
Lewis, D. A., A. A. Curley, J. R. Glausier, and D. W. Volk. 2012. 'Cortical parvalbumin interneurons and cognitive dysfunction in schizophrenia', *Trends Neurosci*, 35: 57-67.
Li, J., S. Han, H. Li, N. D. Udeshi, T. Svinkina, D. R. Mani, C. Xu, R. Guajardo, Q. Xie, T. Li, D. J. Luginbuhl, B. Wu, C. N. McLaughlin, A. Xie, P. Kaewsapsak, S. R. Quake, S. A. Carr, A. Y. Ting, and L. Luo. 2020. 'Cell-Surface Proteomic Profiling in the Fly Brain Uncovers Wiring Regulators', *Cell*, 180: 373-86 e15.
Lim, L., D. Mi, A. Llorca, and O. Marin. 2018. 'Development and Functional Diversification of Cortical Interneurons', *Neuron*, 100: 294-313.
Liu, G., W. Li, L. Wang, A. Kar, K. L. Guan, Y. Rao, and J. Y. Wu. 2009. 'DSCAM functions as a netrin receptor in commissural axon pathfinding', *Proc Natl Acad Sci U S A*, 106: 2951-6.
Loh, K. H., P. S. Stawski, A. S. Draycott, N. D. Udeshi, E. K. Lehrman, D. K. Wilton, T. Svinkina, T. J. Deerinck, M. H. Ellisman, B. Stevens, S. A. Carr, and A. Y. Ting. 2016. 'Proteomic Analysis of Unbounded Cellular Compartments: Synaptic Clefts', *Cell*, 166: 1295-+.

Lowe, S. A., J. J. L. Hodge, and M. M. Usowicz. 2018. 'A third copy of the Down syndrome cell adhesion molecule (Dscam) causes synaptic and locomotor dysfunction in Drosophila', *Neurobiol Dis*, 110: 93-101.
Lu, J., J. Tucciarone, N. Padilla-Coreano, M. He, J. A. Gordon, and Z. J. Huang. 2017. 'Selective inhibitory control of pyramidal neuron ensembles and cortical subnetworks by chandelier cells', *Nat Neurosci*, 20: 1377-83.
Martinez-Cue, C., P. Martinez, N. Rueda, R. Vidal, S. Garcia, V. Vidal, A. Corrales, J. A. Montero, A. Pazos, J. Florez, R. Gasser, A. W. Thomas, M. Honer, F. Knoflach, J. L. Trejo, J. G. Wettstein, and M. C. Hernandez. 2013. 'Reducing GABAA alpha5 receptor-mediated inhibition rescues functional and neuromorphological deficits in a mouse model of down syndrome', *J Neurosci*, 33: 3953-66.
Martinez de Lagran, M., X. Altafaj, X. Gallego, E. Marti, X. Estivill, I. Sahun, C. Fillat, and M. Dierssen. 2004. 'Motor phenotypic alterations in TgDyrk1a transgenic mice implicate DYRK1A in Down syndrome motor dysfunction', *Neurobiol Dis*, 15: 132-42.
Matthews, Benjamin J., Michelle E. Kim, John J. Flanagan, Daisuke Hattori, James C. Clemens, S. Lawrence Zipursky, and Wesley B. Grueber. 2007. 'Dendrite Self-Avoidance Is Controlled by Dscam', *Cell*, 129: 593-604.
Mayer, C., C. Hafemeister, R. C. Bandler, R. Machold, R. Batista Brito, X. Jaglin, K. Allaway, A. Butler, G. Fishell, and R. Satija. 2018. 'Developmental diversification of cortical inhibitory interneurons', *Nature*, 555: 457-62.
Mendoza, E., J. Colomb, J. Rybak, H. J. Pfluger, T. Zars, C. Scharff, and B. Brembs. 2014. 'Drosophila FoxP Mutants Are Deficient in Operant Self-Learning', *PLoS One*, 9.
Mi, D., Z. Li, L. Lim, M. Li, M. Moissidis, Y. Yang, T. Gao, T. X. Hu, T. Pratt, D. J. Price, N. Sestan, and O. Marin. 2018. 'Early emergence of cortical interneuron diversity in the mouse embryo', *Science*, 360: 81-85.
Mishra, A., B. Knerr, S. Paixao, E. R. Kramer, and R. Klein. 2008. 'The protein dendrite arborization and synapse maturation 1 (Dasm-1) is dispensable for dendrite arborization', *Mol Cell Biol*, 28: 2782-91.
Mishra, A., M. H. Traut, L. Becker, T. Klopstock, V. Stein, and R. Klein. 2014. 'Genetic evidence for the adhesion protein IgSF9/Dasm1 to regulate inhibitory synapse development independent of its intracellular domain', *J Neurosci*, 34: 4187-99.
Missler, M., T. C. Sudhof, and T. Biederer. 2012. 'Synaptic cell adhesion', *Cold Spring Harb Perspect Biol*, 4: a005694.
Moller, R. S., S. Kubart, M. Hoeltzenbein, B. Heye, I. Vogel, C. P. Hansen, C. Menzel, R. Ullmann, N. Tommerup, H. H. Ropers, Z. Tumer, and V. M. Kalscheuer. 2008. 'Truncation of the Down syndrome candidate gene DYRK1A in two unrelated patients with microcephaly', *Am J Hum Genet*, 82: 1165-70.
Moriya, H. 2015. 'Quantitative nature of overexpression experiments', *Mol Biol Cell*, 26: 3932-9.
Nakata, K., B. Abrams, B. Grill, A. Goncharov, X. Huang, A. D. Chisholm, and Y. Jin. 2005. 'Regulation of a DLK-1 and p38 MAP kinase pathway by the ubiquitin ligase RPM-1 is required for presynaptic development', *Cell*, 120: 407-20.
Nakazawa, K., V. Zsiros, Z. Jiang, K. Nakao, S. Kolata, S. Zhang, and J. E. Belforte. 2012. 'GABAergic interneuron origin of schizophrenia pathophysiology', *Neuropharmacology*, 62: 1574-83.
Nelson, A. D., R. N. Caballero-Floran, J. C. R. Diaz, J. M. Hull, Y. Yuan, J. Li, K. Chen, K. K. Walder, L. F. Lopez-Santiago, V. Bennett, M. G. McInnis, L. L. Isom, C. Wang, M. Zhang, K. S.

Jones, and P. M. Jenkins. 2019. 'Correction: Ankyrin-G regulates forebrain connectivity and network synchronization via interaction with GABARAP', *Mol Psychiatry*.
Nelson, A. D., R. N. Caballero-Floran, J. C. Rodriguez Diaz, J. M. Hull, Y. Yuan, J. Li, K. Chen, K. K. Walder, L. F. Lopez-Santiago, V. Bennett, M. G. McInnis, L. L. Isom, C. Wang, M. Zhang, K. S. Jones, and P. M. Jenkins. 2018. 'Ankyrin-G regulates forebrain connectivity and network synchronization via interaction with GABARAP', *Mol Psychiatry*.
Nern, A., B. D. Pfeiffer, K. Svoboda, and G. M. Rubin. 2011. 'Multiple new site-specific recombinases for use in manipulating animal genomes', *Proc Natl Acad Sci U S A*, 108: 14198-203.
Neumann, H., R. Schweigreiter, T. Yamashita, K. Rosenkranz, H. Wekerle, and Y. A. Barde. 2002. 'Tumor necrosis factor inhibits neurite outgrowth and branching of hippocampal neurons by a rho-dependent mechanism', *J Neurosci*, 22: 854-62.
Nosheny, R. L., P. V. Belichenko, B. L. Busse, A. M. Weissmiller, V. Dang, D. Das, A. Fahimi, A. Salehi, S. J. Smith, and W. C. Mobley. 2015. 'Increased cortical synaptic activation of TrkB and downstream signaling markers in a mouse model of Down Syndrome', *Neurobiol Dis*, 77: 173-90.
O'Roak, B. J., H. A. Stessman, E. A. Boyle, K. T. Witherspoon, B. Martin, C. Lee, L. Vives, C. Baker, J. B. Hiatt, D. A. Nickerson, R. Bernier, J. Shendure, and E. E. Eichler. 2014. 'Recurrent de novo mutations implicate novel genes underlying simplex autism risk', *Nat Commun*, 5: 5595.
Okui, M., T. Ide, K. Morita, E. Funakoshi, F. Ito, K. Ogita, Y. Yoneda, J. Kudoh, and N. Shimizu. 1999. 'High-level expression of the Mnb/Dyrk1A gene in brain and heart during rat early development', *Genomics*, 62: 165-71.
Osorio, C., P. J. Chacon, M. White, L. Kisiswa, S. Wyatt, A. Rodriguez-Tebar, and A. M. Davies. 2014. 'Selective regulation of axonal growth from developing hippocampal neurons by tumor necrosis factor superfamily member APRIL', *Mol Cell Neurosci*, 59: 24-36.
Park, M., S. Watanabe, V. Y. Poon, C. Y. Ou, E. M. Jorgensen, and K. Shen. 2011. 'CYY-1/cyclin Y and CDK-5 differentially regulate synapse elimination and formation for rewiring neural circuits', *Neuron*, 70: 742-57.
Paul, A., M. Crow, R. Raudales, M. He, J. Gillis, and Z. J. Huang. 2017. 'Transcriptional Architecture of Synaptic Communication Delineates GABAergic Neuron Identity', *Cell*, 171: 522-39 e20.
Pettem, K. L., D. Yokomaku, L. Luo, M. W. Linhoff, T. Prasad, S. A. Connor, T. J. Siddiqui, H. Kawabe, F. Chen, L. Zhang, G. Rudenko, Y. T. Wang, N. Brose, and A. M. Craig. 2013. 'The specific alpha-neurexin interactor calsyntenin-3 promotes excitatory and inhibitory synapse development', *Neuron*, 80: 113-28.
Pfeiffer, B. D., A. Jenett, A. S. Hammonds, T. T. Ngo, S. Misra, C. Murphy, A. Scully, J. W. Carlson, K. H. Wan, T. R. Laverty, C. Mungall, R. Svirskas, J. T. Kadonaga, C. Q. Doe, M. B. Eisen, S. E. Celniker, and G. M. Rubin. 2011. "GAL4 Driver Collection of Rubin Laboratory at Janelia Farm." In.
Poulopoulos, A., G. Aramuni, G. Meyer, T. Soykan, M. Hoon, T. Papadopoulos, M. Zhang, I. Paarmann, C. Fuchs, K. Harvey, P. Jedlicka, S. W. Schwarzacher, H. Betz, R. J. Harvey, N. Brose, W. Zhang, and F. Varoqueaux. 2009. 'Neuroligin 2 drives postsynaptic assembly at perisomatic inhibitory synapses through gephyrin and collybistin', *Neuron*, 63: 628-42.
Prelich, G. 2012. 'Gene overexpression: uses, mechanisms, and interpretation', *Genetics*, 190: 841-54.

Purohit, A. A., W. Li, C. Qu, T. Dwyer, Q. Shao, K. L. Guan, and G. Liu. 2012. 'Down Syndrome Cell Adhesion Molecule (DSCAM) Associates with Uncoordinated-5C (UNC5C) in Netrin-1-mediated Growth Cone Collapse', *The Journal of biological chemistry*, 287: 27126-38.
Ramamoorthi, K., and Y. Lin. 2011. 'The contribution of GABAergic dysfunction to neurodevelopmental disorders', *Trends Mol Med*, 17: 452-62.
Ramón y Cajal, Santiago. 1893. *Nuevo concepto de la histología de los centros nerviosos* (Impr. de Henrich y c.a en comandita, sucesores de N. Ramírez: Barcelona,).
Ran, F. A., P. D. Hsu, J. Wright, V. Agarwala, D. A. Scott, and F. Zhang. 2013. 'Genome engineering using the CRISPR-Cas9 system', *Nature protocols*, 8: 2281-308.
Reeves, R. H., N. G. Irving, T. H. Moran, A. Wohn, C. Kitt, S. S. Sisodia, C. Schmidt, R. T. Bronson, and M. T. Davisson. 1995. 'A mouse model for Down syndrome exhibits learning and behaviour deficits', *Nat Genet*, 11: 177-84.
Reissner, C., J. Stahn, D. Breuer, M. Klose, G. Pohlentz, M. Mormann, and M. Missler. 2014. 'Dystroglycan binding to alpha-neurexin competes with neurexophilin-1 and neuroligin in the brain', *J Biol Chem*, 289: 27585-603.
Roll-Mecak, A., and F. J. McNally. 2010. 'Microtubule-severing enzymes', *Current Opinion in Cell Biology*, 22: 96-103.
Roth, S., L. J. Fulcher, and G. P. Sapkota. 2019. 'Advances in targeted degradation of endogenous proteins', *Cell Mol Life Sci*, 76: 2761-77.
Rueda, N., J. Florez, and C. Martinez-Cue. 2012. 'Mouse Models of Down Syndrome as a Tool to Unravel the Causes of Mental Disabilities', *Neural Plasticity*.
Saito, Y., A. Oka, M. Mizuguchi, K. Motonaga, Y. Mori, L. E. Becker, K. Arima, J. Miyauchi, and S. Takashima. 2000. 'The developmental and aging changes of Down's syndrome cell adhesion molecule expression in normal and Down's syndrome brains', *Acta neuropathologica*, 100: 654-64.
Salehi, A., J. D. Delcroix, P. V. Belichenko, K. Zhan, C. Wu, J. S. Valletta, R. Takimoto-Kimura, A. M. Kleschevnikov, K. Sambamurti, P. P. Chung, W. Xia, A. Villar, W. A. Campbell, L. S. Kulnane, R. A. Nixon, B. T. Lamb, C. J. Epstein, G. B. Stokin, L. S. Goldstein, and W. C. Mobley. 2006. 'Increased App expression in a mouse model of Down's syndrome disrupts NGF transport and causes cholinergic neuron degeneration', *Neuron*, 51: 29-42.
Sanes, J. R., and J. W. Lichtman. 1999. 'Development of the vertebrate neuromuscular junction', *Annu Rev Neurosci*, 22: 389-442.
Sanes, J. R., and R. H. Masland. 2015. 'The types of retinal ganglion cells: current status and implications for neuronal classification', *Annu Rev Neurosci*, 38: 221-46.
Santos, R. A., A. J. C. Fuertes, G. Short, K. C. Donohue, H. Shao, J. Quintanilla, P. Malakzadeh, and S. Cohen-Cory. 2018. 'DSCAM differentially modulates pre- and postsynaptic structural and functional central connectivity during visual system wiring', *Neural Dev*, 13: 22.
Schmucker, D., J. C. Clemens, H. Shu, C. A. Worby, J. Xiao, M. Muda, J. E. Dixon, and S. L. Zipursky. 2000. 'Drosophila Dscam is an axon guidance receptor exhibiting extraordinary molecular diversity', *Cell*, 101: 671-84.
Scotti, M. M., and M. S. Swanson. 2016. 'RNA mis-splicing in disease', *Nat Rev Genet*, 17: 19-32.
Shen, L., Z. Xiao, Y. M. Pan, M. Fang, C. S. Li, D. Chen, L. Wang, Z. Q. Xi, F. Xiao, and X. F. Wang. 2011. 'Altered Expression of Dscam in Temporal Lobe Tissue From Human and Experimental Animals', *Synapse*, 65: 975-82.

Shi, Lei, Hung-Hsiang Yu, Jacob S. Yang, and Tzumin Lee. 2007. 'Specific Drosophila Dscam Juxtamembrane Variants Control Dendritic Elaboration and Axonal Arborization', *J. Neurosci.*, 27: 6723-28.
Shi, S. H., T. Cheng, L. Y. Jan, and Y. N. Jan. 2004. 'The immunoglobulin family member dendrite arborization and synapse maturation 1 (Dasm1) controls excitatory synapse maturation', *Proc Natl Acad Sci U S A*, 101: 13346-51.
Siarey, R. J., J. Stoll, S. I. Rapoport, and Z. Galdzicki. 1997. 'Altered long-term potentiation in the young and old Ts65Dn mouse, a model for Down Syndrome', *Neuropharmacology*, 36: 1549-54.
Soba, P., S. Zhu, K. Emoto, S. Younger, S. J. Yang, H. H. Yu, T. Lee, L. Y. Jan, and Y. N. Jan. 2007. 'Drosophila sensory neurons require Dscam for dendritic self-avoidance and proper dendritic field organization', *Neuron*, 54: 403-16.
Sorra, K. E., and K. M. Harris. 2000. 'Overview on the structure, composition, function, development, and plasticity of hippocampal dendritic spines', *Hippocampus*, 10: 501-11.
Steinecke, A., E. Hozhabri, S. Tapanes, Y. Ishino, H. Zeng, N. Kamasawa, and H. Taniguchi. 2017. 'Neocortical Chandelier Cells Developmentally Shape Axonal Arbors through Reorganization but Establish Subcellular Synapse Specificity without Refinement', *Eneuro*, 4.
Sterne, G. R., J. H. Kim, and B. Ye. 2015a. 'Dysregulated Dscam levels act through Abelson tyrosine kinase to enlarge presynaptic arbors', *Elife*, 4.
Sterne, Gabriella R, Jung Hwan Kim, and Bing Ye. 2015b. 'Dysregulated Dscam levels act through Abelson tyrosine kinase to enlarge presynaptic arbors', *Elife*, 4: e05196.
Sudhof, T. C. 2012. 'The Presynaptic Active Zone', *Neuron*, 75: 11-25.
———. 2018. 'Towards an Understanding of Synapse Formation', *Neuron*, 100: 276-93.
Szentagothai, J. 1975a. 'The 'module-concept' in cerebral cortex architecture', *Brain Res*, 95: 475-96.
———. 1975b. 'Module-Concept in Cerebral-Cortex Architecture', *Brain Res Dev Brain Res*, 95: 475-96.
Tai, Y., N. B. Gallo, M. Wang, J. R. Yu, and L. Van Aelst. 2019. 'Axo-axonic Innervation of Neocortical Pyramidal Neurons by GABAergic Chandelier Cells Requires AnkyrinG-Associated L1CAM', *Neuron*, 102: 358-72 e9.
Tai, Y., J. A. Janas, C. L. Wang, and L. Van Aelst. 2014. 'Regulation of chandelier cell cartridge and bouton development via DOCK7-mediated ErbB4 activation', *Cell Rep*, 6: 254-63.
Takahashi, H., K. Katayama, K. Sohya, H. Miyamoto, T. Prasad, Y. Matsumoto, M. Ota, H. Yasuda, T. Tsumoto, J. Aruga, and A. M. Craig. 2012. 'Selective control of inhibitory synapse development by Slitrk3-PTPdelta trans-synaptic interaction', *Nat Neurosci*, 15: 389-98, S1-2.
Takahashi, H., K. Takahashi, and F. C. Liu. 2009. 'FOXP genes, neural development, speech and language disorders', *Adv Exp Med Biol*, 665: 117-29.
Takano, T., C. Xu, Y. Funahashi, T. Namba, and K. Kaibuchi. 2015. 'Neuronal polarization', *Development*, 142: 2088-93.
Taniguchi, H., J. Lu, and Z. J. Huang. 2013. 'The spatial and temporal origin of chandelier cells in mouse neocortex', *Science*, 339: 70-4.
Terenzio, M., G. Schiavo, and M. Fainzilber. 2017. 'Compartmentalized Signaling in Neurons: From Cell Biology to Neuroscience', *Neuron*, 96: 667-79.
Tremblay, R., S. Lee, and B. Rudy. 2016. 'GABAergic Interneurons in the Neocortex: From Cellular Properties to Circuits', *Neuron*, 91: 260-92.

Turner, T. N., F. Hormozdiari, M. H. Duyzend, S. A. McClymont, P. W. Hook, I. Iossifov, A. Raja, C. Baker, K. Hoekzema, H. A. Stessman, M. C. Zody, B. J. Nelson, J. Huddleston, R. Sandstrom, J. D. Smith, D. Hanna, J. M. Swanson, E. M. Faustman, M. J. Bamshad, J. Stamatoyannopoulos, D. A. Nickerson, A. S. McCallion, R. Darnell, and E. E. Eichler. 2016. 'Genome Sequencing of Autism-Affected Families Reveals Disruption of Putative Noncoding Regulatory DNA', *American journal of human genetics*, 98: 58-74.
Uezu, A., D. J. Kanak, T. W. A. Bradshaw, E. J. Soderblom, C. M. Catavero, A. C. Burette, R. J. Weinberg, and S. H. Soderling. 2016. 'Identification of an elaborate complex mediating postsynaptic inhibition', *Science*, 353: 1123-29.
Um, J. W., G. Pramanik, J. S. Ko, M. Y. Song, D. Lee, H. Kim, K. S. Park, T. C. Sudhof, K. Tabuchi, and J. Ko. 2014. 'Calsyntenins function as synaptogenic adhesion molecules in concert with neurexins', *Cell Rep*, 6: 1096-109.
Van Doren, M., A. L. Williamson, and R. Lehmann. 1998. 'Regulation of zygotic gene expression in Drosophila primordial germ cells', *Curr Biol*, 8: 243-6.
van Spronsen, M., E. Y. van Battum, M. Kuijpers, V. R. Vangoor, M. L. Rietman, J. Pothof, L. F. Gumy, W. F. van Ijcken, A. Akhmanova, R. J. Pasterkamp, and C. C. Hoogenraad. 2013. 'Developmental and activity-dependent miRNA expression profiling in primary hippocampal neuron cultures', *PLoS One*, 8: e74907.
Waite, A., S. C. Brown, and D. J. Blake. 2012. 'The dystrophin-glycoprotein complex in brain development and disease', *Trends Neurosci*, 35: 487-96.
Wang, J., X. J. Ma, J. S. Yang, X. Y. Zheng, C. T. Zugates, C. H. J. Lee, and T. Lee. 2004a. 'Transmembrane/juxtamembrane domain-dependent Dscam distribution and function during mushroom body neuronal morphogenesis', *Neuron*, 43: 663-72.
Wang, J., X. Ma, J. S. Yang, X. Zheng, C. T. Zugates, C. H. Lee, and T. Lee. 2004b. 'Transmembrane/juxtamembrane domain-dependent Dscam distribution and function during mushroom body neuronal morphogenesis', *Neuron*, 43: 663-72.
Wang, J., C. T. Zugates, I. H. Liang, C. H. J. Lee, and T. M. Lee. 2002. 'Drosophila Dscam is required for divergent segregation of sister branches and suppresses ectopic bifurcation of axons', *Neuron*, 33: 559-71.
Wang, T. Y., H. Guo, B. Xiong, H. A. F. Stessman, H. D. Wu, B. P. Coe, T. N. Turner, Y. L. Liu, W. J. Zhao, K. Hoekzema, L. Vives, L. Xia, M. N. Tang, J. J. Ou, B. Y. Chen, Y. D. Shen, G. L. Xun, M. Long, J. Lin, Z. N. Kronenberg, Y. Peng, T. Bai, H. H. Li, X. Y. Ke, Z. M. Hu, J. P. Zhao, X. B. Zou, K. Xia, and E. E. Eichler. 2016. 'De novo genic mutations among a Chinese autism spectrum disorder cohort', *Nat Commun*, 7.
Wang, X., G. R. Sterne, and B. Ye. 2014. 'Regulatory mechanisms underlying the differential growth of dendrites and axons', *Neurosci Bull*, 30: 557-68.
Wang, X., J. Tucciarone, S. Jiang, F. Yin, B. S. Wang, D. Wang, Y. Jia, X. Jia, Y. Li, T. Yang, Z. Xu, M. A. Akram, Y. Wang, S. Zeng, G. A. Ascoli, P. Mitra, H. Gong, Q. Luo, and Z. J. Huang. 2019. 'Genetic Single Neuron Anatomy Reveals Fine Granularity of Cortical Axo-Axonic Cells', *Cell reports*, 26: 3145-59 e5.
Wang, Y., A. Gupta, M. Toledo-Rodriguez, C. Z. Wu, and H. Markram. 2002. 'Anatomical, physiological, molecular and circuit properties of nest basket cells in the developing somatosensory cortex', *Cereb Cortex*, 12: 395-410.
Wei, H. Y., H. Y. Kyung, P. J. Kim, and C. Desplan. 2020. 'The diversity of lobula plate tangential cells (LPTCs) in the Drosophila motion vision system', *Journal of Comparative Physiology a-Neuroethology Sensory Neural and Behavioral Physiology*, 206: 139-48.

Wills, Z., J. Bateman, C. A. Korey, A. Comer, and D. Van Vactor. 1999. 'The tyrosine kinase Abl and its substrate enabled collaborate with the receptor phosphatase Dlar to control motor axon guidance', *Neuron*, 22: 301-12.
Wills, Z., M. Emerson, J. Rusch, J. Bikoff, B. Baum, N. Perrimon, and D. Van Vactor. 2002. 'A Drosophila homolog of cyclase-associated proteins collaborates with the Abl tyrosine kinase to control midline axon pathfinding', *Neuron*, 36: 611-22.
Wills, Z., L. Marr, K. Zinn, C. S. Goodman, and D. Van Vactor. 1999. 'Profilin and the Abl tyrosine kinase are required for motor axon outgrowth in the Drosophila embryo', *Neuron*, 22: 291-9.
Woo, J., S. K. Kwon, J. Nam, S. Choi, H. Takahashi, D. Krueger, J. Park, Y. Lee, J. Y. Bae, D. Lee, J. Ko, H. Kim, M. H. Kim, Y. C. Bae, S. Chang, A. M. Craig, and E. Kim. 2013. 'The adhesion protein IgSF9b is coupled to neuroligin 2 via S-SCAM to promote inhibitory synapse development', *J Cell Biol*, 201: 929-44.
Woo, T. U., R. E. Whitehead, D. S. Melchitzky, and D. A. Lewis. 1998. 'A subclass of prefrontal gamma-aminobutyric acid axon terminals are selectively altered in schizophrenia', *Proc Natl Acad Sci U S A*, 95: 5341-6.
Wu, C. L., Y. P. Wairkar, C. A. Collins, and A. DiAntonio. 2005. 'Highwire function at the Drosophila neuromuscular junction: Spatial, structural, and temporal requirements', *Journal of Neuroscience*, 25: 9557-66.
Xiang, Y., Q. Yuan, N. Vogt, L. L. Looger, L. Y. Jan, and Y. N. Jan. 2010. 'Light-avoidance-mediating photoreceptors tile the Drosophila larval body wall', *Nature*, 468: 921-6.
Xiong, X., X. Wang, R. Ewanek, P. Bhat, A. Diantonio, and C. A. Collins. 2010. 'Protein turnover of the Wallenda/DLK kinase regulates a retrograde response to axonal injury', *J Cell Biol*, 191: 211-23.
Yamakawa, K., Y. K. Huo, M. A. Haendel, R. Hubert, X. N. Chen, G. E. Lyons, and J. R. Korenberg. 1998. 'DSCAM: a novel member of the immunoglobulin superfamily maps in a Down syndrome region and is involved in the development of the nervous system', *Human Molecular Genetics*, 7: 227-37.
Yang, B., J. B. Treweek, R. P. Kulkarni, B. E. Deverman, C. K. Chen, E. Lubeck, S. Shah, L. Cai, and V. Gradinaru. 2014. 'Single-Cell Phenotyping within Transparent Intact Tissue through Whole-Body Clearing', *Cell*, 158: 945-58.
Yang, J. M., C. J. Shen, X. J. Chen, Y. Kong, Y. S. Liu, X. W. Li, Z. Chen, T. M. Gao, and X. M. Li. 2018. 'erbb4 Deficits in Chandelier Cells of the Medial Prefrontal Cortex Confer Cognitive Dysfunctions: Implications for Schizophrenia', *Cereb Cortex*.
———. 2019. 'erbb4 Deficits in Chandelier Cells of the Medial Prefrontal Cortex Confer Cognitive Dysfunctions: Implications for Schizophrenia', *Cereb Cortex*, 29: 4334-46.
Yang, J. S. J., J. M. Bai, and T. M. Lee. 2008. 'Dynein-Dynactin Complex Is Essential for Dendritic Restriction of TM1-Containing Drosophila Dscam', *PLoS ONE*, 3.
Yap, K., and E. V. Makeyev. 2016. 'Functional impact of splice isoform diversity in individual cells', *Biochemical Society transactions*, 44: 1079-85.
Ye, B., J. H. Kim, L. Yang, I. McLachlan, S. Younger, L. Y. Jan, and Y. N. Jan. 2011. 'Differential regulation of dendritic and axonal development by the novel kruppel-like factor dar1', *J Neurosci*, 31: 3309-19.
Ye, B., D. Liao, X. Zhang, P. Zhang, H. Dong, and R. L. Huganir. 2000. 'GRASP-1: a neuronal RasGEF associated with the AMPA receptor/GRIP complex', *Neuron*, 26: 603-17.

Ye, B., Y. Zhang, W. Song, S. H. Younger, L. Y. Jan, and Y. N. Jan. 2007. 'Growing dendrites and axons differ in their reliance on the secretory pathway', *Cell*, 130: 717-29.
Yogev, S., and K. Shen. 2017. 'Establishing Neuronal Polarity with Environmental and Intrinsic Mechanisms', *Neuron*, 96: 638-50.
Yuan, J. S., A. Reed, F. Chen, and C. N. Stewart, Jr. 2006. 'Statistical analysis of real-time PCR data', *BMC bioinformatics*, 7: 85.
Zhan, X. L., J. C. Clemens, G. Neves, D. Hattori, J. J. Flanagan, T. Hummel, M. L. Vasconcelos, A. Chess, and S. L. Zipursky. 2004. 'Analysis of Dscam diversity in regulating axon guidance in Drosophila mushroom bodies', *Neuron*, 43: 673-86.
Zhang, L., Y. Huang, J. Y. Chen, Y. Q. Ding, and N. N. Song. 2015. 'DSCAM and DSCAML1 regulate the radial migration and callosal projection in developing cerebral cortex', *Brain Res*, 1594: 61-70.
Zhang, P., K. Takeuchi, L. S. Csaki, and K. Reue. 2012. 'Lipin-1 phosphatidic phosphatase activity modulates phosphatidate levels to promote peroxisome proliferator-activated receptor gamma (PPARgamma) gene expression during adipogenesis', *J Biol Chem*, 287: 3485-94.
Zuliani, C., S. Kleber, S. Klussmann, T. Wenger, M. Kenzelmann, N. Schreglmann, A. Martinez, J. A. del Rio, E. Soriano, P. Vodrazka, R. Kuner, H. J. Groene, I. Herr, P. H. Krammer, and A. Martin-Villalba. 2006. 'Control of neuronal branching by the death receptor CD95 (Fas/Apo-1)', *Cell Death Differ*, 13: 31-40.